Analytical
Systems Engineering CORPORATION

25 RAY AVENUE
BURLINGTON, MASSACHUSETTS 01803
(617) 272-7910

ASECR 74-71

# ANALYSIS OF SATELLITE MEASUREMENTS OF TERRESTRIAL RADIO NOISE



By

George Bakalyar
Joseph Caruso
Richard Vargas-Vila
Edward Ziemba

SEPTEMBER 1974



Prepared For

NATIONAL AERONAUTICS & SPACE ADMINISTRATION
Goddard Space Flight Center
Greenbelt, Maryland 20771

Final Report On: Contract NAS5-23224, Article 1, Paragraph B

Period Covered: November 7, 1973 - May 7, 1974

# ABSTRACT

Worldwide distributions of terrestrial radio noise as monitored by RAE I have been generated and compared with CCIR predictions. These contour maps show the global morphology of radio noise at 6.55 and 9.18 MHz for Fall, Winter, Spring and Summer during the local time blocks of 00-08 LT and 16-24 LT. These computer produced maps show general agreement with CCIR predictions over large land masses. The RAE and CCIR maps diverge at high latitudes over Asia and frequently over ocean regions. Higher noise levels observed by RAE at high latitudes are attributed to magnetospheric emission. Higher noise levels observed by RAE over Asia are attributable to high power transmitters.

Analysis of RAE noise observations in conjunction with various geophysical phenomena showed no obvious correlation. For certain, high latitude noise levels are greater than mid and low latitude noise levels for all seasons and times of day for both hemispheres. Higher noise temperatures of enhanced radiation are almost always observed on the lower Vee antenna. This observation coupled with the observation that the enhanced noise temperatures at higher frequencies drops off sooner than it does at lower frequencies leads to the conclusion that the source of enhanced radiation is between the satellite and the F-layer.

Results of an investigation of RAE noise levels over the South Atlantic geomagnetic anomaly are inconclusive. Some of the HF noise contour maps reveal enhanced noise levels over the geomagnetic anomaly. However, analysis of individual RAE passes over the same area show little difference from control passes. Clearly, a more detailed investigation is required.

# TABLE OF CONTENTS

# 1.0 INTRODUCTION

From the time it became evident that the Radio Astronomy Explorer (RAE) I Satellite could provide a means of determining the global characteristics of HF terrestrial radio noise, Analytical Systems Engineering Corporation has been privileged to fulfill a leading role both in the initiation and implementation of this basic research. The results of these investigations have been communicated to the scientific community through publications and symposium papers.

One of the more important and exciting results to date has been the generation of contour maps of worldwide terrestrial noise distributions for the discrete frequencies of 3.93, 4.7, 6.55 and 9.18 MHz during specific periods for the months of July, August, October and December. Since contour map generation was carried out manually, severe limitations were imposed on the number of maps one could reasonably expect to generate. Further, since the data base used to provide the maps was not complete, the number of measurements utilized to arrive at the average noise factor as a function of geographic location and local time was less than optimum in many instances.

For the present effort, the complete data base in the form of magnetic tapes was utilized. Additionally, NASA/GSFC computer programs developed for mapping galactic noise were adapted for terrestrial noise mapping. The result has been the generation of fourteen seasonal noise contour maps for Fall, Winter, Spring and Summer at the frequencies 6.55 and 9.18 MHz during the local time blocks 00-08 LT and 16-24 LT. Characteristic features of the contours are discussed in Section 2.0 of this report as well as their comparison with CCIR contours of global terrestrial

noise. A further topic considered in Section 2.0 is the manner in which the noise contours were generated.

A major portion of the present report concerns itself with RAE I observations over high latitude regions. Since RAE spends nearly 25% of its time over auroral latitudes large amounts of data are available for the investigation of the many absorption and emission processes occurring in the regions of the auroral oval and the mid-latitude trough. Since both absorption and emission play predominant roles under many circumstances, a careful analysis of the RAE data is required to determine the relative importance of these competing factors. The analytical results, although interesting in themselves, have a further significance insofar as they help to explain some of the characteristic features of the seasonal noise contour maps.

In accordance with our judgement that precipitating particles may enhance the noise levels observed by RAE, it is reasonable to assume that in the neighborhood of the South Atlantic geomagnetic anomaly, noise levels may also be either enhanced or lessened. In this region, the electron mirror points are much lower than elsewhere due to the anomalously small values of the magnetic field at the earth's surface. Hence, large amounts of electrons are deposited from the trapping regions in the locale of the South Atlantic anomaly.

A further objective of our effort involved an attempt to determine whether RAE had measured enhanced noise levels during the January, 1969 artificial aurora experiment because of the synchrotron radiation associated with the injection of high energy electrons into the magnetosphere. A description of the analysis of the high latitude events,

observations over the South Atlantic anomaly, and the artificial aurora experiment, together with the conclusions of these investigations, are the subjects of Section 3.0.

Section 4.0 highlights significant conclusions regarding both the seasonal noise contour maps and RAE's ability to provide significant information concerning high latitude magnetospheric processes as well as noise emission over the geomagnetic anomaly.

# 2.0 MORPHOLOGY OF TERRESTRIAL RADIO NOISE

The importance of accurately assessing the RF noise environment near the Earth's surface is a well established fact which needs very little elaboration. It is sufficient to indicate that noise imposes fundamental limitations on all communications, and efficient communication system dictates that one describe the noise environment as accurately as possible. The CCIR predictions of global terrestrial noise levels presently represent the most reliable and most frequently used source of noise information.

The end we seek to achieve by using the RAE observations to generate global noise contours is to provide empirial noise mappings based on global observations of noise power to serve as a basis for comparison with the CCIR predictions. Since the CCIR predictions rest on measurements taken at but 16 land based observational stations (shown in Figure 2-1), a propagation model must be invoked to predict the noise magnitude at locations removed from the observation points. The CCIR predictions are, therefore, vulnerable to criticism over certain regions. RAE observations prove extremely valuable, since they furnish empirical data taken over the full spatial extent of these regions.



There are, however, two criticisms which can be leveled against noise contours determined from RAE observational data. The most fundamental criticism is that major contributions to the noise power measured by RAE at a particular instant have their origins in sources which are not immediately below the RAE in the neighborhood of the subsatellite point. If this were the case, noise contour mapping would not be possible since the source locations of the major contributions are unknown. Herman,

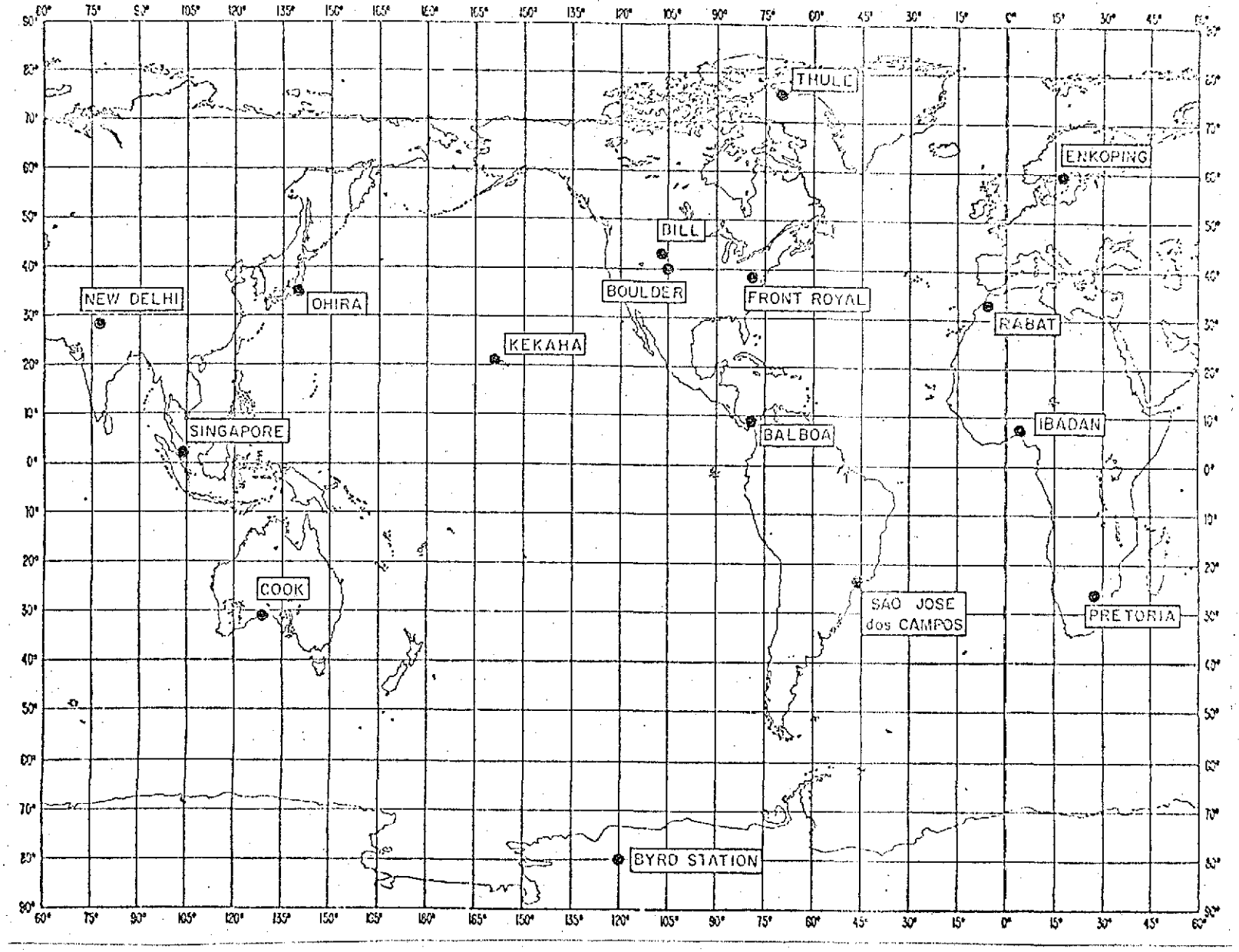


FIGURE 2-1 RADIO NOISE STATIONS USING ARN-2 RECORDERS

et al. (1973) have provided ample evidence that this is not the case. On the contrary, in most instances, the major contribution to the noise power at any given time does, in fact, have its origin in the immediate neighborhood of the subsatellite point. This clearly indicates that RAE noise contours are a valid representation of the terrestrial noise power distribution as a function of time and geographic location. At high latitudes, RF noise generation processes in the magnetosphere appear to contribute significantly to the total noise power and this must be given careful consideration, as will be indicated in more detail later in this report.

A further criticism involves the lack of spatial resolution as observations are taken at lower frequencies. It is true that at 3.93 MHz and below, the projected antenna beamwidth is substantial. However, the noise contours were generated for the frequencies 9.18 and 6.55 MHz where spatial resolution is quite acceptable. In fact, the projected beamwidth at 9.18 MHz covers approximately $13^{o}$ of latitude and $27^{o}$ longitude at the equator. Consequently, although only under special circumstances do we possess sufficient resolution to differentiate between various types of sources (e.g. thunderstorms, man made noise, etc.), the total noise power can be contoured with a reasonable degree of confidence.

The following sections discuss the methods used to map the RAE noise data, the RAE noise level contours and their comparison with CCIR predictions.

## 2.1 Computer Processing of RAE Noise Tapes

Manual mapping of the RAE terrestrial noise distribution has been made in geographic coordinates for selected intervals by restricting the times of interest to periods when RAE was nominally over earth's night side (Herman, Caruso and Stone, 1973). For 1968 data, in the local time block periods of 20-24LT, 00-04LT and 04-08LT, the ephemeris information printed out at 15-minute UT intervals was manually searched to find local times falling into the above LT time blocks. Usually only 2 points within a block were found. At these points the universal time and geographic location of the satellite were noted, and the noise magnitude at that UT time was extracted from the whole-orbit RV data tabulated on microfilm and converted to decibels (dB) above $288^{\circ}K$. On base maps cast in modified-cylindrical (geographic) coordinates, each noise magnitude was recorded at its appropriate location, and then isolines of constant dB noise in 5 dB increments were drawn manually through the data points, as illustrated in Figure 2-2 for 9.18 MHz in December, 1968.

This technique yielded good maps for studying the gross features of worldwide distributions, but it perforce neglected all the data between 15-minute UT intervals and therefore omitted detailed geographic variations. The ephemeris for 1969 was printed out at 10-minute intervals increasing the number of available data points by 50%, and the manual mapping technique suffered from having too much data and increased processing time per map.



In order to determine the variability of world distributions as a function of frequency, time block and season, and to determine the statistical fluctuations within a season, it is necessary to construct a larger number of maps than is feasible with manual techniques. The only way to adequately

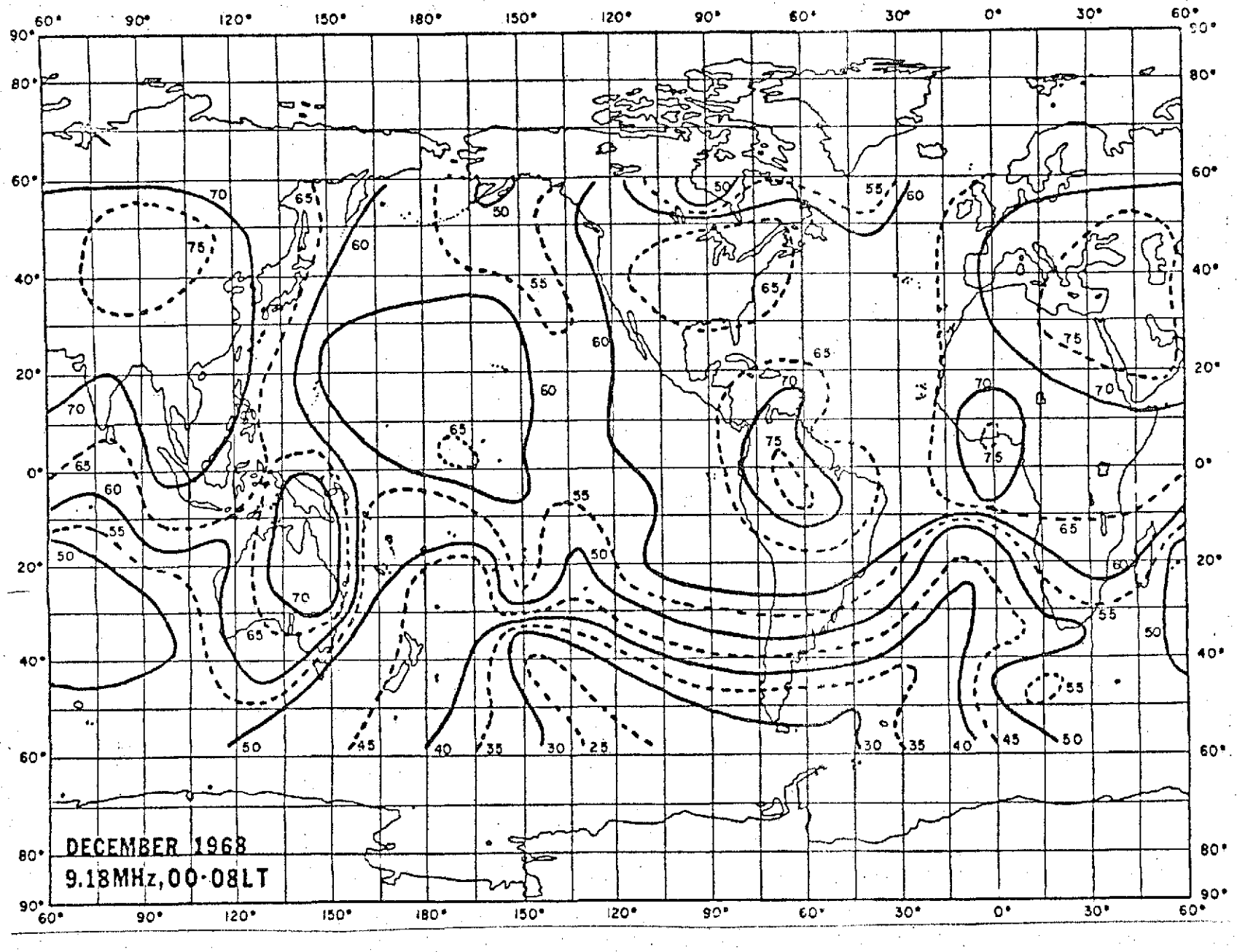


FIGURE 2-2 NOISE CONTOUR MAP OF RAE NOISE DISTRIBUTION
(AFTER HERMAN, CARUSO AND STONE, 1973)

attack this problem therefore, is to utilize computer mapping techniques.

## SOFTWARE

An investigation into existing NASA software was performed. While there was software which produced data similar to our objectives, it appeared to be a simple matter to code new algorithms which produced the exact data required. The first data which was checked was the October 15-23, 1968 period at 9.18 MHz.

The computer generated noise contour map for the October 15-23, 1968 period at 9.18 MHz compares quite favorably with the manually generated map (under an earlier contract) for the same period. The digital output of the noise factors ($F_a$) for geographic block sizes of $10^\circ$ of latitude $15^\circ$ of longitude, and $5^\circ$ by $5^\circ$ were plotted on base maps and contours were manually drawn at 5 dB intervals. The $10^\circ$ by $15^\circ$ plots are most suitable and the remaining maps are presented in this format.

A comparison with the earlier map indicates that all of the significant features are retained. However, several new characteristics have been manifested which are a direct result of using the digital information rather than reading the data points from the microfilm which involves some additional averaging.

The specific shapes of the contour lines vary somewhat from map to map. This is to be expected since some judgement is involved and different individuals do tend to produce slightly different overall contours, while retaining all of the significant features of the map.

A further conclusion of this preliminary analysis is that a block size of $10^\circ$ by $15^\circ$ is optimum and that an averaging process of the data eliminating only those points which

are clearly not representative (e.g., equipment malfunction) yields the most valid experimental values of noise factor. In summary, 1) the criteria for map generation was established, 2) the computer software was decided to be accurate and operable producing a test map in all essential features comparable to the reference map, and 3) the RAE data base has been compressed and is available as input to the data generating routine.

It became necessary to slightly revise the selection of time periods to be mapped. Originally we had intended to use data gathered in 1968 for the summer season. Since the onboard recorder was operable at this time, however, RV data is not available for this period and we have chosen summer of 1970 as an alternative. Hence, it was decided to produce twenty-four seasonal maps for three 8-hour local time blocks and two frequencies, 9.18 and 6.55 MHz, for the year 1970 (except December 1969 was used instead of December 1970).

For an individual map the procedure was:

1. Select data points at specified intervals ($10^{o}$X $15^{o}$) within a preselected 8 hour local time block.

2. Incorporate the noise temperatures into the running average for that set of geographic coordinates and the local times for each of the selected data points.

3. Convert the noise temperature to noise factor $F_a$ in dB above $288^{o}$K and store.

4. Plot values of average noise factor at the appropriate geographic coordinates on a modified cylindrically projected

world map or other suitable projection.

5. Generate contour curves of constant noise factor in 5dB increments.

This procedure was followed and data (i.e., actual noise factor value) were calculated. These data were then used as input to the existing NASA contour mapping routines. Many of the contours are not totally useful since observational periods during daylight time blocks yield scant information. The 00-08 and 16-24 local time blocks resulted in useable contours. Hence, 16 noise contour maps were obtained. The contours obtained from the NASA program were not all closed due to lack of data in certain areas. These were manually closed and continental outlines added to the plots.

## 2.2 Global HF Noise Contour Maps

Before beginning the discussion of the RAE noise level contours and their subsequent comparison with CCIR predictions, a brief description of the general features of the CCIR noise predictions will be presented.

In general, there is pronounced noise activity over the continental land masses where it is well known that abundant thunderstorm activity occurs. Over the northern and southern ocean regions, the noise levels are consis-

tently low; this is also true at the higher latitudes. Noise levels are ordinarily higher in the central Pacific and Atlantic Oceans.

At the higher latitudes it is quite reasonable to expect relatively low noise levels since there are few noise sources in these reqions. However, what the noise environment should be over large portions of ocean is not completely obvious. Since there is only one observing station in the Pacific and not a single station in the Atlantic, the CCIR predicted noise levels do not have a strong empirical basis in measurements. This is true to a lesser degree over the continental land masses where, for example, there is one observing station in South America at Sao Jose dos Campos, and one station at Cook, Australia. These facts have not been elicited to demean the CCIR noise prediction contours but only to point out that RAE observations can serve to improve and supplement our knowledge of the noise environment.

Utilizing the RAE magnetic tape data base in conjunction with modified NASA/Goddard sky mapping computer software, fourteen seasonal contour maps were generated at Goddard Space Flight Center. The observational period considered was the year 1970. Noise contours on both 6.55 and 9.18 MHz for Winter, Spring, Summer and Fall in the northern hemisphere for the local time blocks 00-08 LT and 16-24 LT were generated. The noise contours are displayed in Figures 2-3 through 2-16. The CCIR predictions for similar periods are shown in Figures 2-17 through 2-24.

Insofar as was possible, the contours as graphed by the computer plotting software were not modified since it was judged that this would insure against any preconceived notions insinuating their way into the contours. This is an important consideration and the results of adopting this policy become evident when the RAE and CCIR maps are compared. The CCIR contours are smooth; there are very few anomalies; the high noise source concentrations are where one would expect and they remain localized over the continental land masses from season to season; the contours are always of similar shape over Northern and Southern Ocean regions. In short, the CCIR predictions are "predictable." On the other hand, the RAE contours, while reflecting many of the gross characteristics exhibited in the CCIR noise predictions, are more disjointed and display on occassion high noise levels over oceans and at the higher latitudes. Furthermore, the contours are not as uniform from season to season, nor are they as smooth and "continuous" as the CCIR maps.

In some instances it was necessary to close or complete contours which were unfinished by the plotting routine primarily as a result of gaps in the data. In all cases but one it was possible to legitimately close the contours on the basis of the trends indicated by neighboring data points supplemented by insight into the morphology of terrestrial radio noise. This was not possible for the Spring contours for the 0-8 local time block due to the paucity of Northern Hemisphere data.

Figures 2-5 and 2-6 depict the Spring contours for

the local time block from 00-08 LT at the frequencies 6.55 and 9.18 MHz respectively. Considerable data is lacking in the northern hemisphere but the contours are complete enough to illustrate a number of interesting features. The high noise levels over South America and portions of Africa and Madagascar are expected, although the South American peak level is much further south than anticipated. The low noise levels in South Pacific and Atlantic Oceans are also predictable using CCIR as a standard of comparison although the contour structure is quite different. It is worthwhile reiterating that the impulse to modify the contours was firmly resisted. Since there is nothing really sacrosanct about the contouring routines and, in some cases, there appeared to be sound reasons for rejecting the manner in which a particular contour was drawn, this precept was, at times, difficult to accept. However, as indicated earlier, the contouring routines are consistent and objective, and the appearance of sound reasons may simply be a guise for preconceived notions of how the contours should appear.

A unique feature of Figure 2-6 is the high noise level over China extending a considerable distance into the Pacific Ocean. This structure is not predicted by CCIR and is thought to result in large measure from HF transmitters located on the Chinese and Russian mainland. An ionospheric "iris" of sufficient diameter would allow noise from ground based transmitters to reach RAE over these regions of the Pacific.

Figures 2-7 and 2-8 represent the contours for the same season and frequencies for the time block 16-24LT. The characteristics are quite similar to 0-8LT contours. However, there is much more Northern Hemisphere data and Figure 2-7 manifests high noise levels over much of the U.S. Note the high noise factor off the coast of Brazil over the re-

gion of the geomagnetic anomaly.

Figures 2-9 and 2-10 illustrate the summer contours for the 0-8LT block at 6.55 and 9.18 MHz. Figure 2-10 is strikingly similar to the CCIR noise predictions for the same period as witnessed by the preponderance of intense noise sources over the continental landmasses and low noise factors over ocean areas. Note the high noise factor in the Mexico-Florida region. On the other hand, there are significant differences, among which are high noise levels over China, Russia, and the Northern Pacific. Additionally, the noise power is of greater magnitude in the Northern Central Atlantic. The high values of noise power between $40^{\circ}$ and $60^{\circ}$ south latitude are possibly the result of RF noise generated in the magnetosphere. Again, notice the high noise factor in the neighborhood of the South Atlantic anomaly in both figures.

The contours shown in Figures 2-11 and 2-12 for the summer season and the 16-24 local time block exhibit features like those of the 0-8LT time block. An important feature depicted in Figure 2-11 is the high noise level at $7^{\circ}$ south latitude and $327^{\circ}$ east longitude over the region of the South Atlantic geomagnetic anomaly. The noise factor is some 10 dB higher at this geographic location than in any of the surrounding regions. As is well known, in the region of the magnetic anomaly the field strength is low, allowing electrons to penetrate deeper into the atmosphere. As an electron penetrates more deeply, the probability that scattering may change its pitch angle is increased and, hence, the likelihood that it may impart its energy to other particles also is increased. This type of scattering is responsible for the continous removal of trapped electrons with small pitch angles. A priori, it is not clear whether increased absorption or enhanced noise due to RF

emission will predominant. Figure 2-11 is another instance of an enhancement over the anomaly at 6.55 MHz.

One further feature of Figure 2-11 should be emphasized. Our basic concern has been directed toward a comparison of the relative locations of high and low noise power regions with little regard to the absolute magnitude of the noise. In fact, if one begins to compare the magnitude of the noise indicated on the RAE and CCIR contours, the comparison is generally favorable. By way of illustration consider the high noise factor over Africa at $5^{o}$ north latitude and $12^{o}$ east longitude. The noise factor as measured by RAE at 6.55 MHz over this region is approximately 55 dB. Over the same geographic location, for the equivalent season and time block, the CCIR predictions (Figure 2-22) indicate a noise factor of approximately 90 dB at 1 MHz. Using Figure 2-25, the noise factor at 1 MHz can be scaled to its appropriate value at 6.55 MHz. At 1 MHz one chooses the value 90 dB to select the correct parametric curve. Moving down the curve to the value 6.55 MHz on the abscissa, a value of $F_a$ equal to approximately 56 dB is read on the ordinate. This is a rather favorable comparison. The example also helps to make manifest the close kinship between the RAE contours and CCIR predictions in regions where there is agreement. Because of the different natures of the contours, and the invariably consistent contrast between high noise levels over the equatorial landmasses and low noise levels over the oceans in the case of the CCIR predictions, the similarities between RAE and CCIR are somewhat obscured. This is somewhat the situation of Figure 2-11 where the high over Africa, which is equal in magnitude to the CCIR predicted value, is less obviously visible since the noise factors in the neighboring ocean regions are of comparable value and the shape of the local contours do not instinctively cause the eye to focus on the African high. The facts illuminated by this discourse

can be easily duplicated in many other instances, and the reader may reaffirm these facts with very little difficulty by repeating this process using almost any of the RAE contours over locations where there is a general correspondence of gross characteristics for both the RAE and CCIR contours.

Figure 2-14, The Fall contour for 0-8LT at 9.18 MHz, is of interest because of the extremely low noise factor at $40^{\circ}$ north latitude, $200^{\circ}$ east longitude surrounded by extremely high noise factors. This structure is singularly unique amongst the fourteen contours and we have not arrived at any sound explanations, although receiver saturation is the most plausible explanation.

Features of the remaining maps display characteristics much like those already described with the exception of Figure 2-11, where high noise powers are observed over the South Atlantic geomagnetic anomaly. Large noise factors over the anomaly, as we have indicated, were measured by RAE for Spring at 6.55 MHz for 16-24LT; during the Summer on both 9.18 and 6.55 MHz for the period 0-8LT, and on 6.55 MHz for 16-24LT; during the Fall on 9.18 MHz for the period 16-24LT. The nine remaining contours do not exhibit any unique structure over this region. Since each contour is derived from a substantial data base, the high noise levels are clearly indicative of the average behavior over this geographic location, an average which is not strongly weighted by any bizarre, rarely present phenomenon. Clearly, this argument applies with equal validity for those instances where the high noise power structure is absent. There is no readily obvious explanation regarding both the presence and absence of the high noise power and how it depends on season, time of day, and frequency. For the present, we defer further discussion of the noise characteristics over the anomaly until we have occasion to present the analysis of the individual RAE orbit data over the region in Section 3.4.

The RAE noise contours, we feel, represent a valuable contribution to our knowledge of the terrestrial noise environment and we wish to re-emphasize and summarize their salient features. In many respects the contours compare favorably with the CCIR predictions, exhibiting, in general, high noise factors over the continental land masses and low noise levels over ocean regions. Where they differ, there are reasonable explanations in most instances. For example, the high noise levels over some portions of the ocean and the East Asian mainland are very likely accurate representations since they are firmly grounded in empirical data. The CCIR predictions are based on little or no data, and therefore suspect. The enhanced noise levels at high latitudes are attributed to magnetospheric emission processes, and therefore are not representative of the noise power on Earth's surface.

In those cases where no acceptable explanation of the noise structure is forthcoming, it is not necessary that the RAE results be repudiated. We emphasize once again that the contours are based on observational data, and theoretical predictions not verified by empirical data can become the bane of knowledge if the theory is ultimately shown to be inaccurate; consequently our reliance on empirical data.

The RAE HF noise contours, we contend, have expanded our knowledge of the terrestrial noise environment and are an important source of empirical observations over those global regions which heretofore have proved to be inaccessible. The RAE contours supplement and enhance the CCIR worldwide noise predictions and therefore will be of importance to both the scientific researcher and the communications system designer.

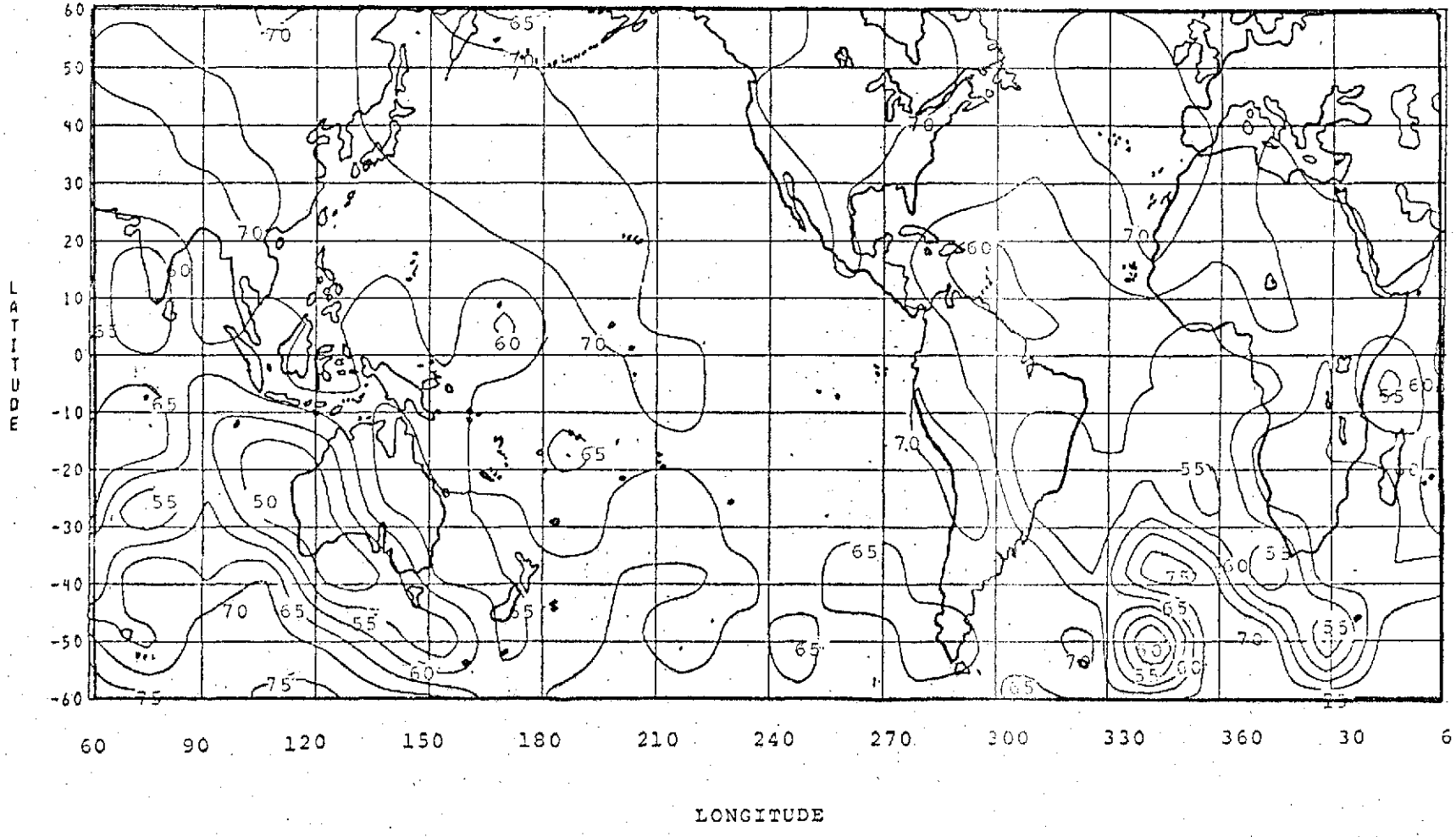


FIGURE 2-3 RAE NOISE CONTOURS FOR WINTER 1970, 6.55MHz (0-8 LT)

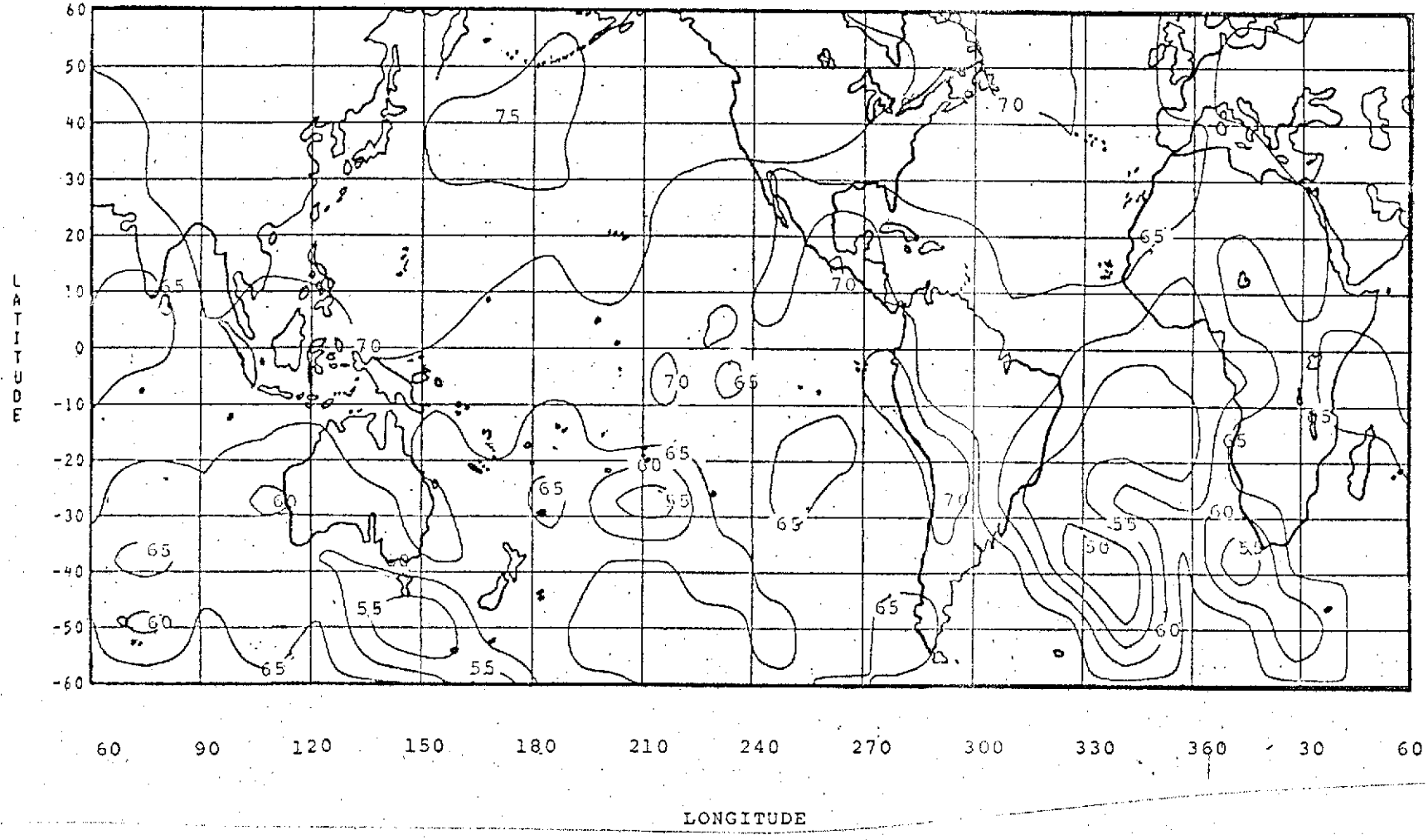


FIGURE 2-4 RAE NOISE CONTOURS FOR WINTER 1970, 9.18MHz (0-8 LT)

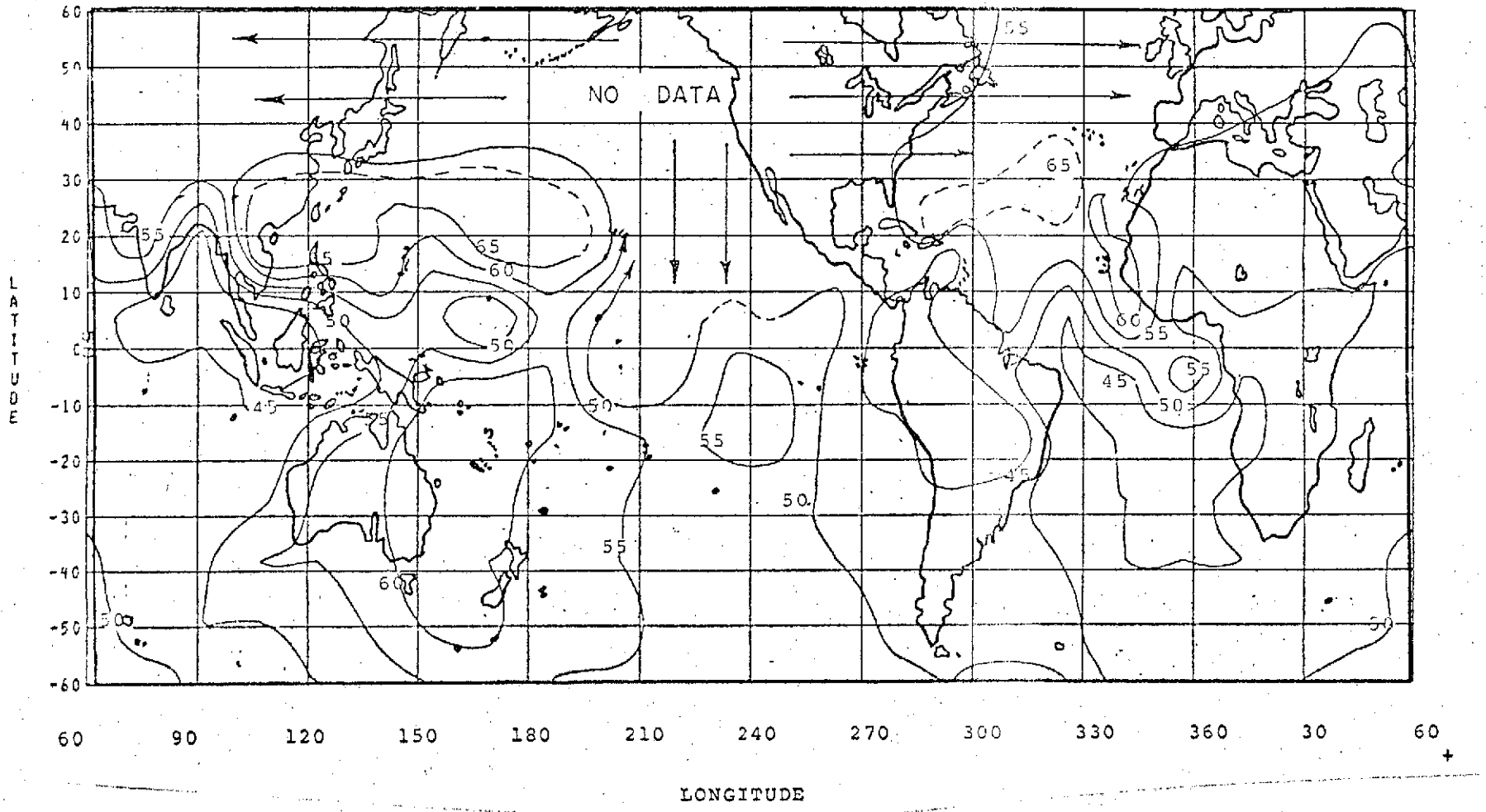


FIGURE 2-5 RAE NOISE CONTOURS FOR SPRING 1970, 6.55MHz (0-8 LT)

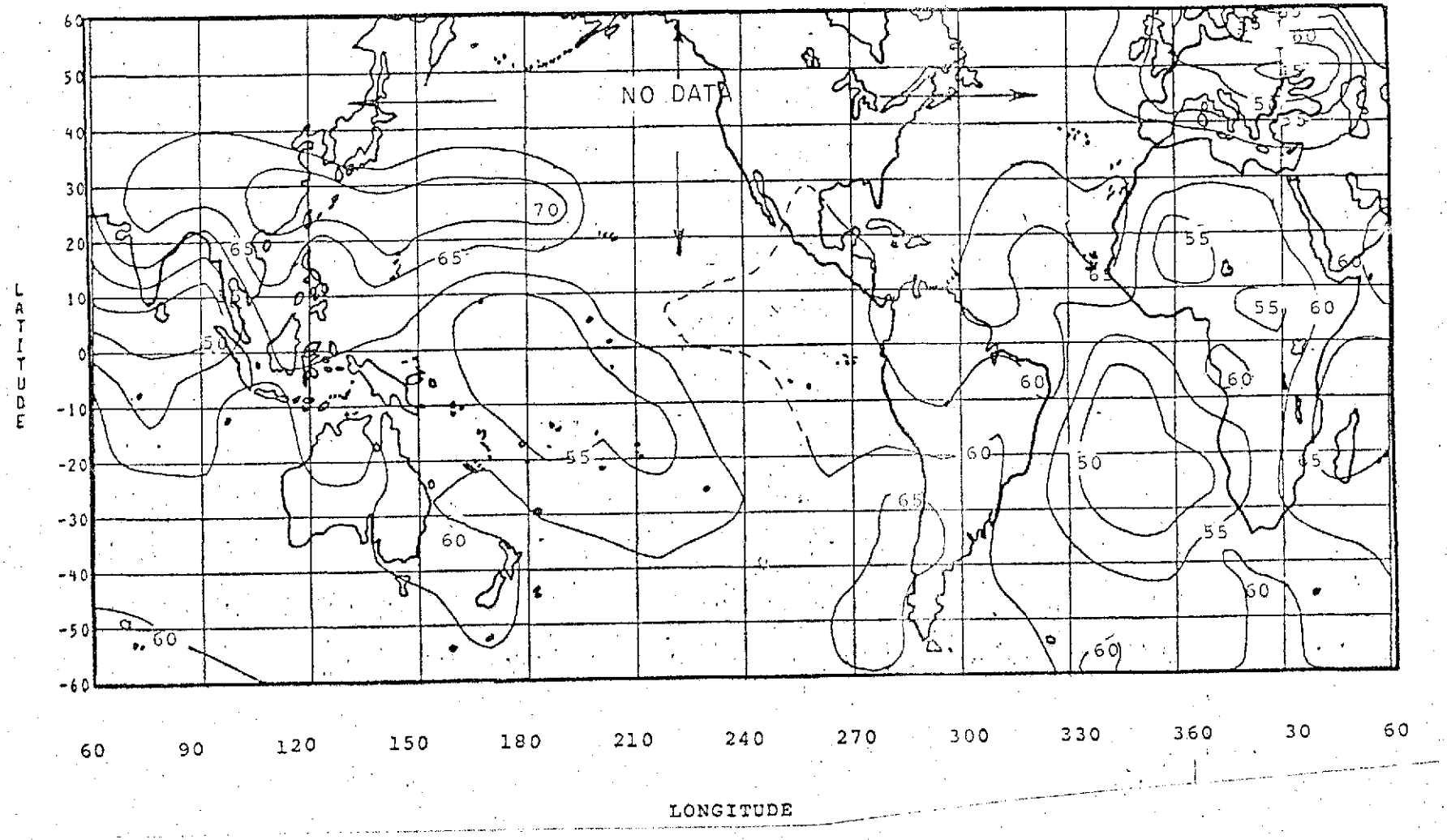


FIGURE 2-6 RAE NOISE CONTOURS FOR SPRING 1970, 9.18MHz (0-8 LT)

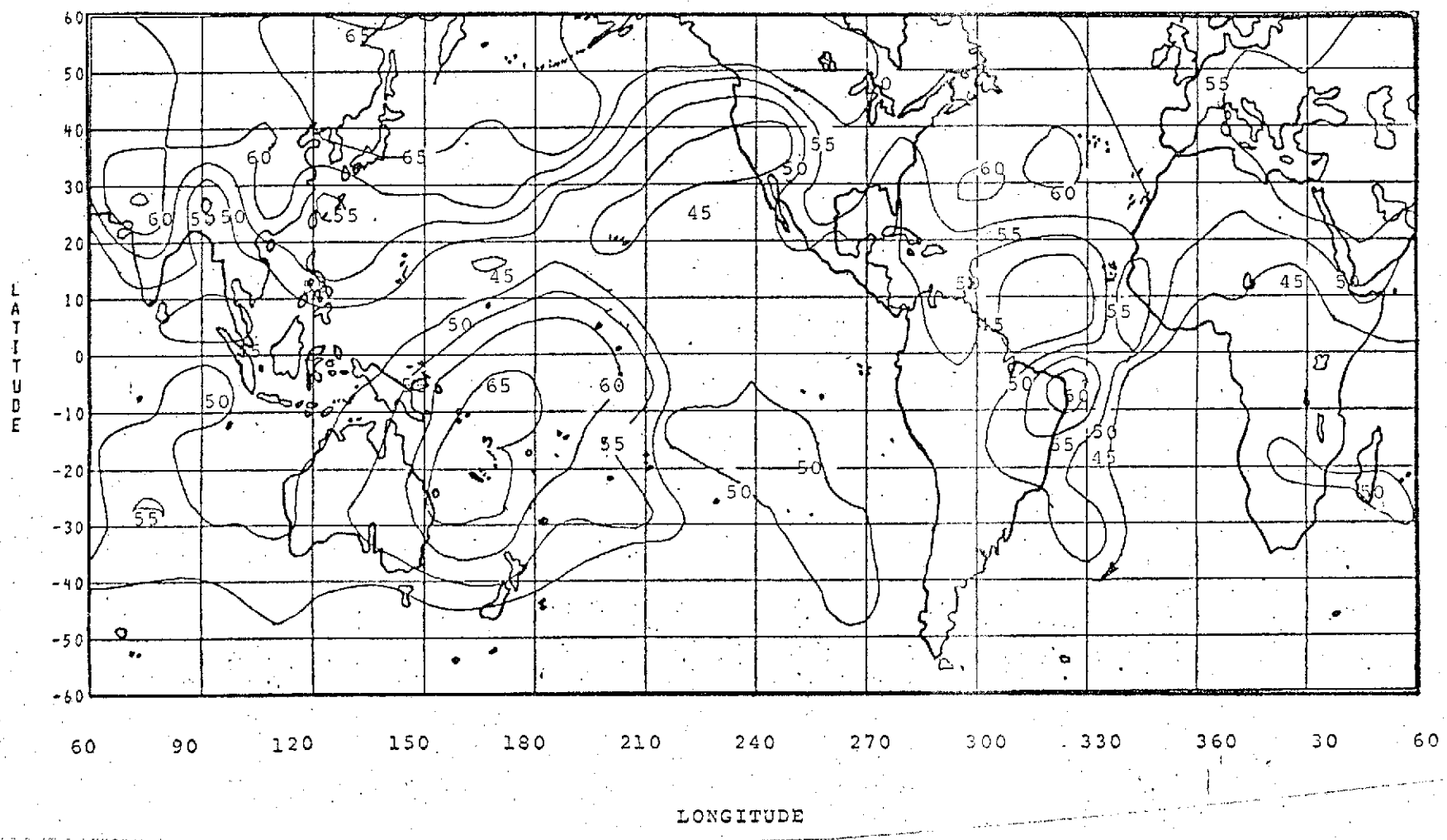


FIGURE 2-7 RAE NOISE CONTOURS FOR SPRING 1970, 0.55MHz (16-24 LT)

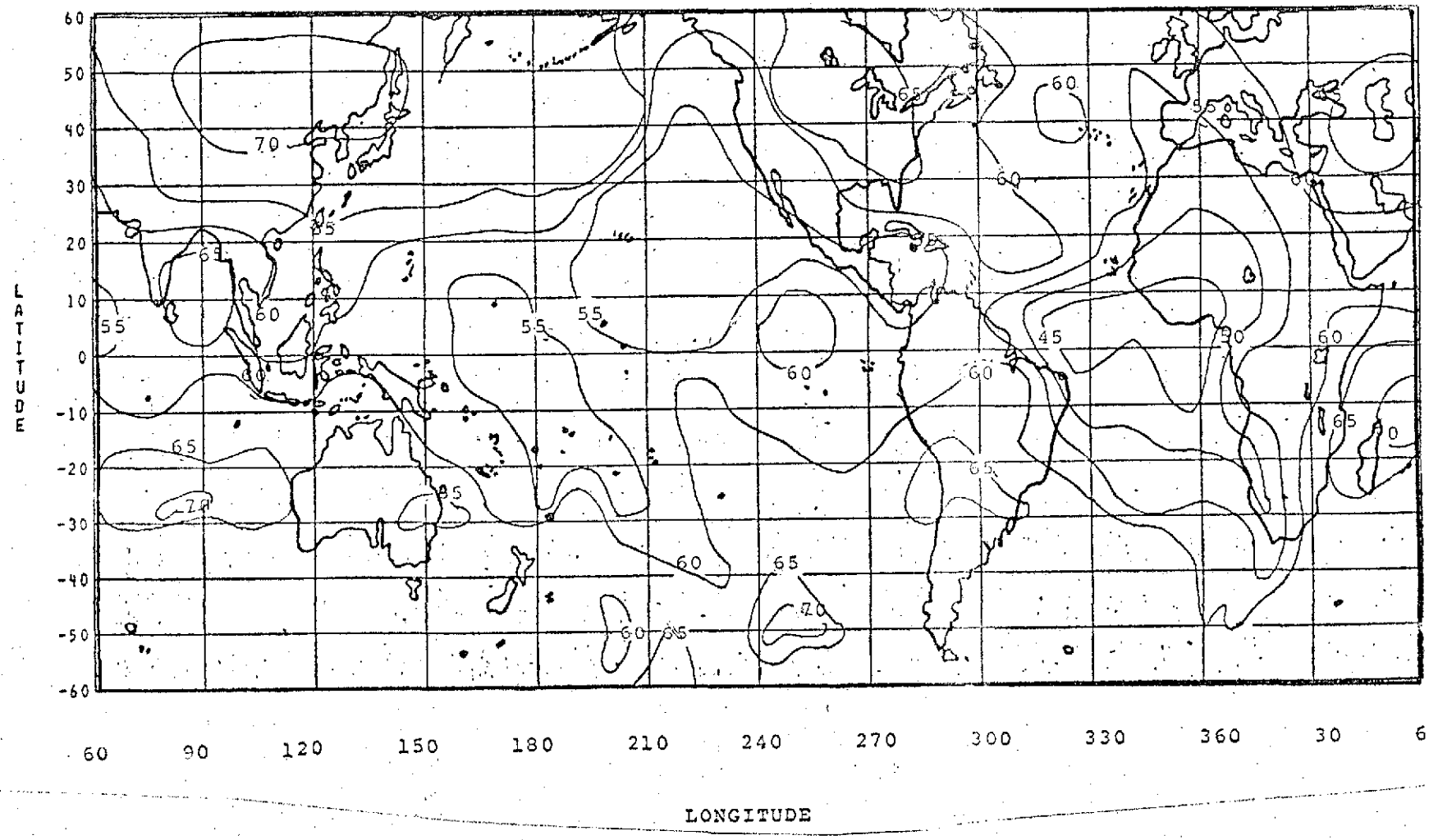


FIGURE 2-8 RAE NOISE CONTOURS FOR SPRING 1970, 9.18MHz (16-24 LT)

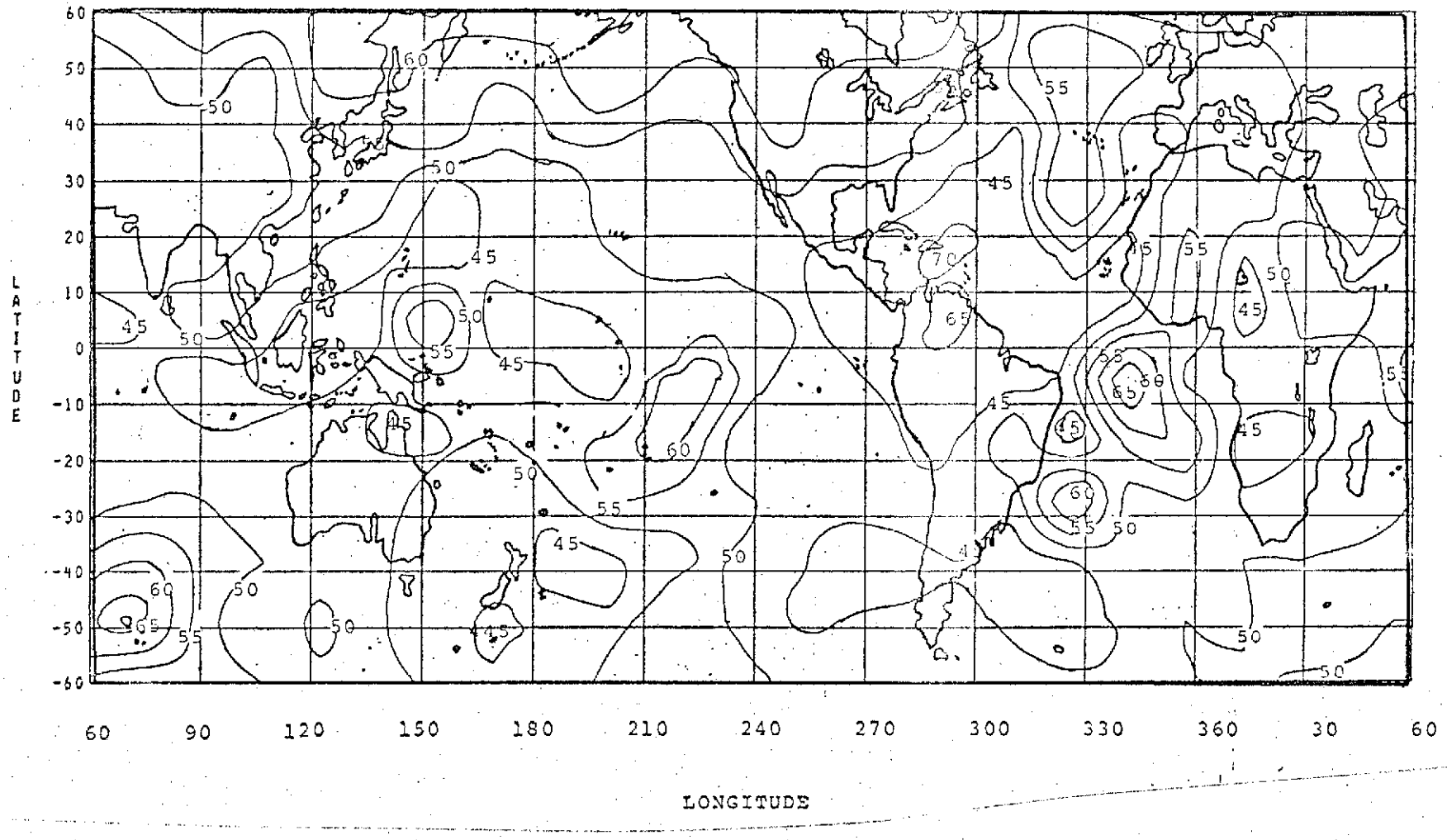


FIGURE 2-9 RAE NOISE CONTOURS FOR SUMMER 1970, 6.55MHz (0-8 LT)

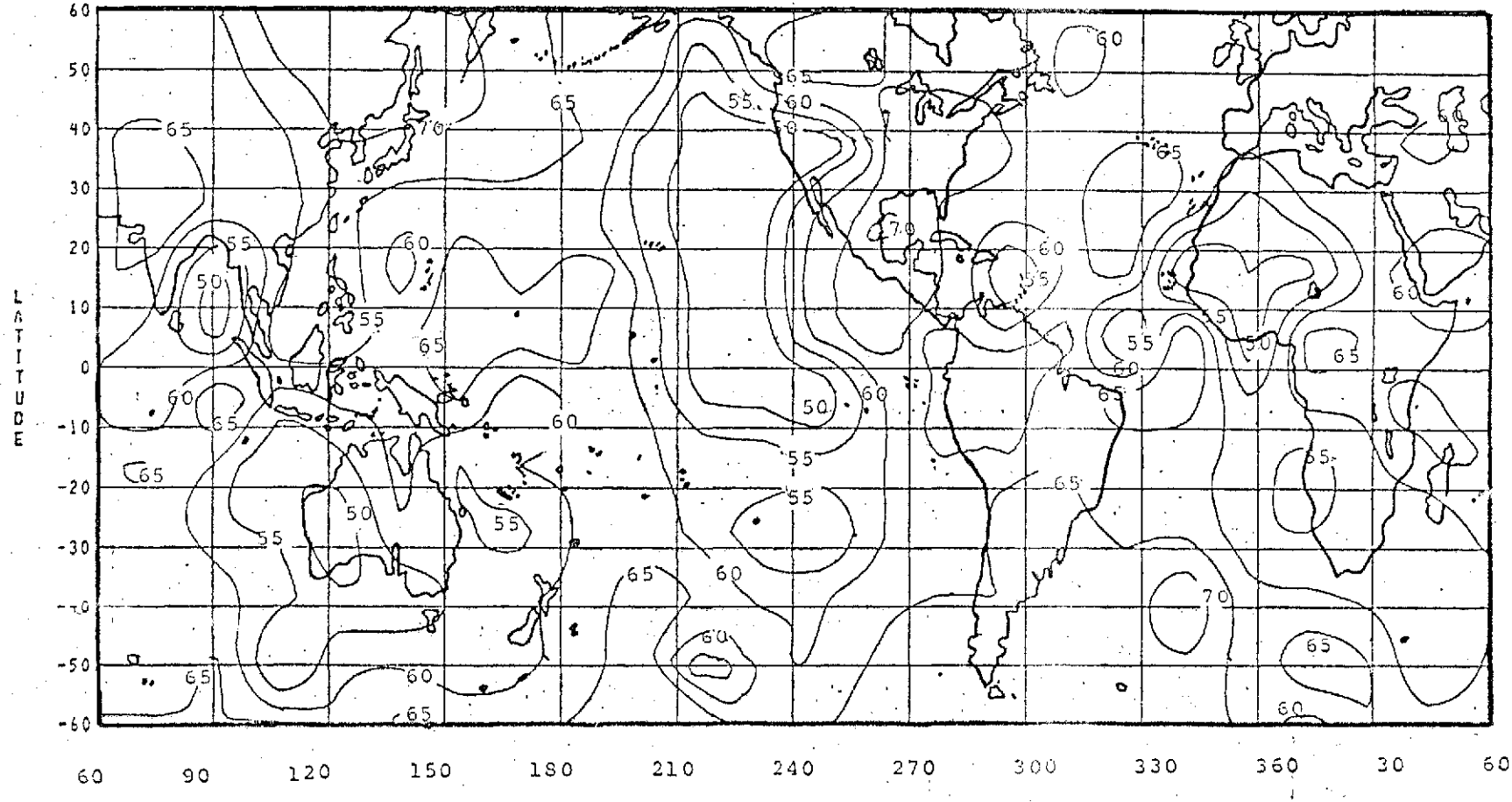


FIGURE 2-10 RAE NOISE CONTOURS FOR SUMMER 1970, 9.18MHz (0-8 LT)

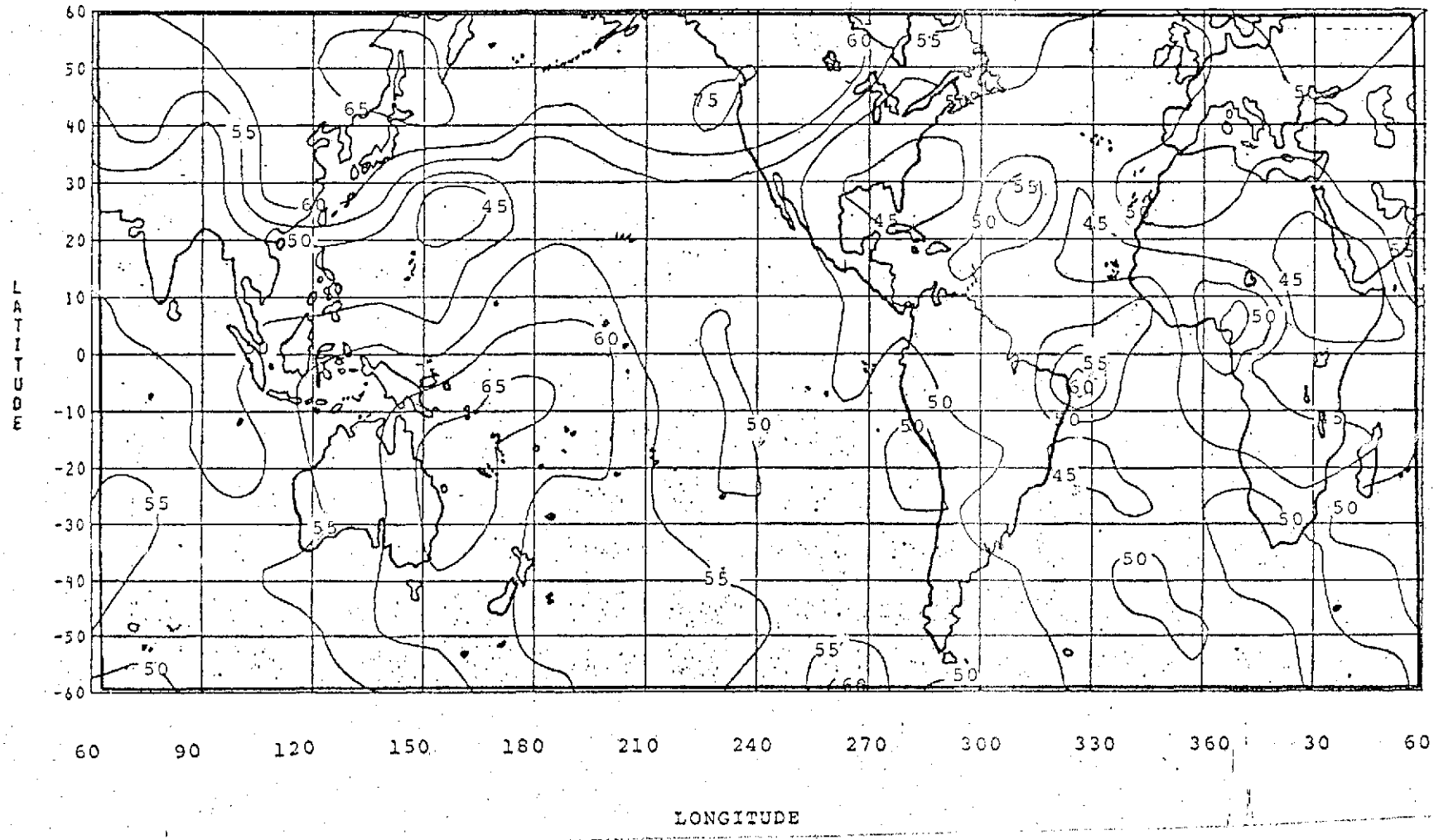


FIGURE 2-11 RAE NOISE CONTOURS FOR SUMMER 1970, 6.55MHz (16-24 LT)

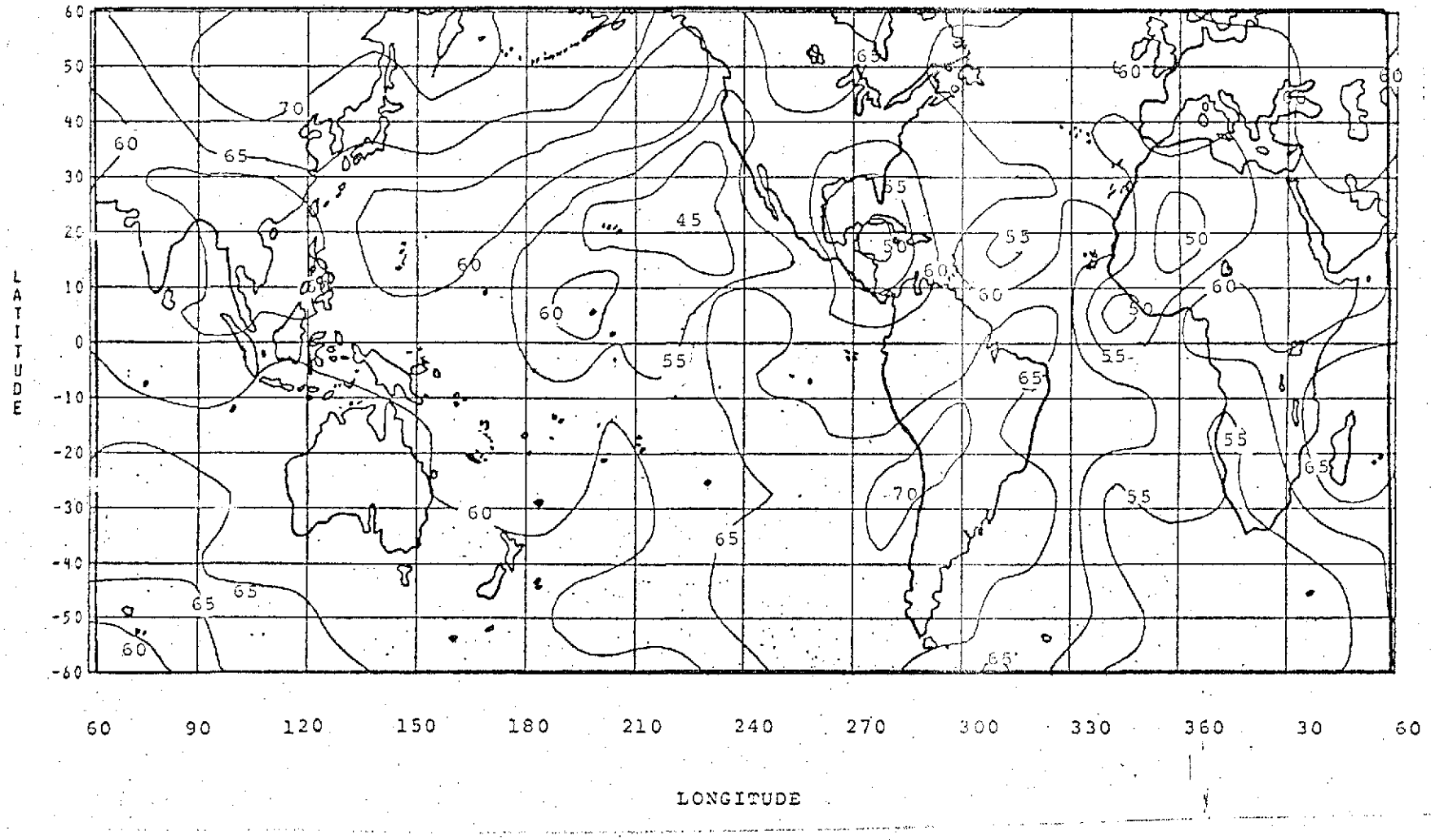


FIGURE 2-12 RAE NOISE CONTOURS FOR SUMMER 1970, 9.18MHz (16-24 LT)

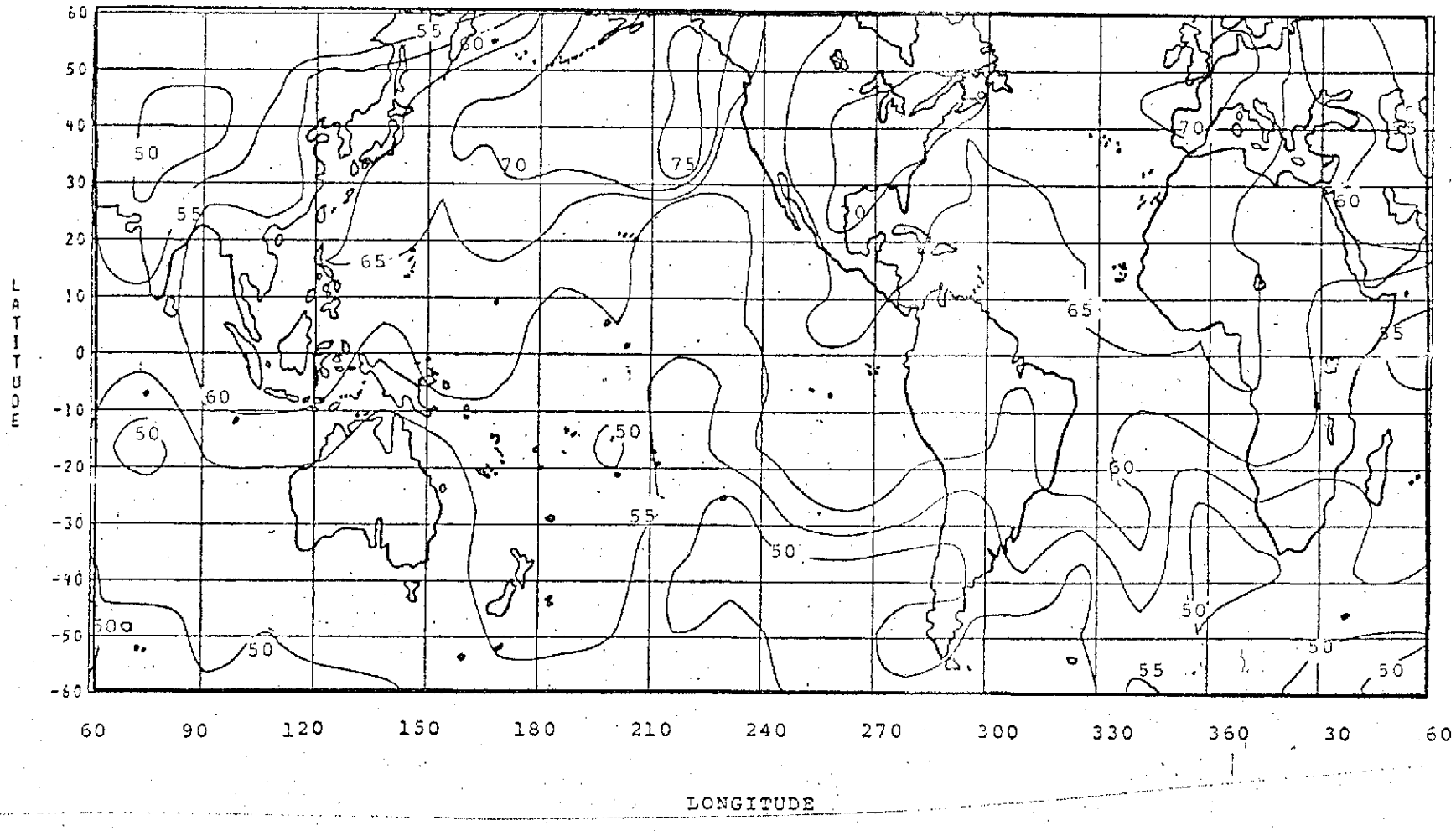


FIGURE 2-13 RAE NOISE CONTOURS FOR FALL 1970, 6.55MHz (0-8 LT)

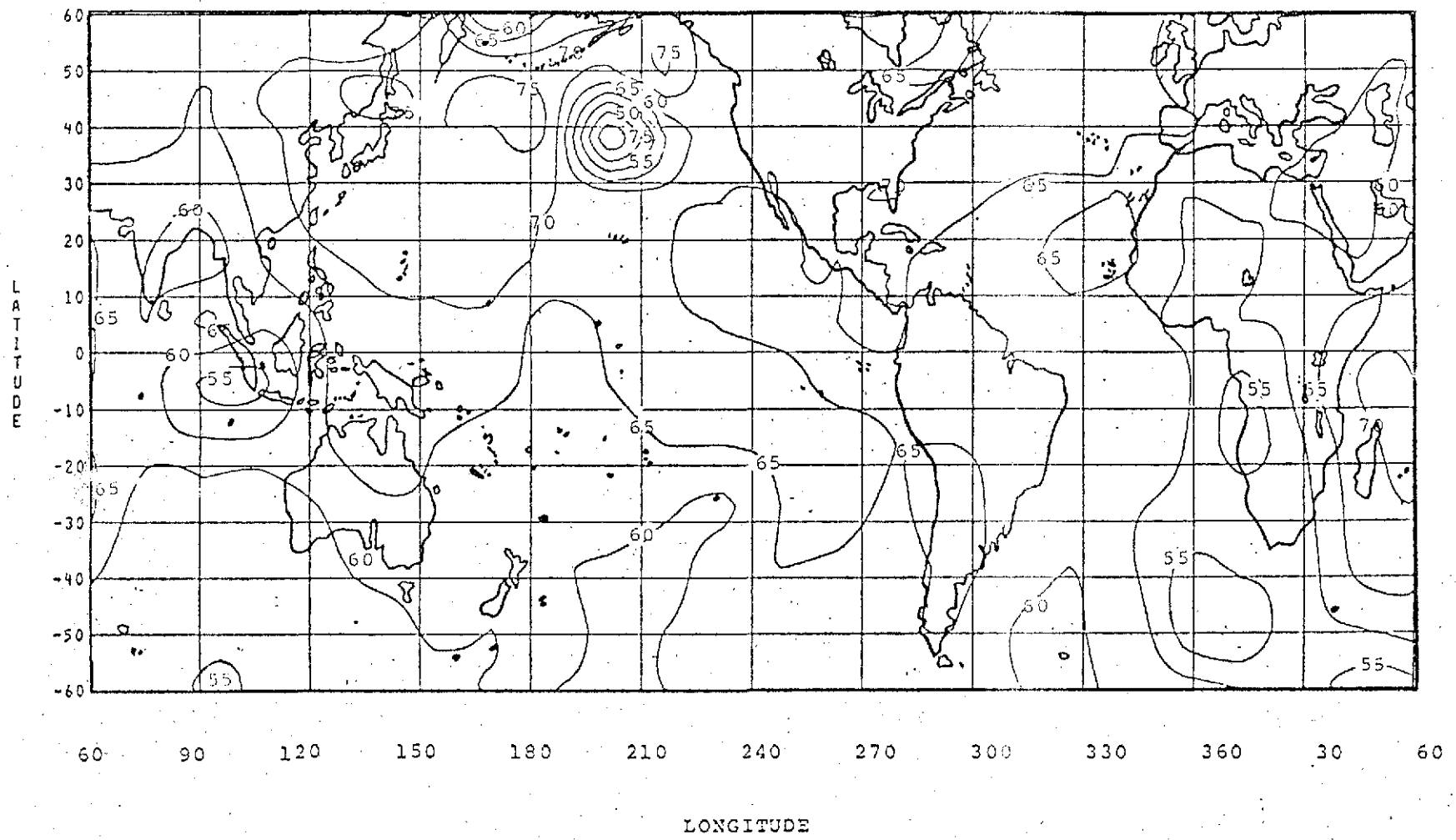


FIGURE 2-14 RAE NOISE CONTOURS FOR FALL 1970, 9.18MHz (0-8 LT)

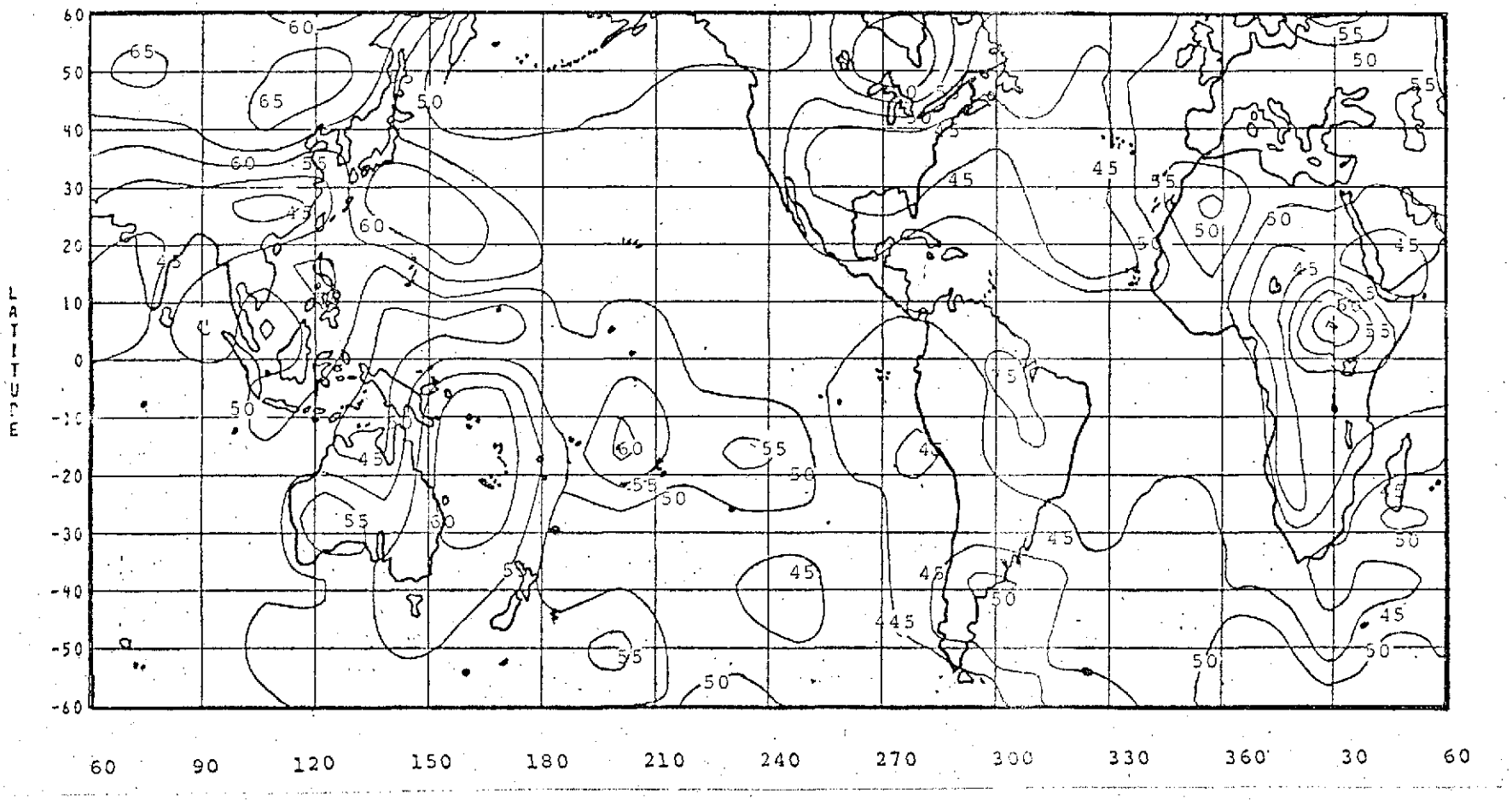


FIGURE 2-15 RAE NOISE CONTOURS FOR FALL 1970, 6.55MHz (16-24 LT)

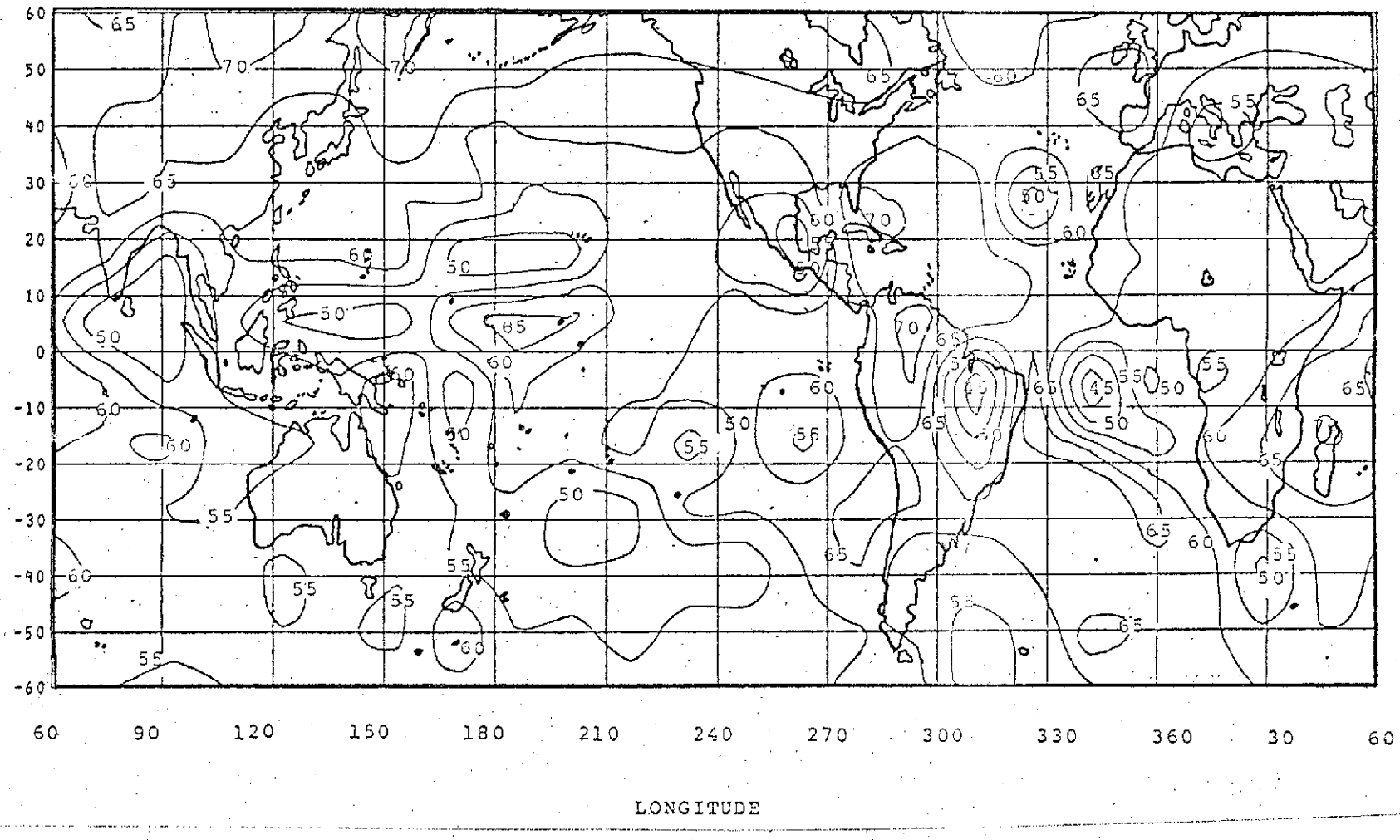


FIGURE 2-16 RAE NOISE CONTOURS FOR FALL 1970, 9.18MHz (16-24 LT)

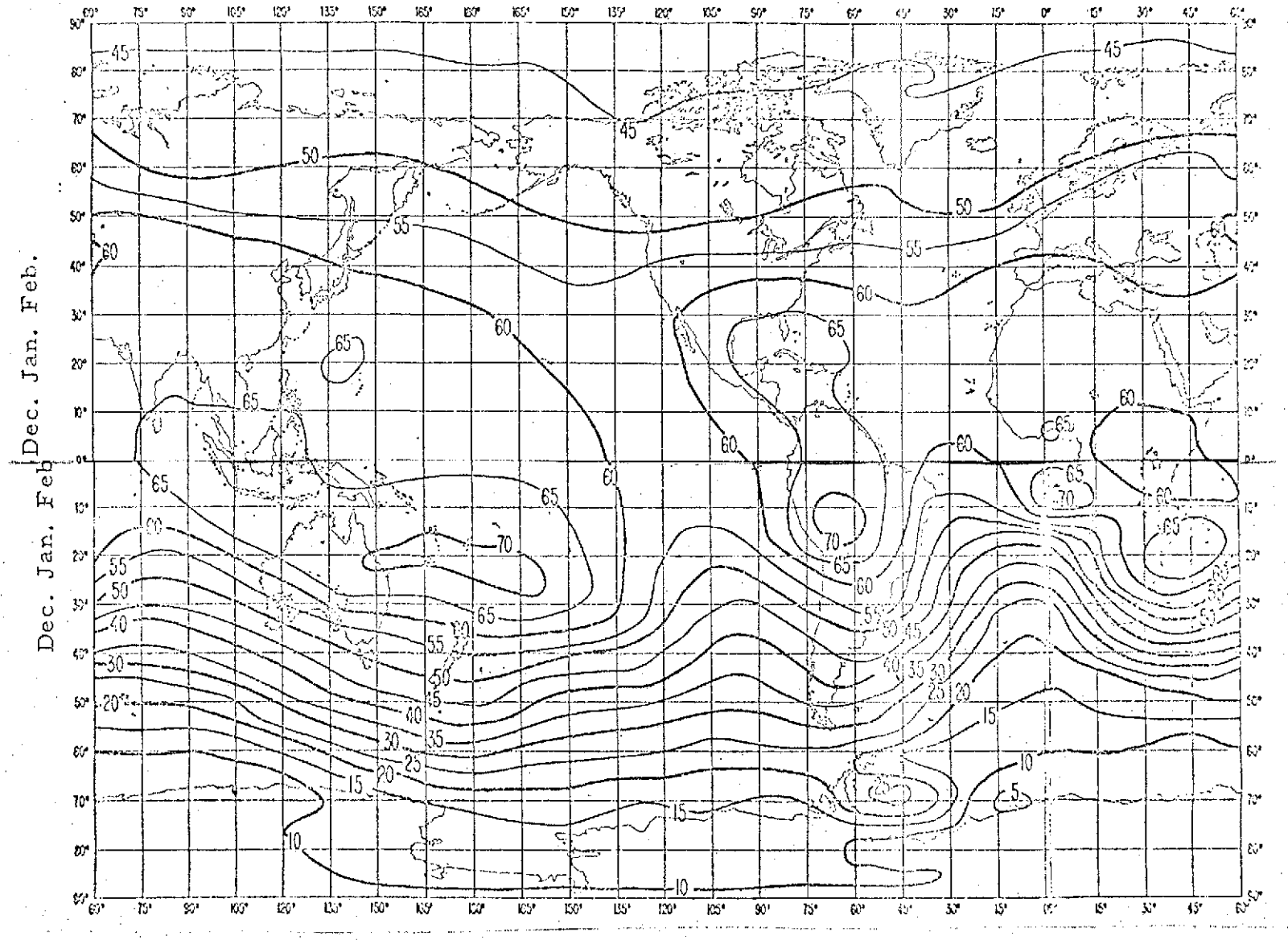


Figure 2-17. Expected Values of Atmospheric Radio Noise, $F_{am}$, in db Above $kT_0b$ at 1 Mc/s for Winter Season, 0400-0800 hrs.

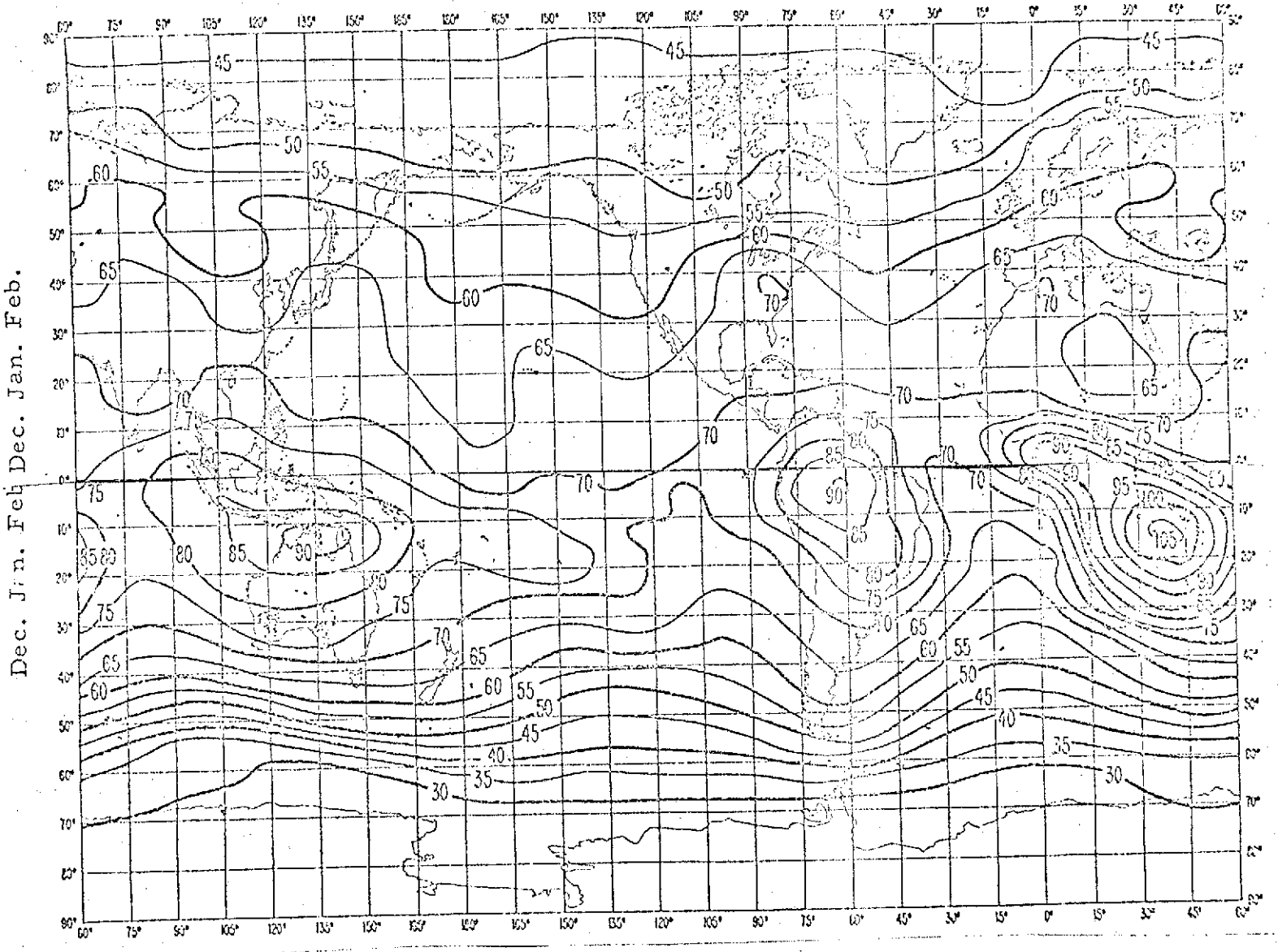


Figure 2-18. Expected Values of Atmospheric Radio Noise, $F_{am}$, in db Above $kT_0b$ at 1 Mc/s for Winter Season, 2000-2400 hrs.

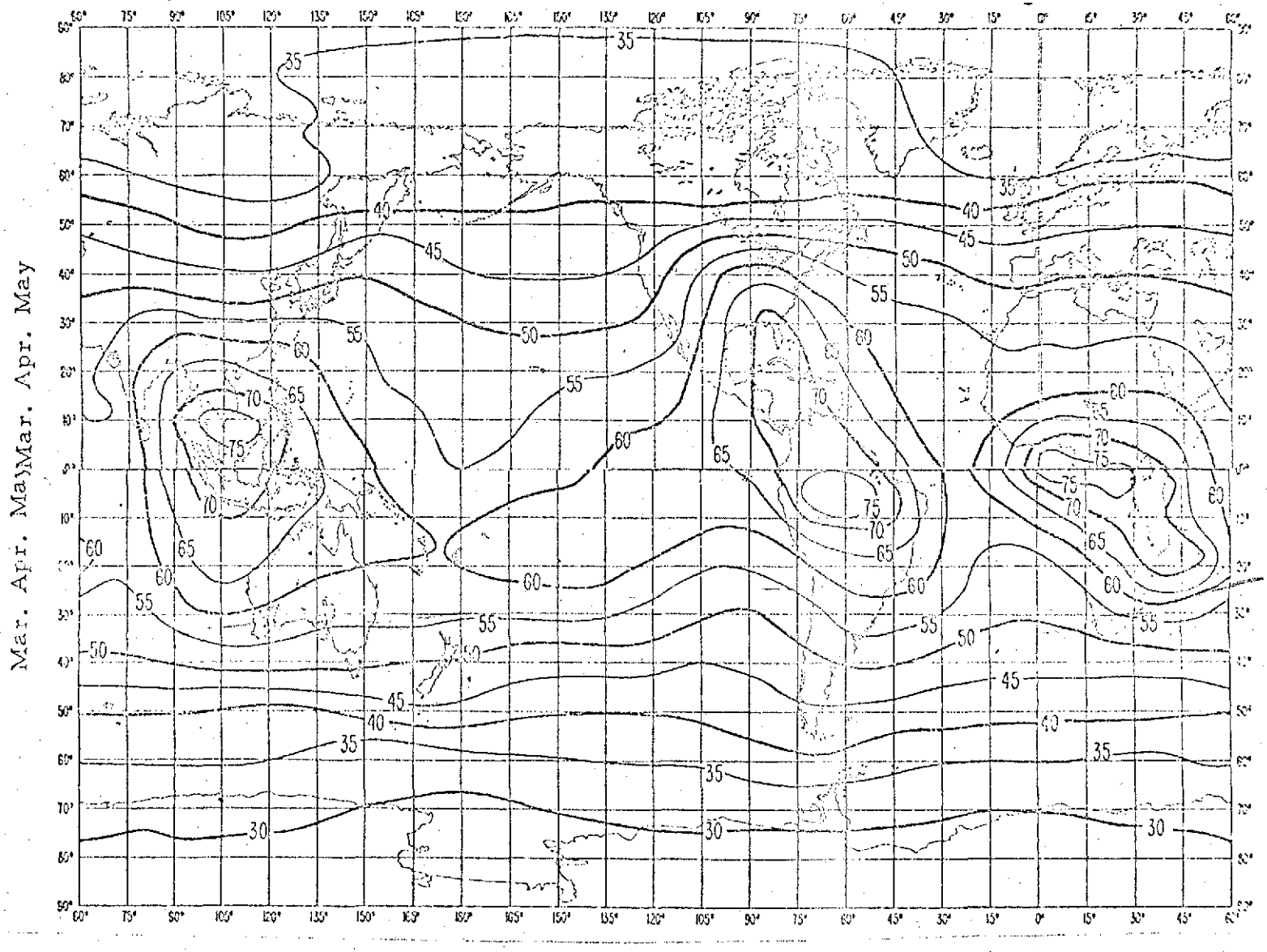


Figure 2-19. Expected Values of Atmospheric Radio Noise, $F_{am}$, in db Above $kT_0b$ at 1 Mc/s for Spring Season, 0400-0800 hrs.

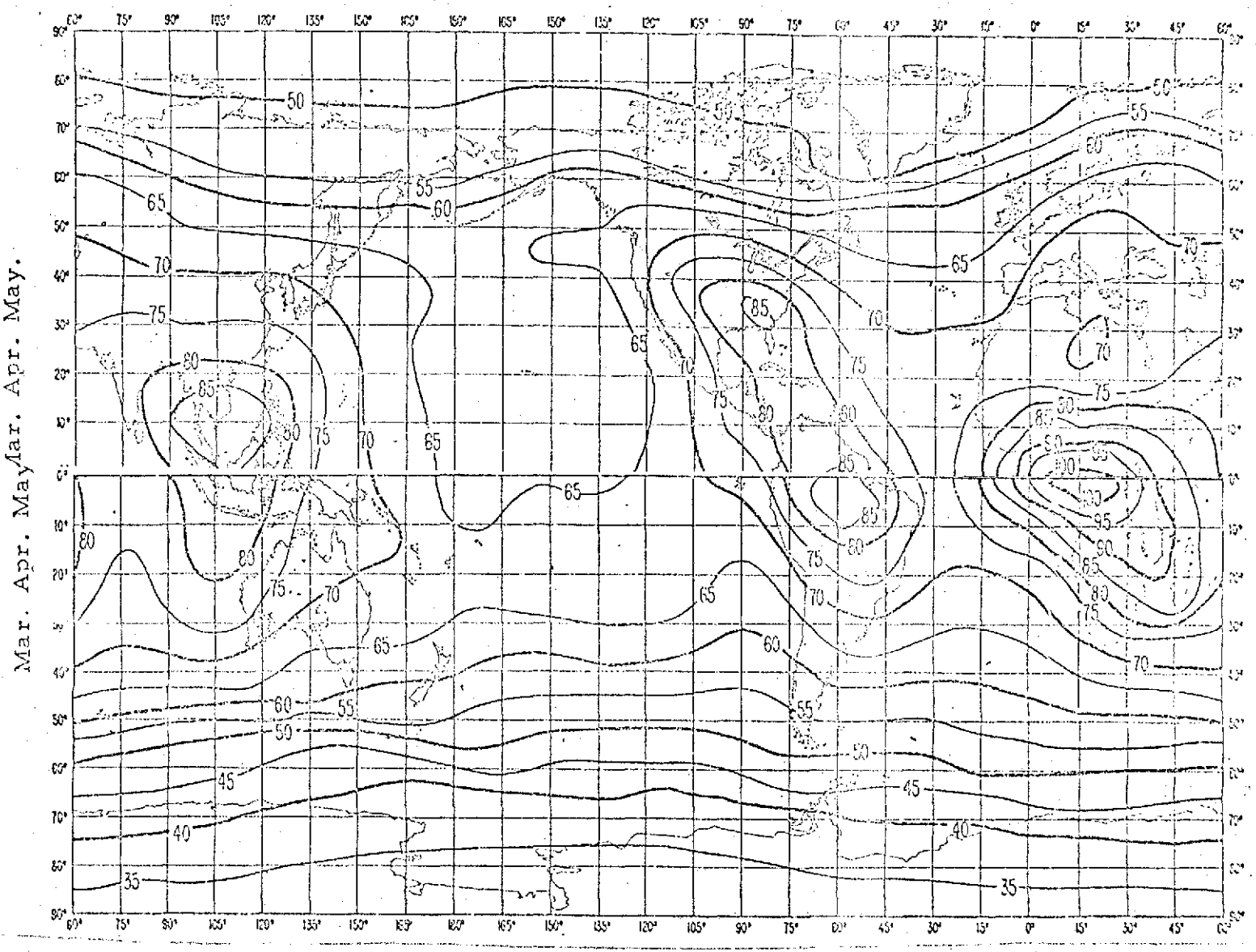


Figure 2-20. Expected Values of Atmospheric Radio Noise, $F_{am}$, in db Above $kT_0b$ at 1 Mc/s for Spring Season, 2000-2400 hrs.

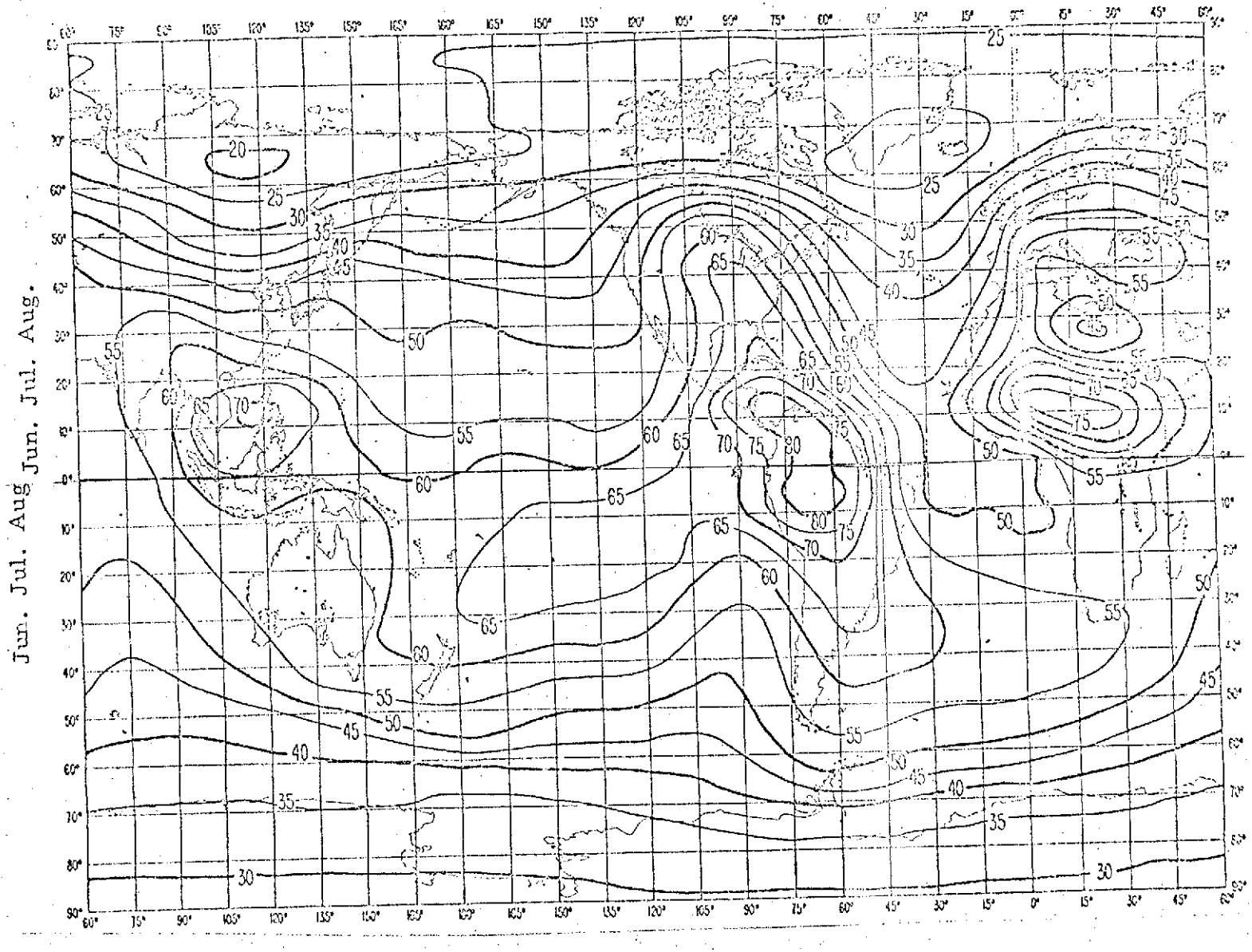


Figure 2-21. Expected Values of Atmospheric Radio Noise, $F_{am}$, in db Above $kT_0b$ at 1 Mc/s for Summer Season 0400-0800 hrs.

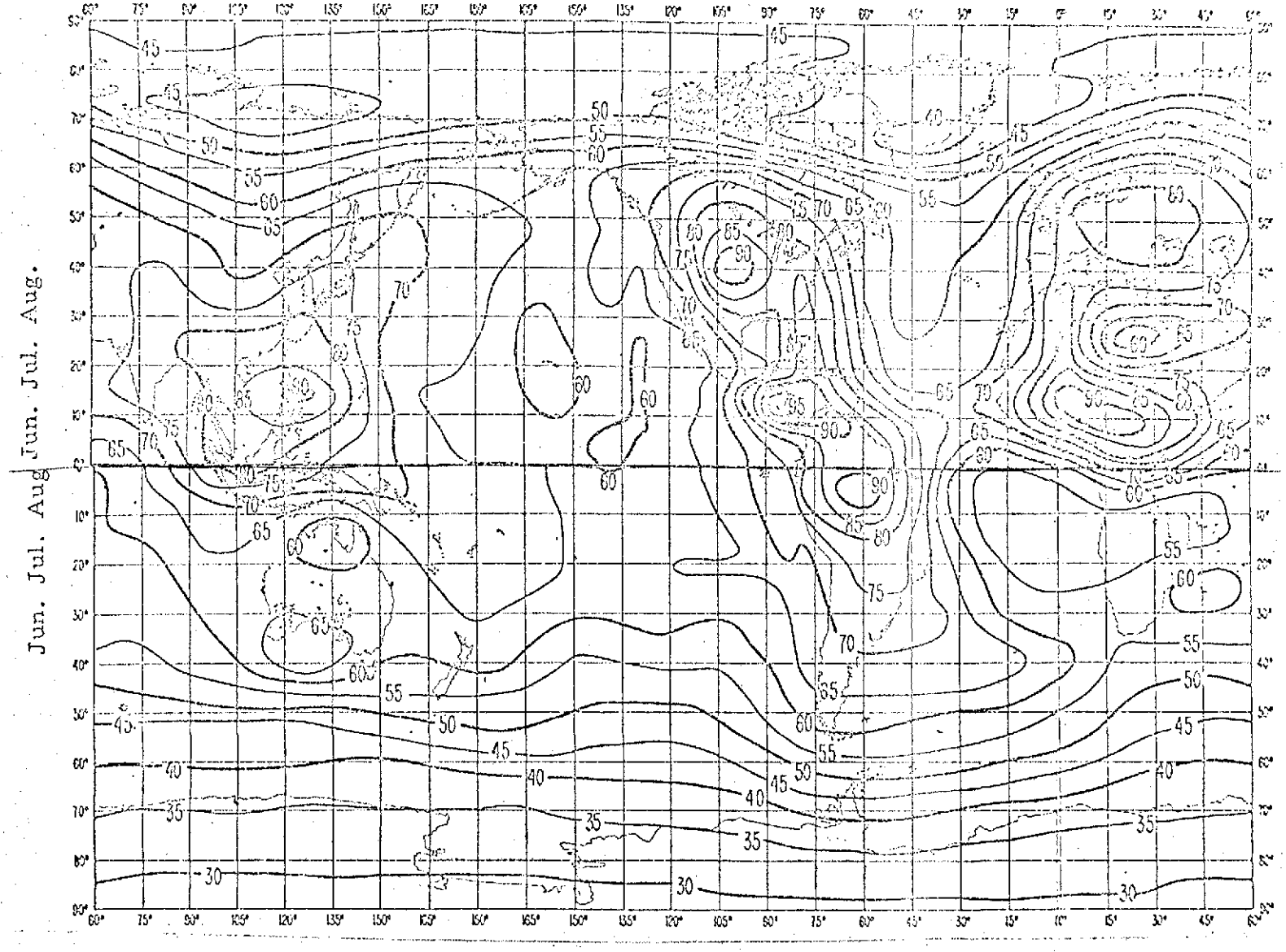


Figure 2-22. Expected Values of Atmospheric Radio Noise, $F_{am}$, in db Above $kT_0b$ at 1 Mc/s for Summer Season, 2000-2400 hrs.

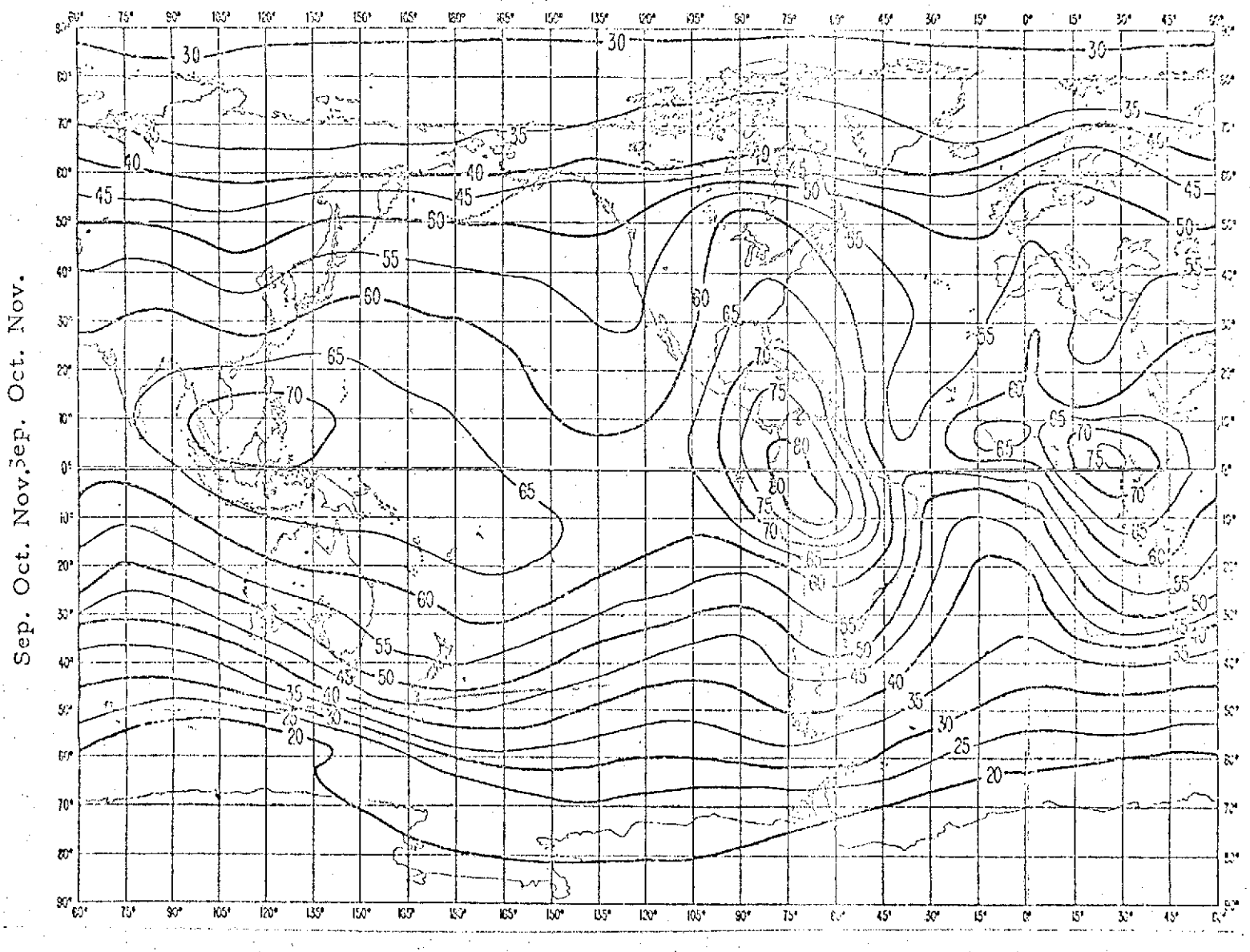


Figure 2-23. Expected Values of Atmospheric Radio Noise, $F_{am}$, in db Above $kT_0b$ at 1 Mc/s for Fall Season, 0400-0800 hrs.

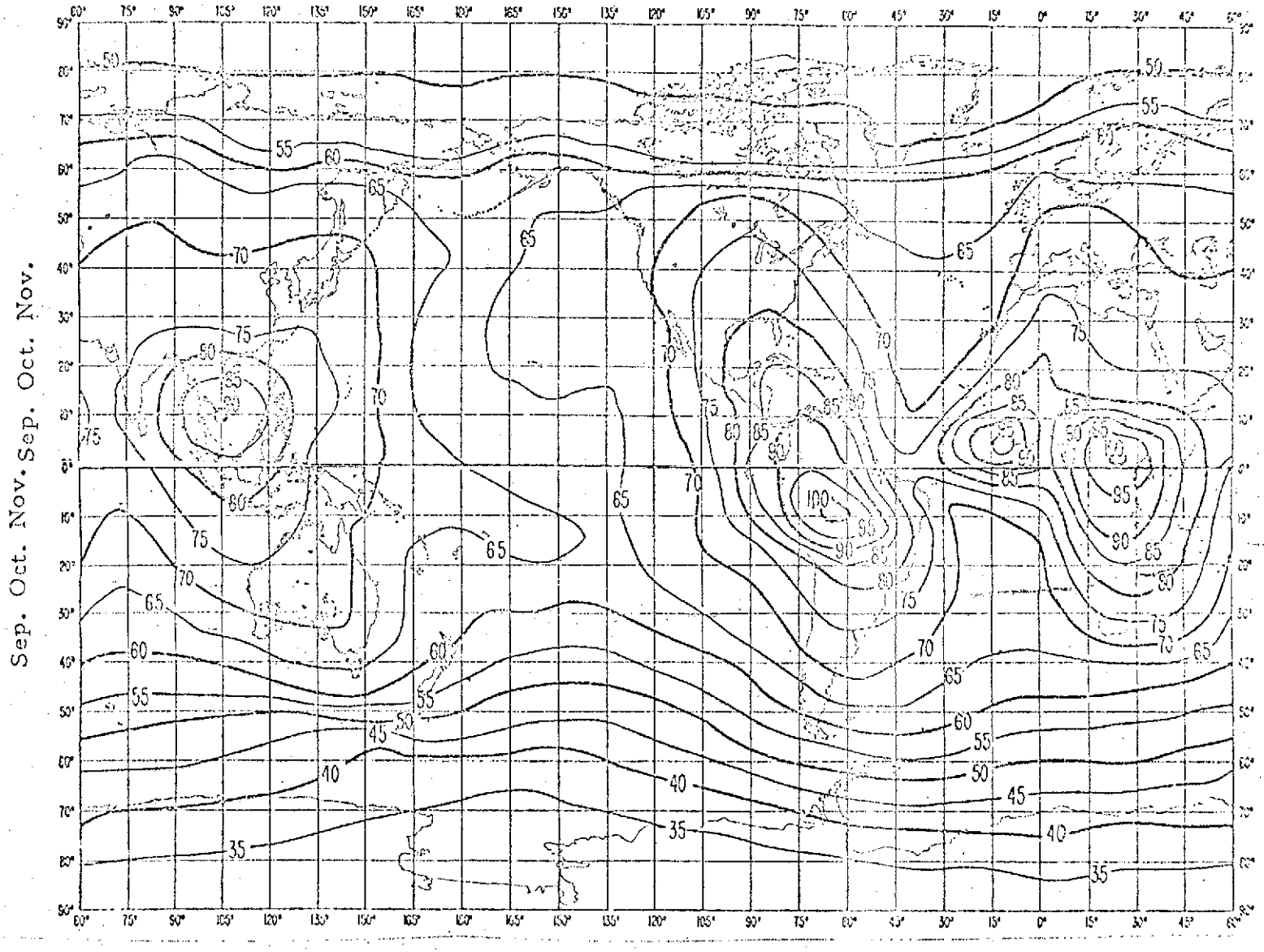


Figure 2-24. Expected Values of Atmospheric Radio Noise, $F_{am}$, in db Above $kT_0b$ at 1 Mc/s for Fall Season 2000-2400 hrs.

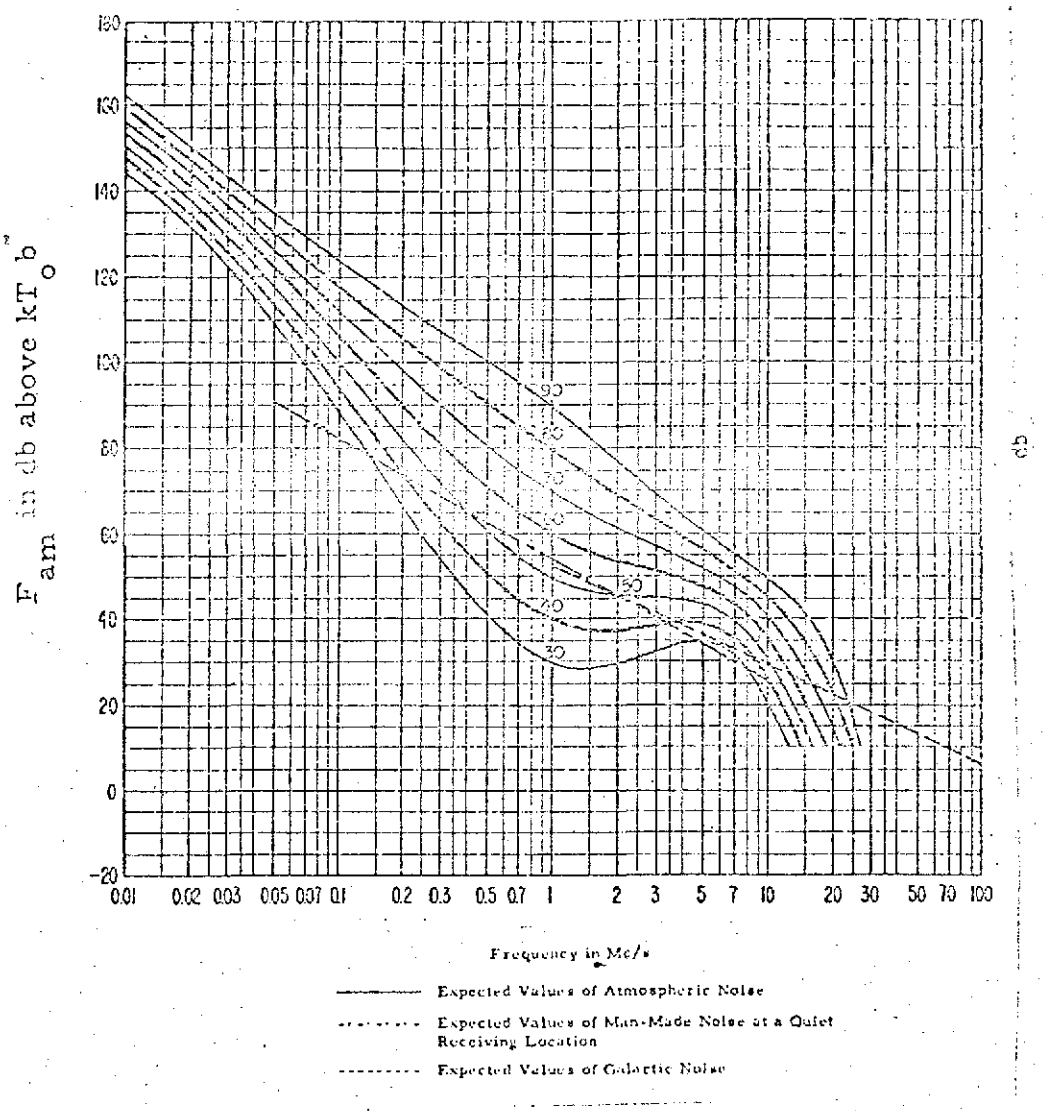


Figure 2-25. Variation of Radio Noise with Frequency Summer Season, 2000-2400 hrs.

# 3.0 SPECIFIC GEOPHYSICAL PHENOMENA

Analyses of the RAE I noise data (Herman, Caruso and Stone, 1973) have shown the importance of the location and strength of terrestrial noise sources upon the noise level in near space. Just as important has been the ionosphere intervening between the terrestrial noise source and the satellite receiver. This was emphasized on data taken as the satellite approached a region of low peak ionospheric electron density or low critical frequency. The terrestrial noise was seen to increase on successively lower frequencies as received by RAE, producing the typical "ground breakthrough" pattern.

Other ionospheric phenomena besides the sunrise/sunset terminator, were chosen to consider their effects on terrestrial noise as seen by RAE. The ionospheric features analyzed were chosen because their spatial location is well established. These phenomena are: the midlatitude trough (Muldrew, 1965); Polar Cap Absorption (PCA) events (Bailey, 1964), and the South Atlantic Magnetic Anomaly (Dessler, 1959). Each of these is a well defined area where there is an obvious variation in either the F-region or D-region electron density compared to the surrounding area. Decreased F-region densities, as in the trough, or increased densities of the magnetic anomaly will be detected through the spatial variation of the ground breakthrough. D-region enhancements caused by a PCA event or perhaps originating in the magnetic anomaly will produce a decrease in signal strength due to the resultant non-deviative absorption in the enhanced D-region. The F-region and D-region effects can result in similar effects upon the RAE data. Thus, it will be the spatial variation of the data that will reveal the location of the geophysical phenomena. However, determining whether

one is seeing an F-region or D-region effect will be difficult if not impossible.

The effects described are tied closely to the Earth's magnetic field and energetic particles, electrons and protons that are guided to ionospheric heights from space by the field. These particles can be emanating sufficient RF energy in the frequency range of the RAE data to be detected. The most obvious location of such an effect will be the auroral oval. Data taken on trajectories through the oval will be examined. Use of both upper and lower Vee antennas will help establish whether any noise detected is coming from the Earth's surface or ionospheric heights or greater. Since the enhancements in the South Atlantic Anomaly are thought to be due to particle precipitation, this will be examined also.

It is convenient to separate the analysis into two parts. The first concerns high latitude effects (the PCA, auroral oval and the mid-latitude trough). These three compose adjacent regions that extend from the pole to the magnetic L shell of L = 3.5. We will examine the RAE data for ionospheric effects and magnetospheric noise sources. The South Atlantic Anomaly will then be examined both for ionospheric enhancement and noise sources. An experiment was also performed to generate an artificial aurora during a time when RAE data was available (Hess, et al. 1971). This will be examined for increased RF emissions due to the artificial aurora that might be detected by RAE.

## 3.1 High Latitude Phenomenology

The polar cap, auroral oval and finally the mid-latitude trough make up an integral ionospheric-magnetospheric region.

These three effects appear to be related, or have a common cause, through the Earth's magnetic field. Whereas their locations above the Earth's surface are related, their time of occurrence is somewhat separated. The PCA occurs often during magnetically calm periods when there is little significant auroral activity in the auroral zone. The mid-latitude trough is consistently present. Each of these will be discussed briefly in the following paragraphs as individual entities. One should remember their spatial relation to each other and their relation through precipitating particles. These effects will first be examined as an ionization anomaly with emphasis on the PCA and trough. Then the aurora will be examined as a source of RF emissions.

### 3.1.1 THE POLAR CAP ABSORPTION EVENT

While there are many ionization sources affecting the polar cap, that which is to be examined here is the enhanced ionization, particularly in the D-region, which is produced by the invasion of solar cosmic rays a few hours after a solar flare.

Occasionally a solar flare will give rise to intense fluxes of energetic protons that precipitate into the upper atmosphere over the polar caps and auroral oval. The protons will also be accompanied by some electrons and heavier nuclei such as $\alpha$-particles. The geomagnetic field determines the minimum energy that a given species must possess in order to reach the Earth at a particular point. This filtering effect results in the lowest-energy particles having access only to the polar caps.

The actual process of ejection of solar cosmic rays is not well understood. Those producing a PCA are ejected

during or shortly after a type IV radio noise burst and associated optical flares. Flares associated with high energy events tend to lie to the west of the central meridian of the sun. Flare locations near the west limb or even beyond appear most favorable.

The ejected particles appear to travel to the Earth by paths which are usually several times larger than the Earth-sun distance. These two facts conform to the Archimedian spiral structure of the interplanetary magnetic field, which magnetically guides the solar particles from the source to the Earth. This field also appears to store the particles. The ejection process is thought to be short but the PCA duration may be measured in days. The Earth's magnetic field is greatly distorted by the solar wind. As a result the modes of particle entry into the polar cap should be different from those anticipated from the Stormer theory for the dipole geomagnetic field.

The development of the PCA is a three-step pattern. The first stage is a slight increase of absorption near the geomagnetic pole. Next, it develops within the latitude of $65^{\circ}$. Finally it extends down to about $60^{\circ}$. The fully developed PCA has circular symmetry in corrected geomagnetic coordinates, giving a definite cut-off latitude. This has been explained by the existence of a ring current whose magnetic moment must be .4 that of the Earth. It also appears that the solar protons have immediate access to the polar caps because the polar cap field lines merge with the interplanetary field. It would be natural to expect the shape of the PCA area to be oval, reflecting the day-night asymmetry of the auroral oval. Synoptic analysis of PCA has shown a symmetric pattern of particle precipitation. There is, of course, a diurnal variation of a PCA due to sunlight which is reflected in some records, such as riometer absorption.

There are anamalous F-region electron densities in the polar cap, specifically troughs and peaks. The troughs exist mainly on the night side and lie along magnetic isolines. A peak of electron density is observed around geomagnetic noon at $78^{\circ}$ invariant latitude. The ionospheric effect of interest here however is the increased D-region electron density that results from the impinging solar protons. The resulting polar-cap absorption, caused by the increased non-deviative absorption in the D-region, can possibly reduce the noise intensity from terrestrial sources when the RAE is over the polar cap.

The methods of calculating the electron density follow the physical process closely and reveal the process of converting high energy protons to an increased electron density. The first step in the process is to determine the energy loss of the protons at each height within the ionosphere and express this as the volume electron-ion pair production rate as a function of height. Early attempts at this required that the energy spectrum of the particle flux be assumed. Normally exponential or power-law spectra were assumed as was the cut-off energy. It was demonstrated that the exponent was relatively unimportant. Most electron production depends upon the protons just above cutoff.

Once the production rate profile is determined, the electron density profile can in most PCA cases be calculated assuming no other source of ionization. The contribution of that part of the profile above 85 km to the absorption is insignificant. It is recognized that the enormous difference in absorption between day and night during the PCA can be explained if negative ions are found by electron attachment at night and photodetachment of electrons by day. Typical night and day profiles during a PCA are shown in Figure 3-1.

(a)

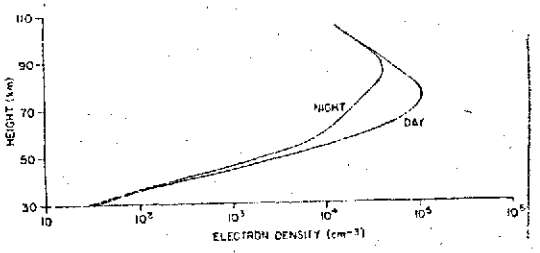


(b)

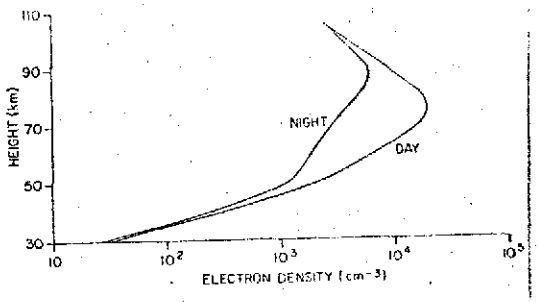


Figure 3-1 Height profiles of electron density during daytime and nighttime steady-state conditions for a low-energy cutoff value of 20 MEV and 40 MEV. (Reid, 1961)

The ability to measure the radiowave absorption that results from the electron density using riometers, and the ability to measure the proton spectra above the ionosphere has led to much work in evaluation of the energy deposition and the various rate coefficients believed to be involved. The riometer, which measures the absorption of galactic noise as seen from the Earth, reveals the effect one expects to see of the absorption of terrestrial noise as viewed from space. Most riometers are operated at the same frequency, 30 MHz, to allow comparison between observations. Data taken at Thule, Greenland for two PCAs is shown in Figure 3-2. In the first illustration a diurnal variation can be seen, of up to an order of magnitude variation of the dB absorption from day to night.

## RAE DETECTION OF PCAs

The absorption as a function of frequency has been found to vary as

$$A(dB)=C(f-f_L)^{-n} \qquad (3-1)$$

where f is the receiving frequency, $f_L$ is the longitudinal component of the electron gyrofrequency. The constant, C, varies with the intensity of the event and the exponent n varies from 1.1 to 1.9 depending upon the proton spectra. Using this relation we can convert the reported riometer absorption at 30 MHz to the RAE frequencies. This will indicate the amount of absorption to be expected when the satellite passes above the polar cap. At the highest frequency, 9.18 MHz, the absorption in dB will be from 3 to 10 times that at 30 MHz. At 2.2 MHz it would increase to at least 14 to 43 times that at 30 MHz. This increase in absorption at low frequencies combined with measured 30 MHz absorption of 10 to 16 dB during some events makes one optimistic that seeing the effects of a

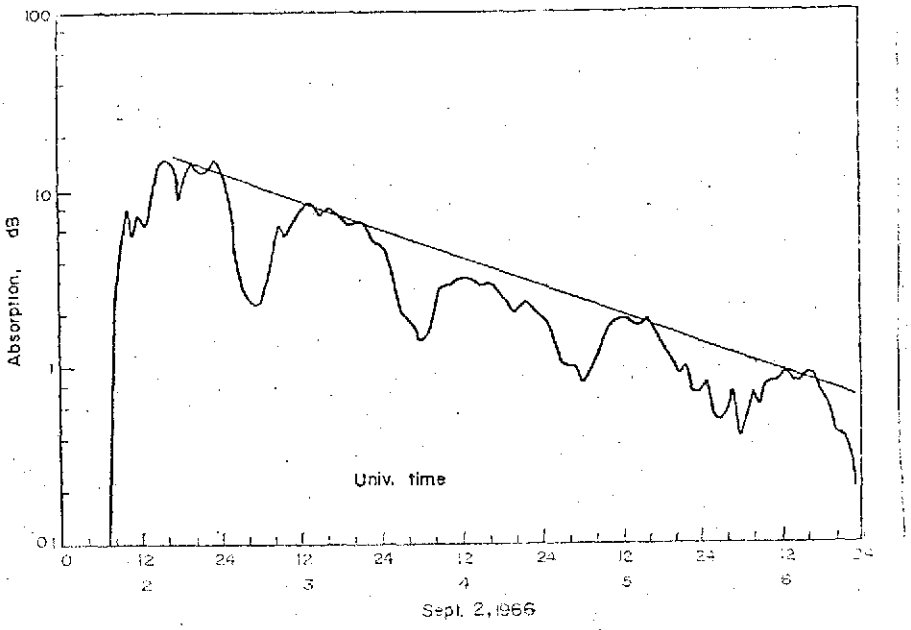


Figure 3-2(a) Plot of dB absorption vs. time for the PCA event of 2 September, 1966, as observed at Thule Greenland, on the 30MHz riometer. The nighttime recovery in absorption is immediately noticeable (from R. Cormier, private communication).

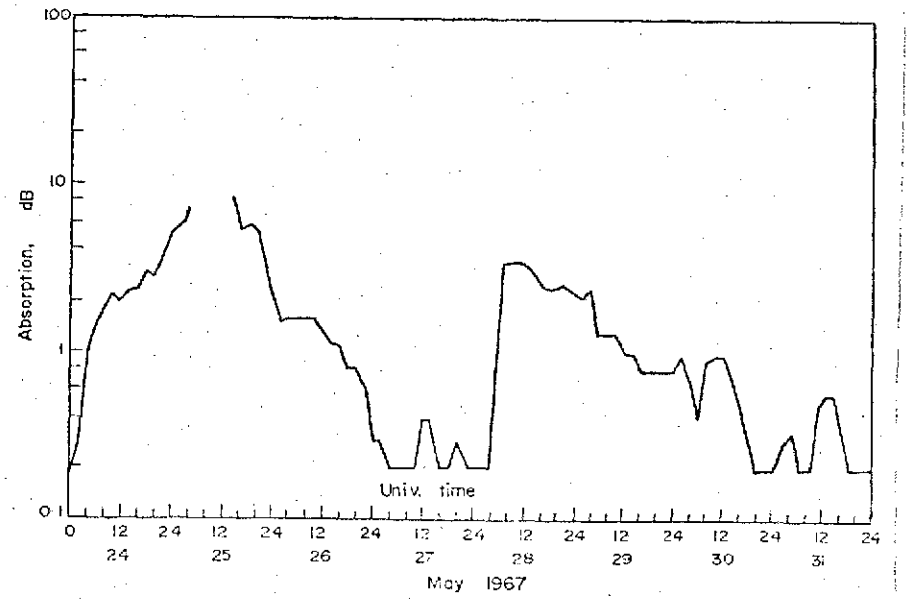


Figure 3-2(b) Plct of dB absorption vs. time for the PCA events of 24 May and 28 May 1967 as observed at Thule, Greenland, on the 30MHz riometer. There is no nighttime recovery since at this season the sun does not set in this region (from R. Cormier, private communication). (Silverman, 1970)

PCA on the RAE data is a sure thing. Such is not the case and analysis of the data will have problems. First, since the orbital inclination is 121° the satellite only reaches geographic latitudes of 59°. Therefore interception of the polar cap will be most likely on those orbits over the eastern United States and Canada, in particular when the orbital plane is such that the northern most point of the trajectory crosses the longitude of the Earth's corrected geomagnetic pole at about 81°W geographic. On this optimum trajectory through the polar cap the northern most geomagnetic latitude will be 73°, well within the PCA lower latitude limit of 60°. On the opposite side the satellite would only reach 45° geomagnetic latitude and be outside even the auroral zone.

It has already been noted with respect to the maps of terrestrial radio noise created from the RAE data that noise sources are not expected at high latitude. In the winter, few, if any, thunderstorms are expected to occur at latitudes (geographic) higher than 30°. Further, the large maximum over the whole of Europe and Asia are far removed from the Polar Cap due to the eccentricity of the magnetic dipole. Thus it seems that any noise leaving the Earth at polar cap latitudes will have first propagated from other sources before escaping, perhaps through one of the polar troughs. These sources could have been many thousands of kilometers from the satellite nadir and any D-region penetration occurred far removed from the PCA effected D-region. We must guard our optimism before searching for PCA effects on the RAE noise data.

## 3.1.2 MIDLATITUDE TROUGH

The introduction of ion trap experiments aboard Sputnik 3 allowed the direct measurement of electron density at ionospheric heights rather than indirect measurement by ground based radio techniques. A variety of experiments since have shown the ionosphere not to be describable by sweeping generalities. It is not a smoothly varying medium. Most of the irregularities however have been shown to be aligned with the geomagnetic field. One of these irregularities has become known as the Midlatitude Trough (Muldrew, 1965; Sharp, 1966).

The midlatitude trough as shown in Figure 3-3 reveals itself on satellite measurements of ion concentration as sharp decreases in ion density of an order of magnitude. This decrease occurs both above and below the F-region peak (Figure 3-4) and can be assumed as a reduction in the electron density of the whole F-region as well as a reduction of the critical frequency. The trough is found surrounding both the north and south magnetic poles. It is most evident at night since solar radiation can tend to "fill" the trough. The poleward side of the trough normally has a much greater gradient, often being an abrupt step-like increase in electron density as in Figure 3-3. The trough is not located in the auroral zone but borders the equatorial side of the auroral zone and will be affected by auroral activity. The trough becomes very narrow during periods of high magnetic index and auroral zone particle flux increases. This is mostly due to the poleward wall, which is the auroral zone, moving equatorward. The equatoral wall of the trough remains in a somewhat stationary location as seen in Figure 3-5.

The cause of this trough is not clear. One theory is that the trough is the ionosphere that would exist if solar

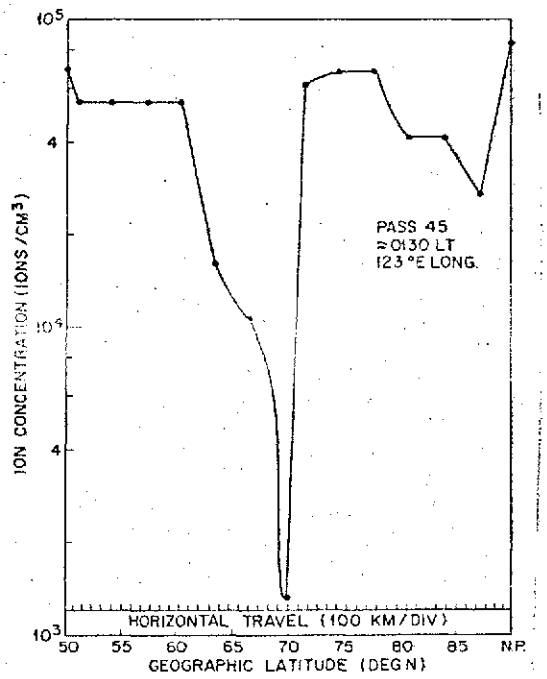


Figure 3-3 A midlatitude trough (Sharp, 1966)

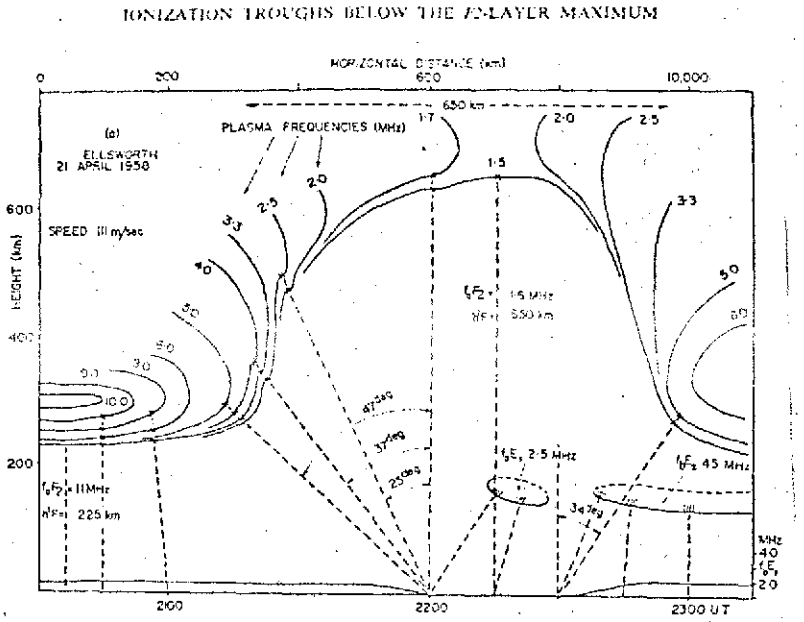


Figure 3-4 Distribution of Ionization for Bottonside Trough on 21 April 1958. (Bowman, 1969)

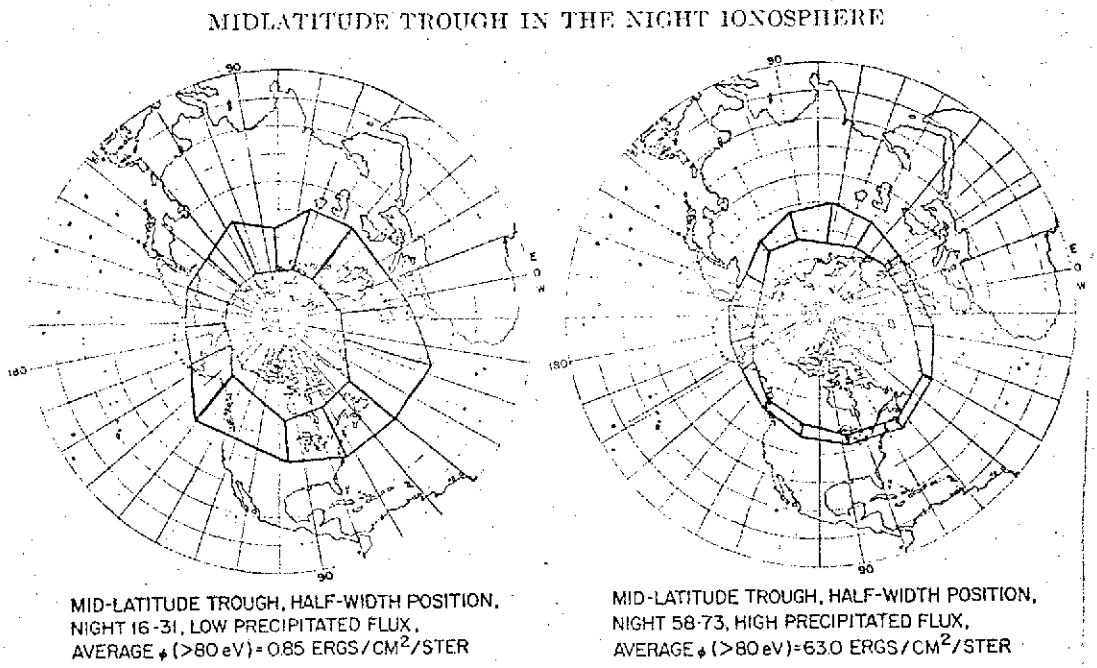


Figure 3-5 Polar-plot comparison of trough half-width and flux precipitated in the auroral zone. (Sharp, 1966)

radiation were the only energy source. The increased density on either side of the trough then would be caused by corpuscular radiation. Since the location of the trough at L=3.5 is the same as Carpenter's "Whistler Knee", it has been suggested that the knee mechanism is responsible for the equatorial side of the trough and the particle precipitation in the polar auroral zone for the poleward side.

It has also been suggested that the trough is due to an ionization sink at the magnetic latitude of the trough. Electric fields in the auroral and airglow phenomena would cause heating of the ionosphere. Therefore an expansion and a reduction of electron concentration would take place. Much work is yet to be done to substantiate either of these explanations or others.

## TROUGH DETECTION WITH RAE

The trough is seen to vary from $10^{\circ}$ to $20^{\circ}$ in width, described as the difference in latitude between the half-depth points. This is approximately the maximum resolution possible with the RAE antennas as depicted in Figure 3-6. At the highest frequency, 9.18 MHz, the travelingwave antenna has a beamwidth of $13^{\circ}X27^{\circ}$. Thus, if the satellite trajectory crosses normal to the trough and the sharpest antenna pattern is aligned with the trough it may be possible to see an increase in noise, reflecting the decreased electron density. In other words, one might expect a sharp increase in ground breakthrough as the satellite crosses the trough.

However, bear in mind that the one explanation of the trough involved particle precipitation on either side of the trough. This could cause increased noise due to synchrotron radiation prior to and after the trough, masking its presence.

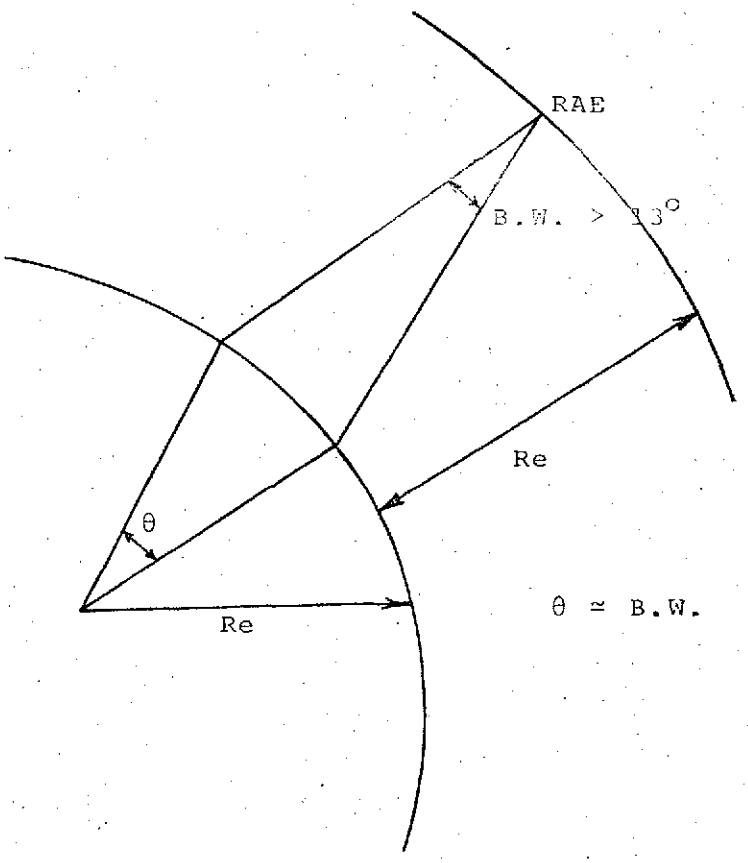


Figure 3-6. RAE Spatial Resolution

## 3.2 RAE 1 Noise Measurements

It has become apparent in recent years that several ionospheric phenomena affecting HF radiowave propagation are intimately related to energetic charged particle precipitation from the magnetosphere as discussed in Section 3.1. In addition to producing ionospheric absorption which can affect radio noise propagating from the ground to RAE altitudes, these particles may produce RF emissions in the RAE band of frequencies as discussed in Section 3.3.

Energetic particle precipitation takes place principally at geomagnetic latitudes greater than about $\pm$ 60°, although intense events associated with and following solar eruptions may spread equatorward as low as 50° geomagnetic latitude. Phenomenological patterns of particle precipitation exhibit diurnal and geographical variations which are similar to those of auroral ionospheric phenomena. Hence, we would expect the region affecting transionospheric propagation of terrestrial noise to RAE altitudes to be in approximately the same location as the region of auroral RF emissions.

In the north-west quadrant of the globe centered at about 81°W longitude, a given geomagnetic latitude is up to 11° higher than the corresponding geographic latitude. This means that over the U.S. and Canada auroral events can extend as low as 39°N geographic latitude. On the opposite side of the world (south-east quandrant) over Australia the same situation prevails, i.e., -50° geomagnetic latitude corresponds to -39° geographic latitude.

Considering the orbital characteristics of RAE 1, it is evident that the satellite spends about 100 minutes of each orbital period, or 45% of its time, over geographic latitudes

between 40 and 60° in the northern and southern hemisphere. Due to the displacement between geomagnetic and geographic coordinates, RAE spends nearly 25% of its time over auroral latitudes; so a significant portion of the RAE data can be utilized to investigate the effects of polar cap absorption (PCA) events, auroral substorms and the main ionospheric trough on the RF environment at satellite heights.

On the one hand we can expect that ionospheric absorption associated with PCA events and auroral substorms will depress the noise contribution to RAE from sources below the ionosphere, while the low critical frequency found in the main trough would allow noise on lower frequencies than usual to penetrate through the ionospheric shield and reach RAE. On the other hand, we can expect that noise emissions generated by the precipitating particles associated with auroral substorms might enhance the noise level at RAE heights. The relative importance of these several competing factors has been examined.

Before presenting the analysis of noise measurement data taken by RAE 1, we will give a brief description of the characteristics of the satellite, the Vee antennas and the Ryle-Vonberg receivers. A more detailed discussion is given by Weber, Alexander and Stone (1971) and Novaco (1973).

## 3.2.1 SYSTEM CHARACTERISTICS

### THE RAE 1 SATELLITE

The system configuration, shown in Figure 3-7, consists of two 229 meter travelling wave Vee antennas (one directed towards the earth, the other towards the local zenith), a 37 meter dipole bisecting the axis of the Vee antennas, and a 192 meter libration damper. The latter was installed to damp out oscillations about the satellite's axes. The Vee antennas operate at 9 frequencies (0.45, 0.70, 0.90, 1.31, 2.20, 3.93, 4.70, 6.55, and 9.18 MHz). Each frequency is sampled every 72 seconds. The orbit, inclination and precession rate of the satellite were chosen to provide the largest amount of sky coverage in the shortest amount of time. The satellite was placed in a retrograde circular orbit at an altitude of 6,000 km with an inclination of $59^{\circ}$. The precession rate for this orbit is 0.52 degrees per day. It took nearly two years to completely map the sky between the declination limits of $\pm 60^{\circ}$.

### THE VEE AND DIPOLE ANTENNAS

A travelling wave antenna was made by inserting a 600-ohm resistor and odd fraction of a wavelength from the tips of each of the legs of the Vee antennas. This allowed most of the energy to be placed in the front lobes since a travelling wave antenna suppresses the back lobes.

The beam patterns for a travelling wave Vee antenna are shown in Figure 3-8 for 1.31, 3.93 and 6.55 MHz. At 3.93 MHz the beam pattern is an ellipse $23^{\circ}$ X $52^{\circ}$; at 6.55 MHz, the ellipse has narrowed to $14^{\circ}$ X $34^{\circ}$.

Because the electrical characteristics of a simple dipole are understood much better than the travelling wave Vee antenna, data from the RAE dipole have provided the basis for absolute

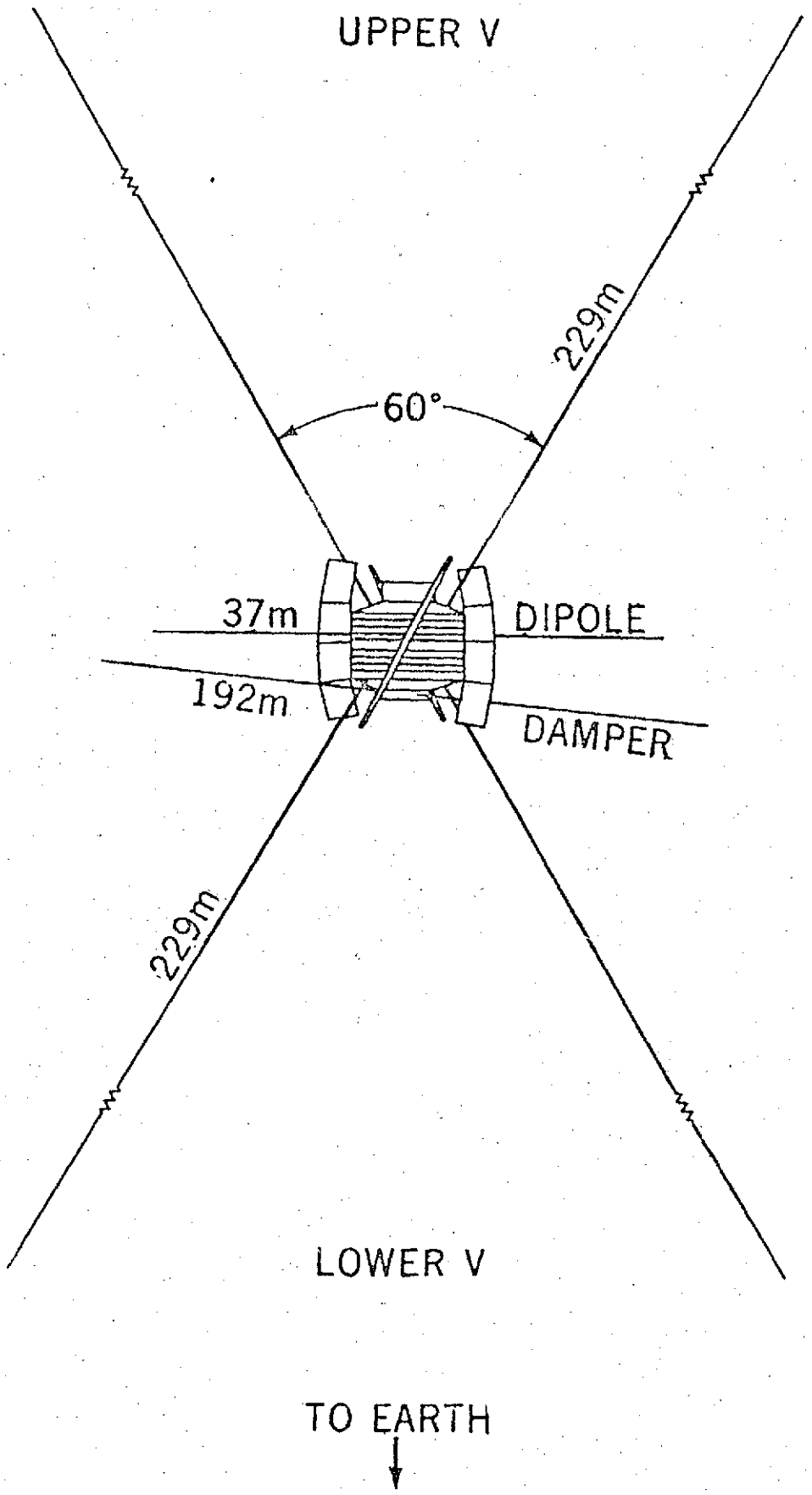


FIGURE 3-7 RAE I CONFIGURATION (WEBER, ALEXANDER & STONE, 1971)

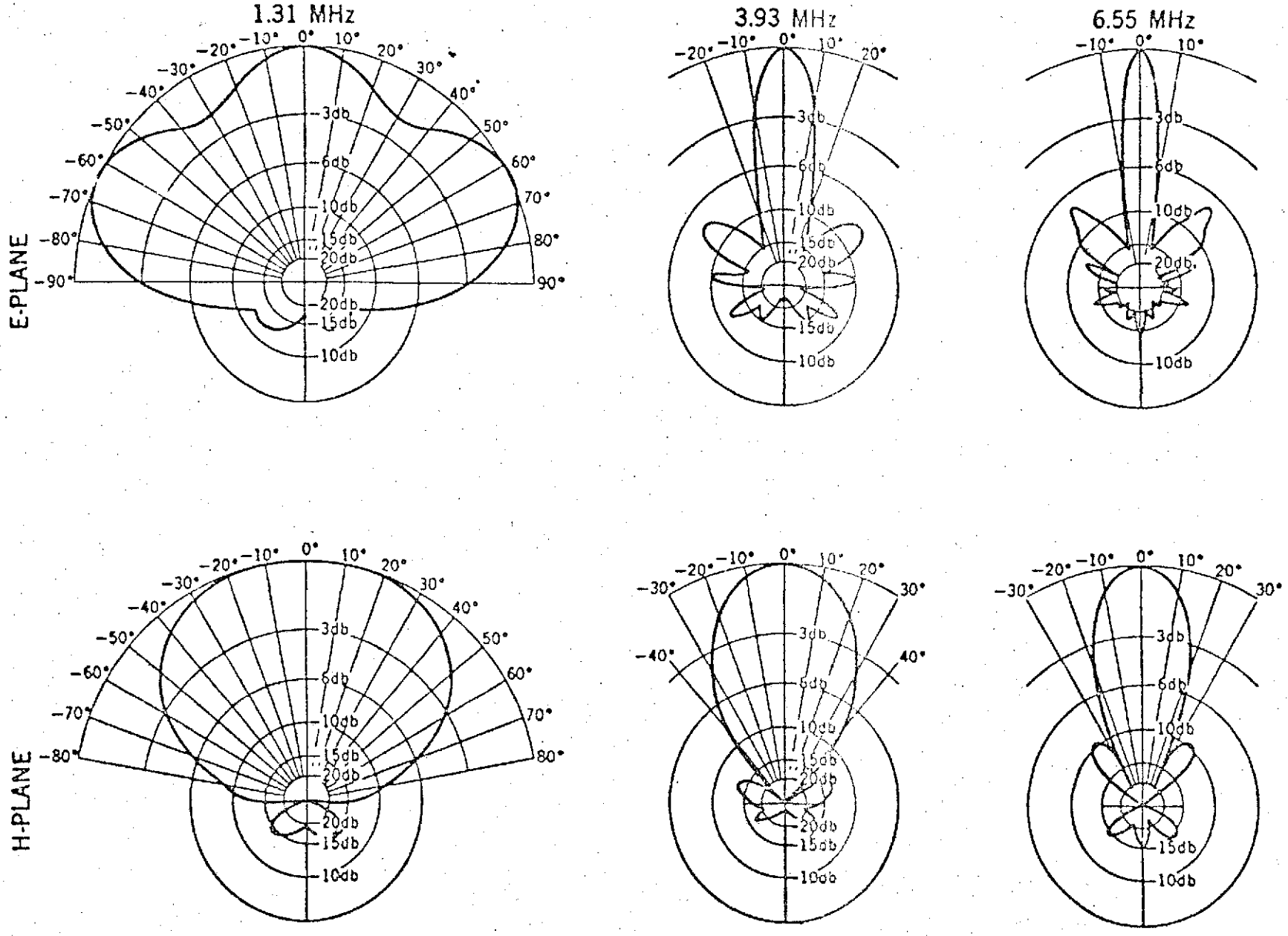


FIGURE 3-8 RAE I ANTENNA PATTERNS (WEBER, ALEXANDER AND STONE, 1971)

sky brightness measurements of other investigations.

Both the dipole and lower Vee are coupled to a burst receiver which steps continuously through its frequency range. The sweeping burst radimeter on the dipole is stepped rapidly through six discrete frequencies from .540 to 2.8 MHz to generate a dynamic spectra. The burst receiver connected to the lower Vee steps through eight frequencies between .245 and 3.93 MHz.

## THE RYLE-VONBERG RECEIVERS

The Ryle-Vonberg receiver was chosen for RAE 1 because it provides the required stability to make precise measurements over many months of unattended operation. This system measures by a null technique and is therefore insensitive to internal changes in system gain or bandwidth. The receiver measures the antenna signal strength by a continuous comparison with an internal voltage-controlled noise source which is adjusted by a servo loop to equal the antenna signal. This system provides a "coarse" measurement by measuring the voltage controlling the noise source. To provide a "fine" measurement (and also redundancy and calibration check) a stable thermistor-bridge power meter was added to the system which measures the output power directly from the noise source. However, the relays in the bridges failed after nine months.

The receiver is sampled at a slow rate, once a second for the "coarse" measurement. Therefore, this receiver's sensitivity is better measured by the peak of the statistical noise instead of the rms statistical noise. This peak noise sensitivity is ≈4%.

## 3.2.2 ANALYSIS OF OBSERVATIONS

To facilitate the investigation of radio noise observations in conjunction with high latitude geophysical processes, a means was needed to plot RAE 1 satellite passes in the same coordinate system as the auroral phenomena. This was most conveniently done by use of a nomographic computer which graphically converts geographical coordinates and universal time into corrected geomagnetic coordinates and geomagnetic local time. This nomographic computer was developed by Whalen (1970) using the corrected geomagnetic coordinate system of Hultqvist. The computer consists of a series of high latitude maps upon which the mean position, size and shape of the auroral oval can be projected for any time of day and magnetic activity.

Using the same technique, a high latitude map upon which the mean position of the main ionospheric trough (after Herman, 1972) can be projected for any time of day and magnetic activity was also developed. The correct auroral oval map and/or main ionospheric trough position to be used is then determined by the magnetic activity.

The projected geographic coordinates as a function of universal time of the position of RAE 1 for the various cases examined were extracted from the ephemeral printouts described in Section 2.1. Magnetic indices for the periods of interest were provided by E.J. Chernosky (Private Communication) of AFCRL.

Two specific examples were chosen for discussion. The first is data from the PCA event which began on 2 November, 1969 at 1200 UT and ended three days later. This event resulted in nearly the highest maximum absorption (11.7 dB on the 30 MHz riometer as measured at Thule) of all the PCA events in 1968 through 1971. The data shown is representative of the winter nighttime data that were examined and unfortunately is not

unique to PCA conditions. The second example, summer nighttime, is from the 1 May, 1969 PCA event (start and end times are unknown). This was a weak event with a maximum absorption of only .5 dB on 30 MHz at Thule.

## WINTER DATA

The data chosen for winter nighttime is from 3 November, 0310-0345 UT. The magnetic index for that particular period is given by Q=3. Knowing this and the time, defines the position of the auroral oval. The position of RAE I is superimposed on the same map as shown in Figure 3-9. Plots of the noise intensity as observed by the burst receiver are shown in Figure 3-10. Noise intensities observed at several frequencies by the Ryle-Vonberg receivers are shown in Figures 3-11 through 3-26.

Examination of the burst receiver data shows an increase in noise level on all frequencies at approximately the time RAE 1 approaches the auroral oval (0315 UT). As RAE 1 passes over the oval, the burst receiver noise levels exceed $10^{10}$ degrees Kelvin. This increase in noise intensity corresponding to passage over the oval is often observed on other data, though not always as clearly as in this example. Further examination of the burst receiver data reveals that the lower frequencies exhibit a more intense response to passage over the oval than the higher frequencies displaying greater enhancements for a longer time.

The noise levels at the higher frequencies drop off sooner than at the lower frequencies. This is the opposite of the ground break through phenomenon observed and reported on by Herman et al (1973). Therefore, it would seem that this noise has its origin above the peak of the F-layer and is not a result of the

mid-latitude trough but of particle precipitation. There certainly is not an obvious reduction in noise level due to polar cap absorption or auroral absorption of terrestrial noise sources within the oval.

All frequencies exhibit enhanced noise levels at least until 0350 UT, at which time the higher frequencies returned to their normal noise level. The lower frequencies maintained noise levels near $10^{10}$ degrees Kelvin until nearly 0400 UT. However, a sharp short-lived decrease in noise level is seen on all frequencies at 0340 UT, the time the satellite leaves the auroral region. It is possible this decrease is due to the satellite's passing over the mid-latitude trough (which, as stated in Section 3.1.2, borders the auroral zone on the equatorial side) and reflects the dirth of particles in the trough region.

A similar frequency response is observed on the R-V receiver data. Generally speaking, the noise intensities are greater at the lower frequencies. In this particular example, the noise level was greatest at .7 MHz.

The R-V receiver which is connected to the upper and lower Vee antennas could shed some light on the spatial distribution of this noise. Examination of R-V receiver data reveals an enhanced noise level which peaks between 0320 UT and 0325 UT. It is stronger on the lower Vee at 700 kHz. At 900 kHz two peaks can be seen, one about 0320 UT and a second at about 0335 UT. Again, the lower Vee noise level is slightly greater at 0320 UT indicating that the source is below the satellite. At 1.31 MHz, the same two enhancements are observed only this time the second peak at 0335 UT is clearly greater on the upper

Vee antenna. At 2.20 MHz the noise intensities are greatly reduced and at 3.93 MHz the noise peaks are no longer visible. However, both peaks are visible at 4.7 MHz with the lower Vee noise intensity being greater in both cases. At 6.5 MHz the structure has again changed until at 9.18 MHz a single peak in intensity is visible with the lower Vee noise still being greater at about 0328UT.

## SUMMER DATA

The second example is data taken on 4 May from 0610-0640UT. The magnetic index is given by Q=3. The RAE 1 track superimposed on the map with the auroral oval for this time is shown in Figure 3-27. Noise levels recorded by the burst receiver are shown in Figure 3-28. The Ryle-Vonberg receiver data are shown in Figures 3-29 through 3-39.

Examination of the burst receiver data between 0620-0635UT (time RAE 1 passes over the auroral oval) shows the greatest response occurs at .245 MHz. Noise level peaks in excess of $10^{10}$ degrees Kelvin can be seen. Enhancements in noise level are also seen at .328 MHz but to a lesser degree. At .490 MHz only two spikes occur at the times RAE 1 approaches and leaves the oval. Two spikes are seen at 0630UT on .540 and .7 MHz. None of the other frequencies respond to passage over the oval until we get to the highest frequency, 3.9 MHz. While the enhanced noise level at 3.9 MHz starts to drop off approximately 10 minutes earlier than at .245 MHz, both frequencies show recovery by 0650 UT. These data are markedly different from the burst receiver data for the winter nighttime example. The enhanced noise levels are greater in the winter case and last for a longer time, particularly on the lower frequencies. In the summer example the enhancements appeared only on frequencies lower than the winter low frequencies, with no other response to passage over the oval until 3.9 MHz.

The R-V receiver data for this example is consistent with the burst receiver data and in contrast to the data shown in the first example. At .45 MHz, noise intensity increases during the period of time the satellite passes over the oval, with a sharp increase at 0634UT. At .7MHz (the frequency which recorded the greatest enhancement in the previous example), only two peaks remain at 0612 and 0633UT. At .9 MHz only the first peak is seen. From 1.3 to 3.9 MHz, there is no response. However, the lower Vee antenna does show enhancements at 3.9 MHz. At 4.7 MHz, the upper Vee measurements show some fluctuations while the lower Vee antenna shows enhancements at 0635 and 0637UT. At 6.5 MHz, many fluctuations are seen during the time the satellite passes over the oval. Although the amount of the enhancements differ, the general structure of the noise level at 6.5 MHz is not unlike that seen at .45 MHz. At 9.18 MHz, the highest frequency, the entire noise level curve is shifted upwards and exhibits a structure entirely different from that seen on other frequencies.

Looking at the data from either example, we have seen fairly complicated responses over a range of frequencies. Looking at both examples together, the data becomes even more complex. No obvious patterns are evident except that there are a lot of inconsistencies. There appears to be a frequency dependence trying to emerge that is more evident in the second example. An in-depth statistical analysis on the wealth of data collected by RAE 1 would most certainly aid analysts in gaining insight into <u>what</u> we are seeing in the data and thus aid scientists in explaining <u>why</u>. Unfortunately that level of effort was beyond the scope of this study.

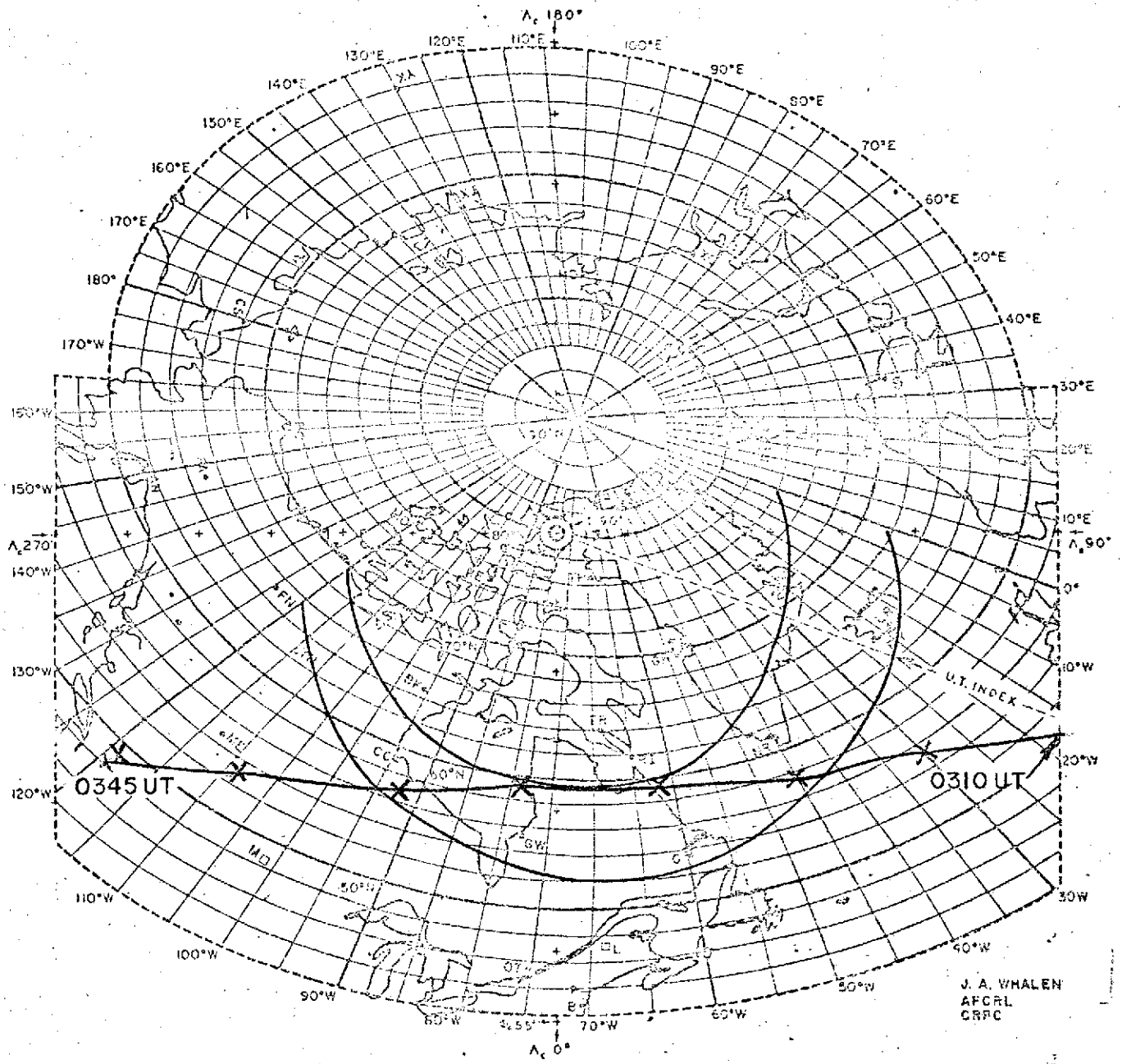


Figure 3-9. Location of Auroral Oval and RAE I Position for 3 November 1969 (0310-0345 UT)

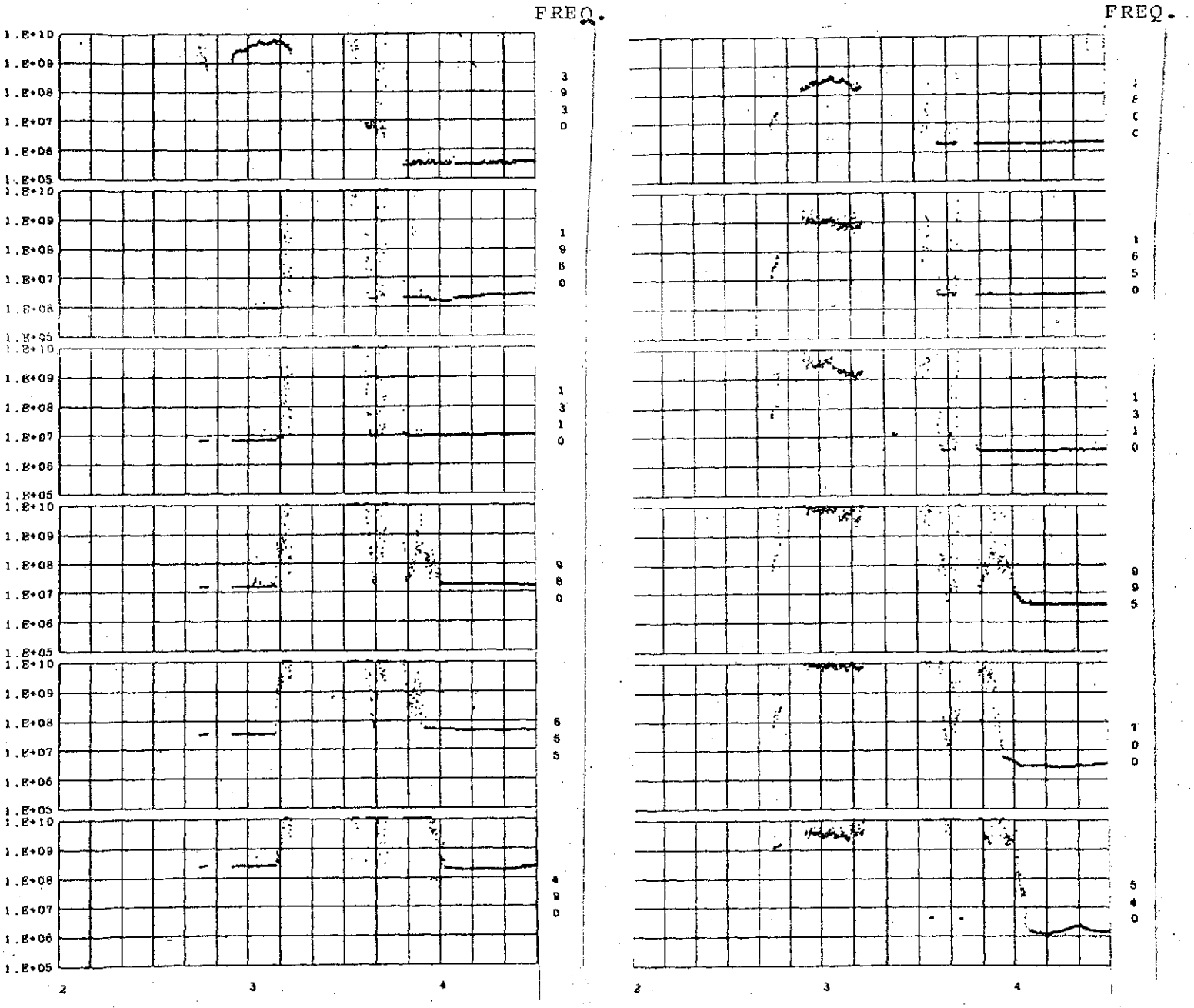


Figure 3-10. RAE I Burst Receiver Data 3 November 1969.

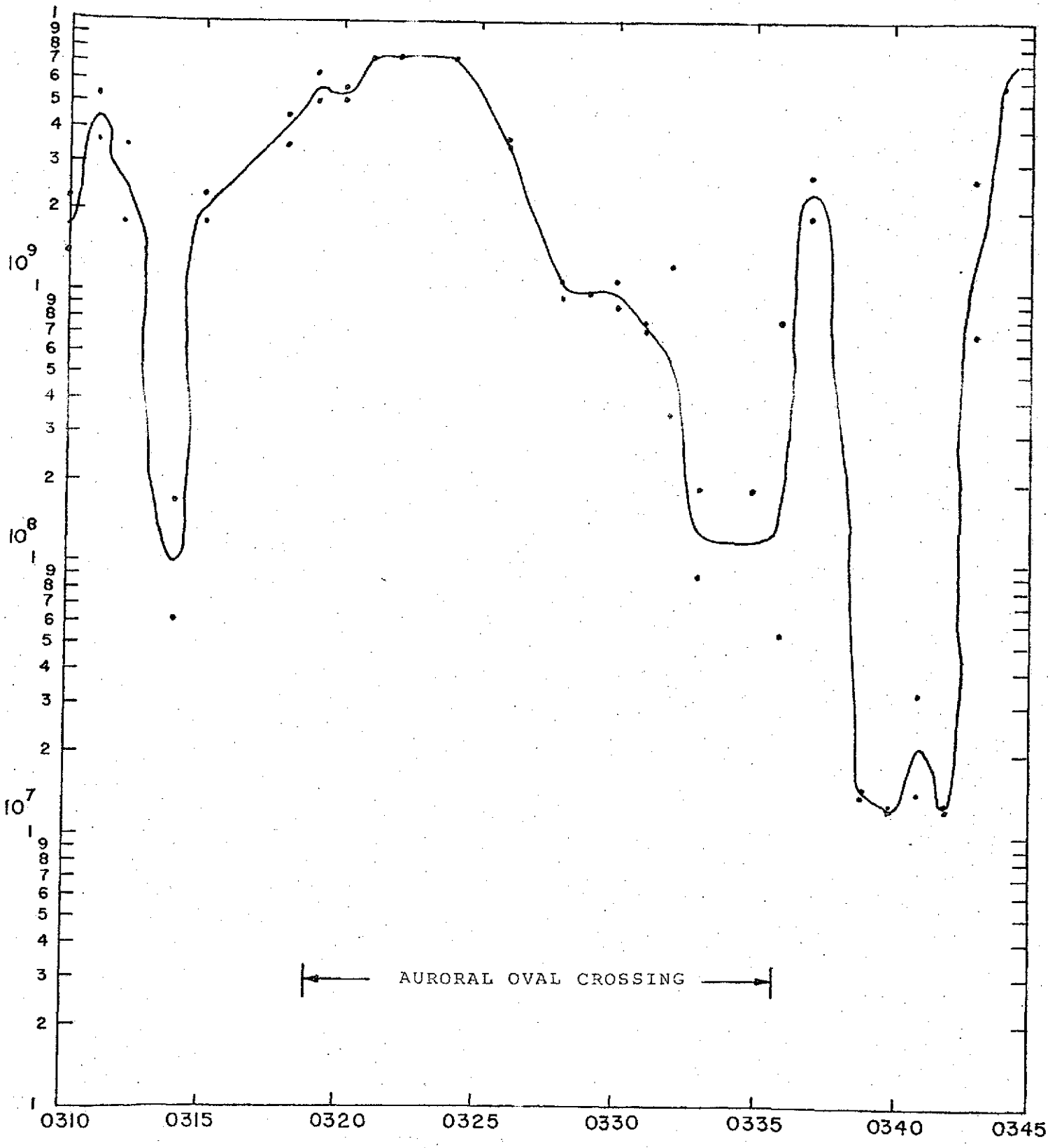


Figure 3-11. RAE I Noise Temperature at 700 kHz on Upper Vee Antenna - 0310 to 0345 UT - 3 November 1969

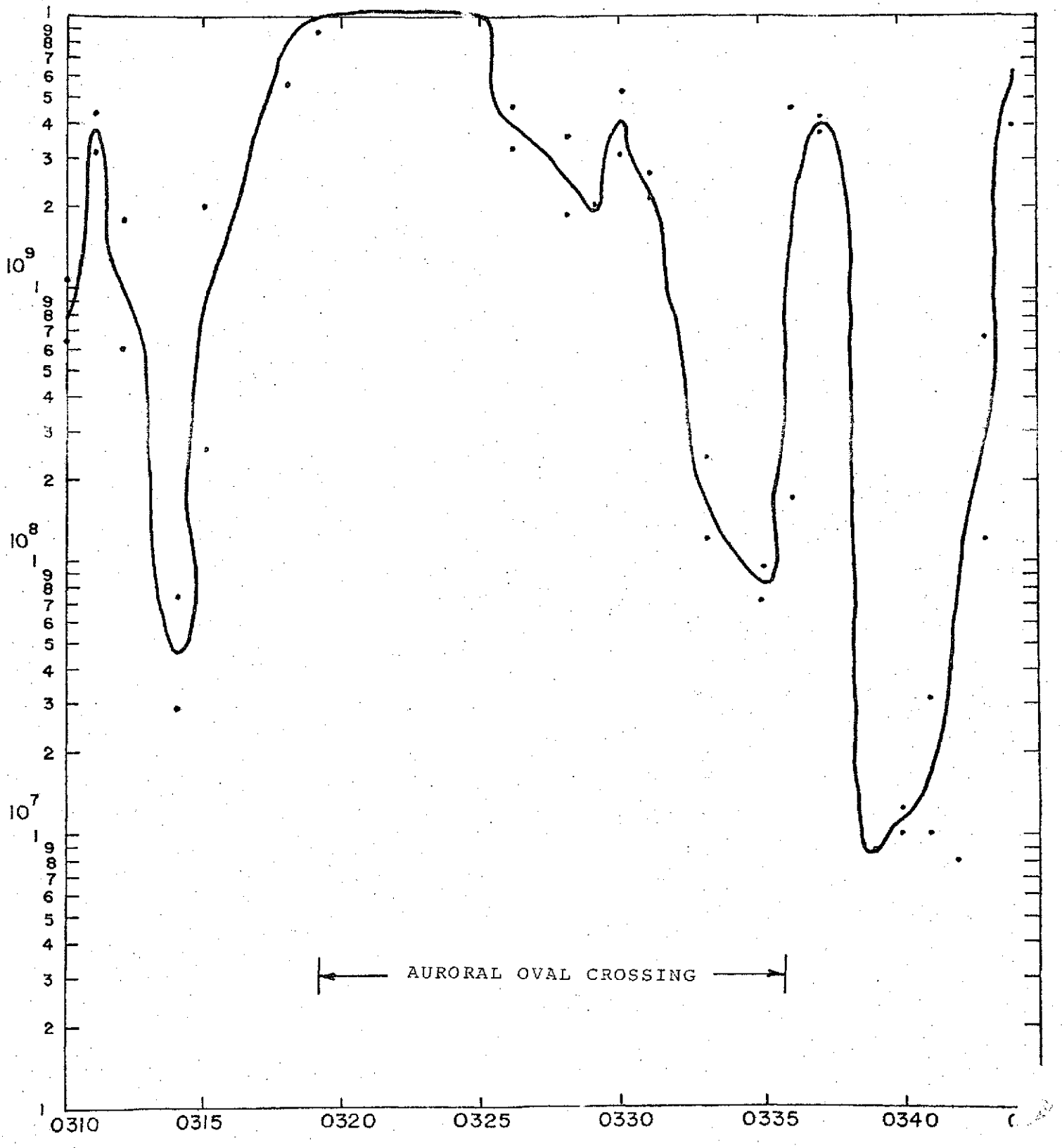


Figure 3-12. RAE I Noise Temperature at 700 kHz on Lower Vee Antenna - 0310 to 0345 UT - 3 November 1969

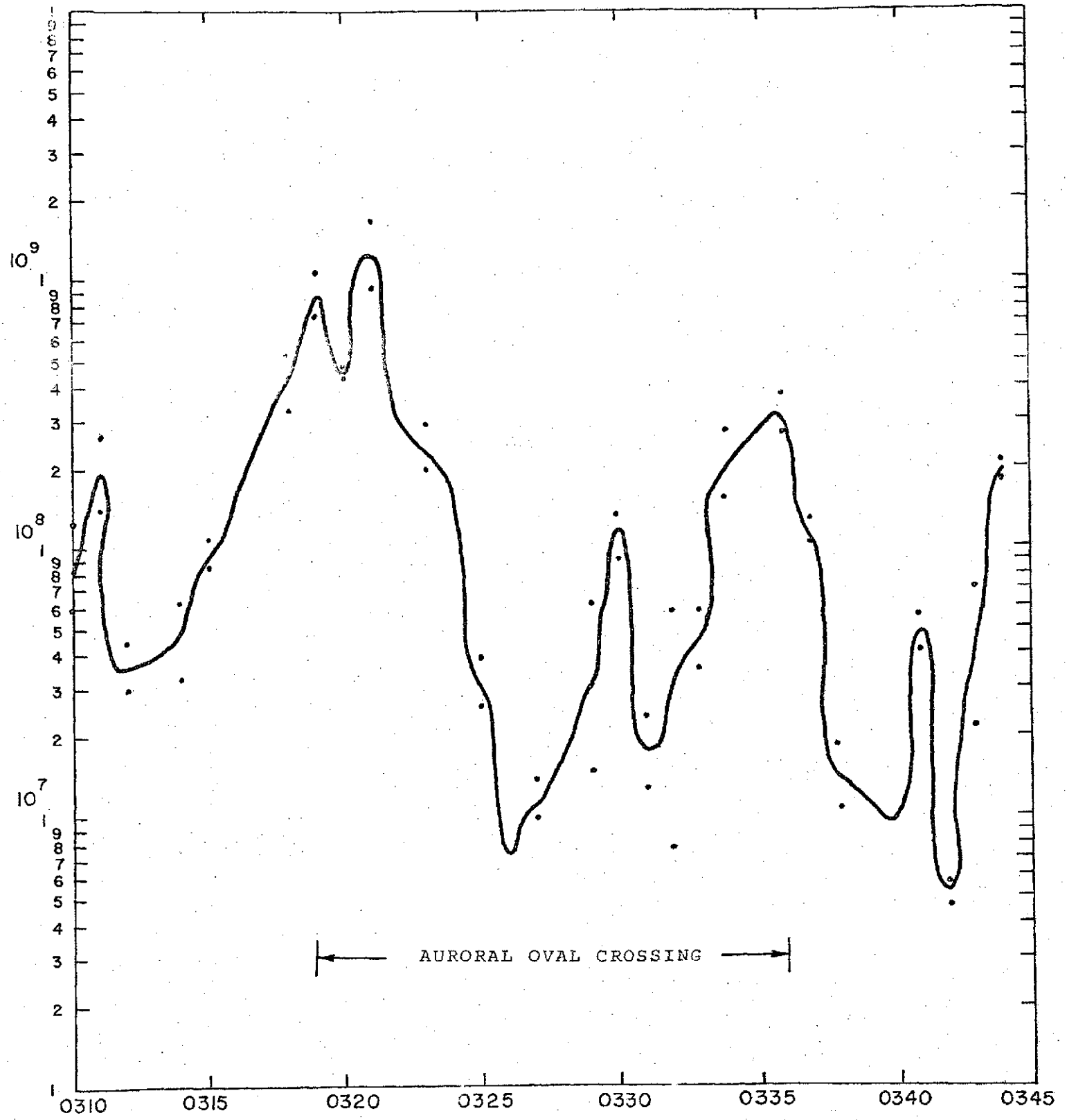


Figure 3-13. RAE I Noise Temperature at 900 kHz on Upper Vee Antenna - 0310 to 0345 UT - 3 November 1969

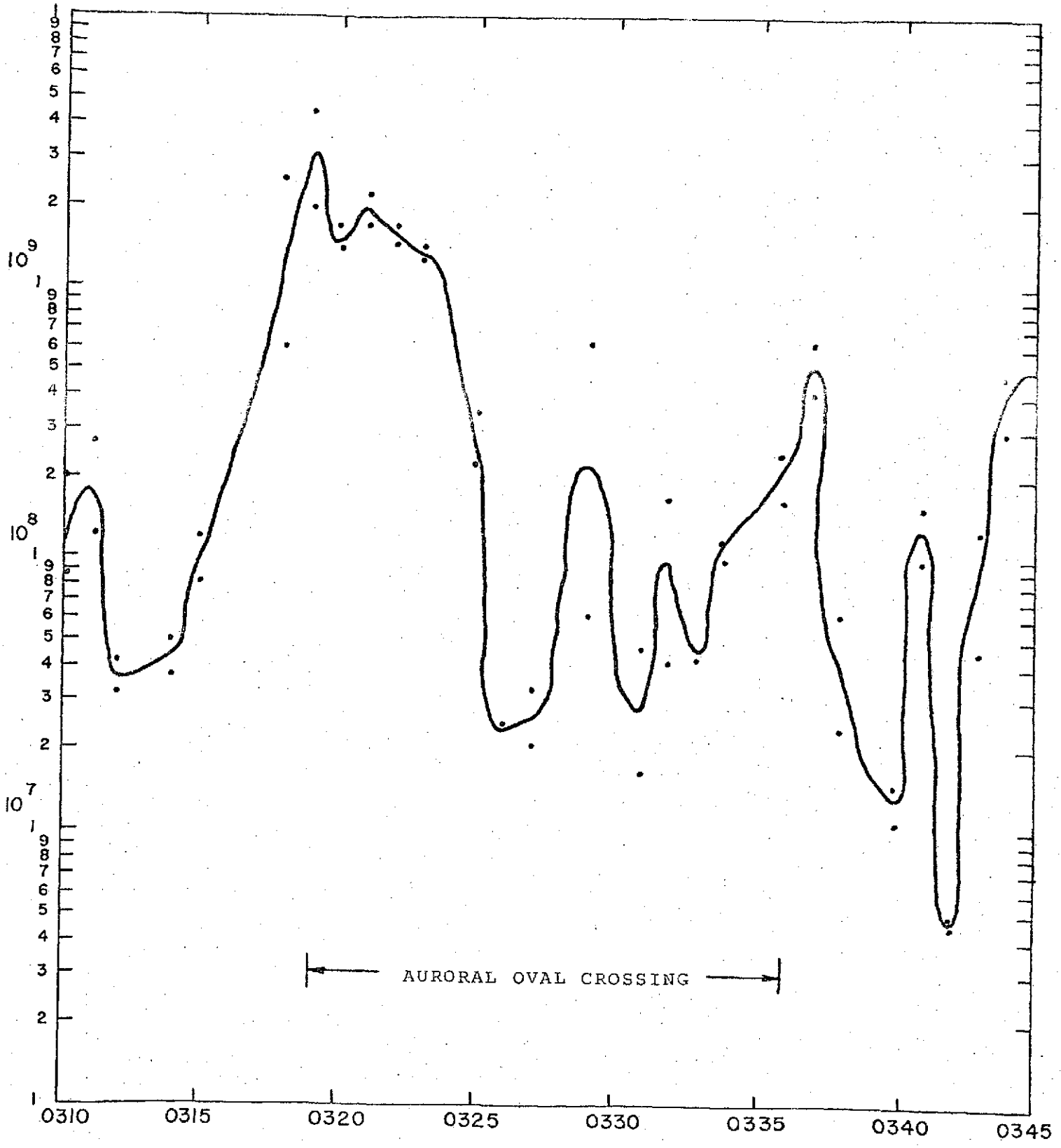


Figure 3-14. RAE I Noise Temperature at 900 kHz on Lower Vee Antenna - 0310 to 0345 UT - 3 November 1969

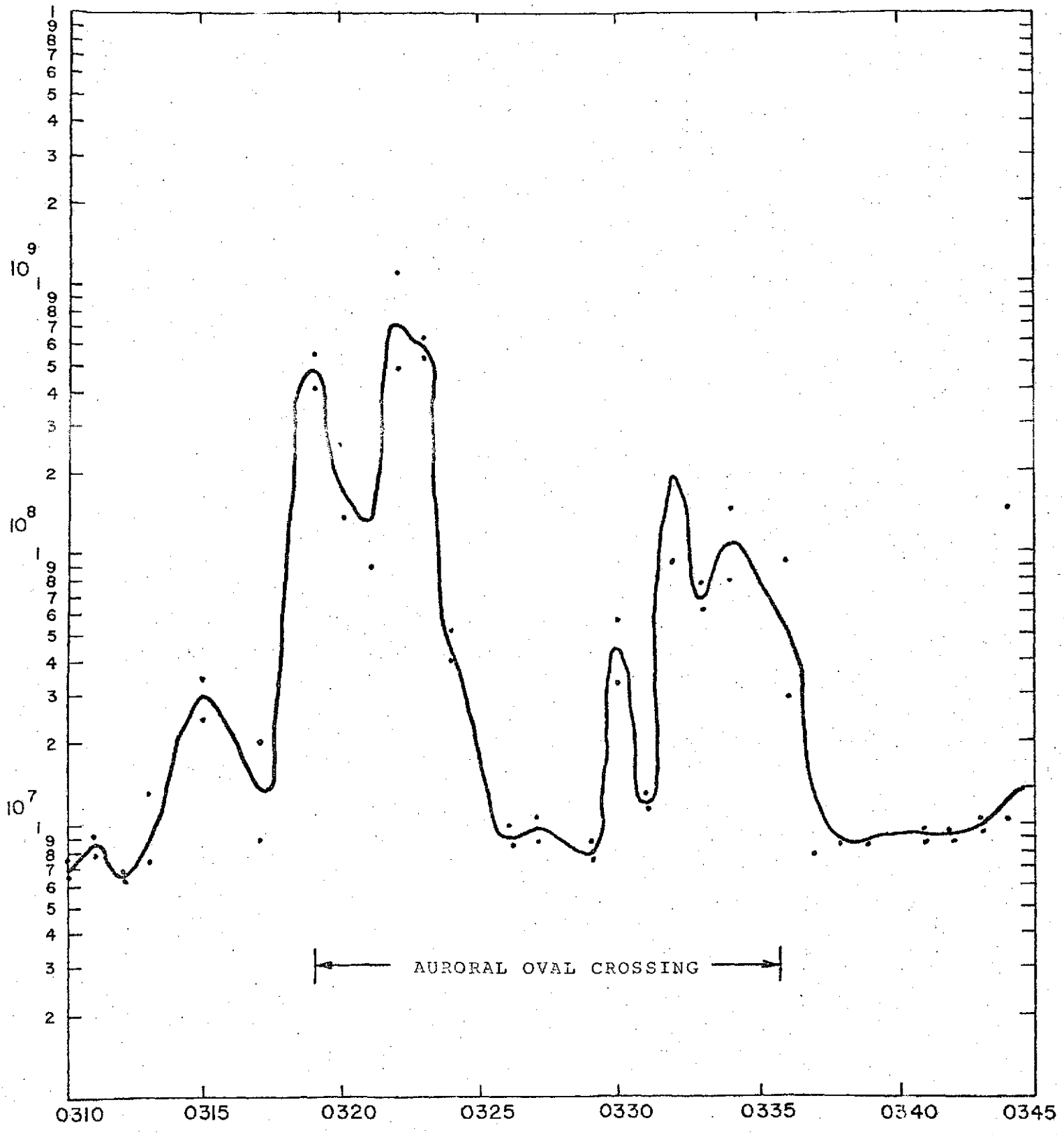


Figure 3-15. RAE I Noise Temperature at 1-3 MHz on Upper Vee Antenna - 0310 to 0345 UT - 3 November 1969

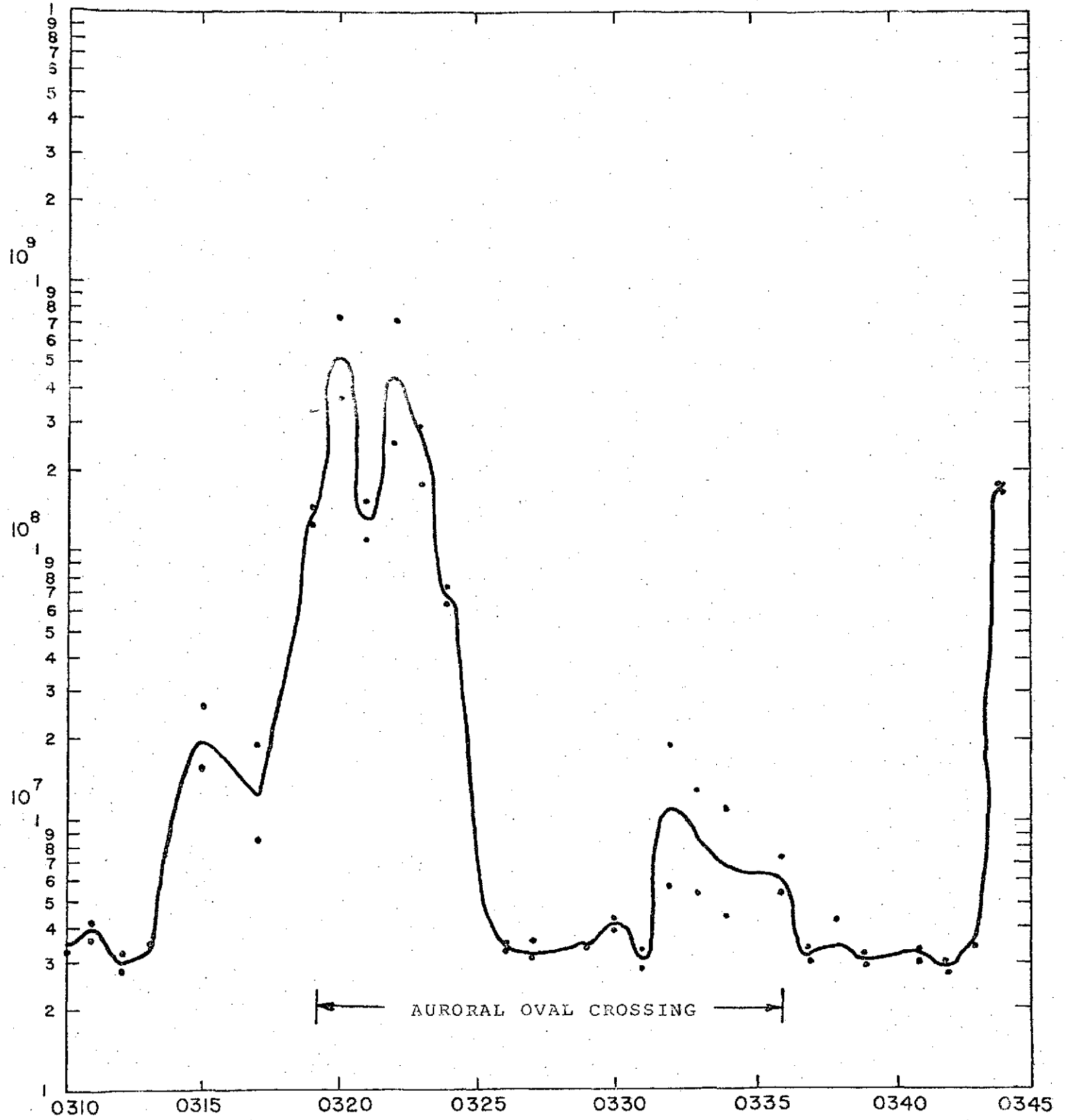


Figure 3-16. RAE I Noise Temperature at 1.3 MHz on Lower Vee Antenna - 0310 to 0345 UT - 3 November 1969

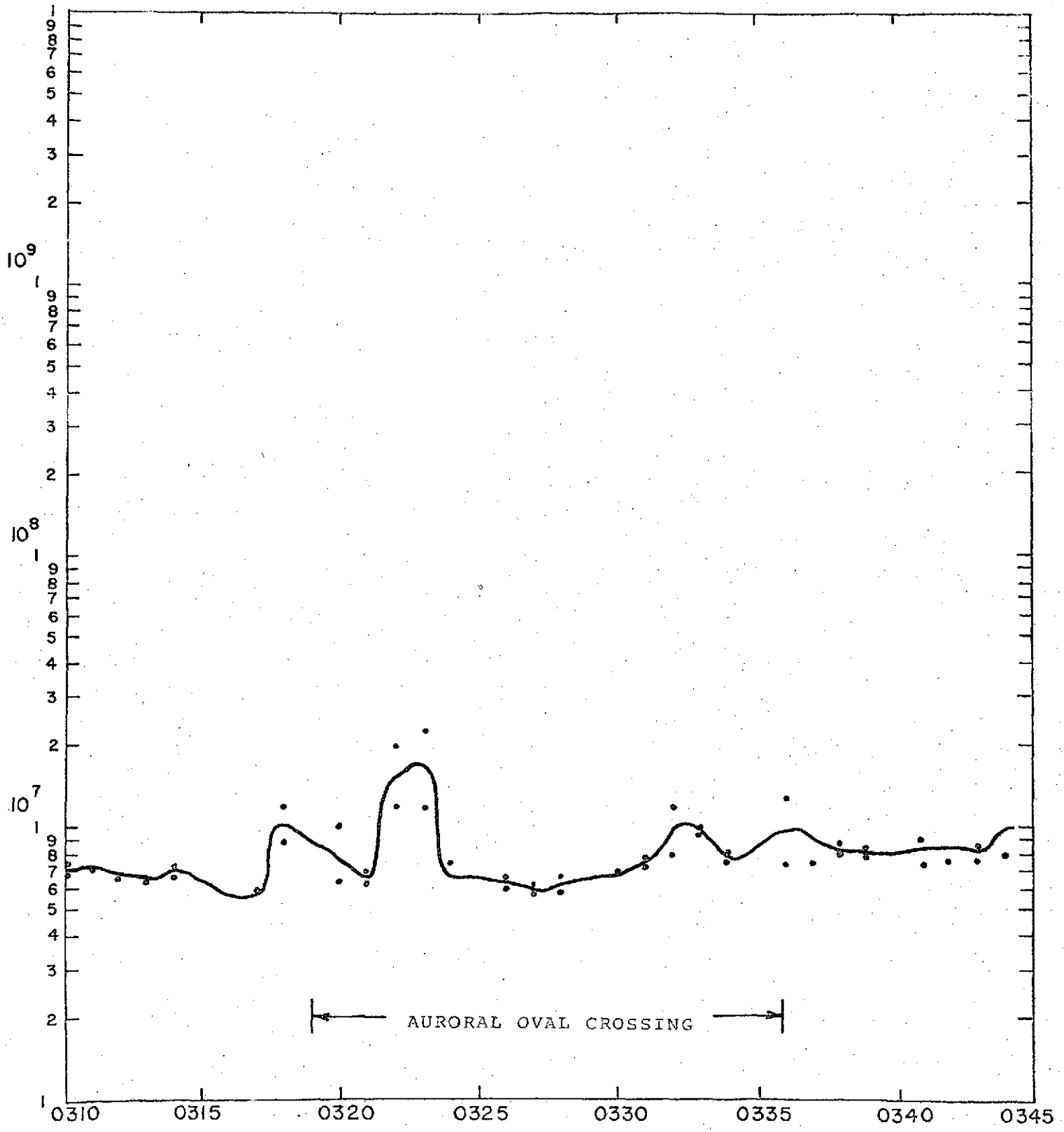


Figure 3-17. RAE I Noise Temperature at 2.2 MHz on Upper Vee Antenna - 0310 to 0345 UT - 3 November 1969

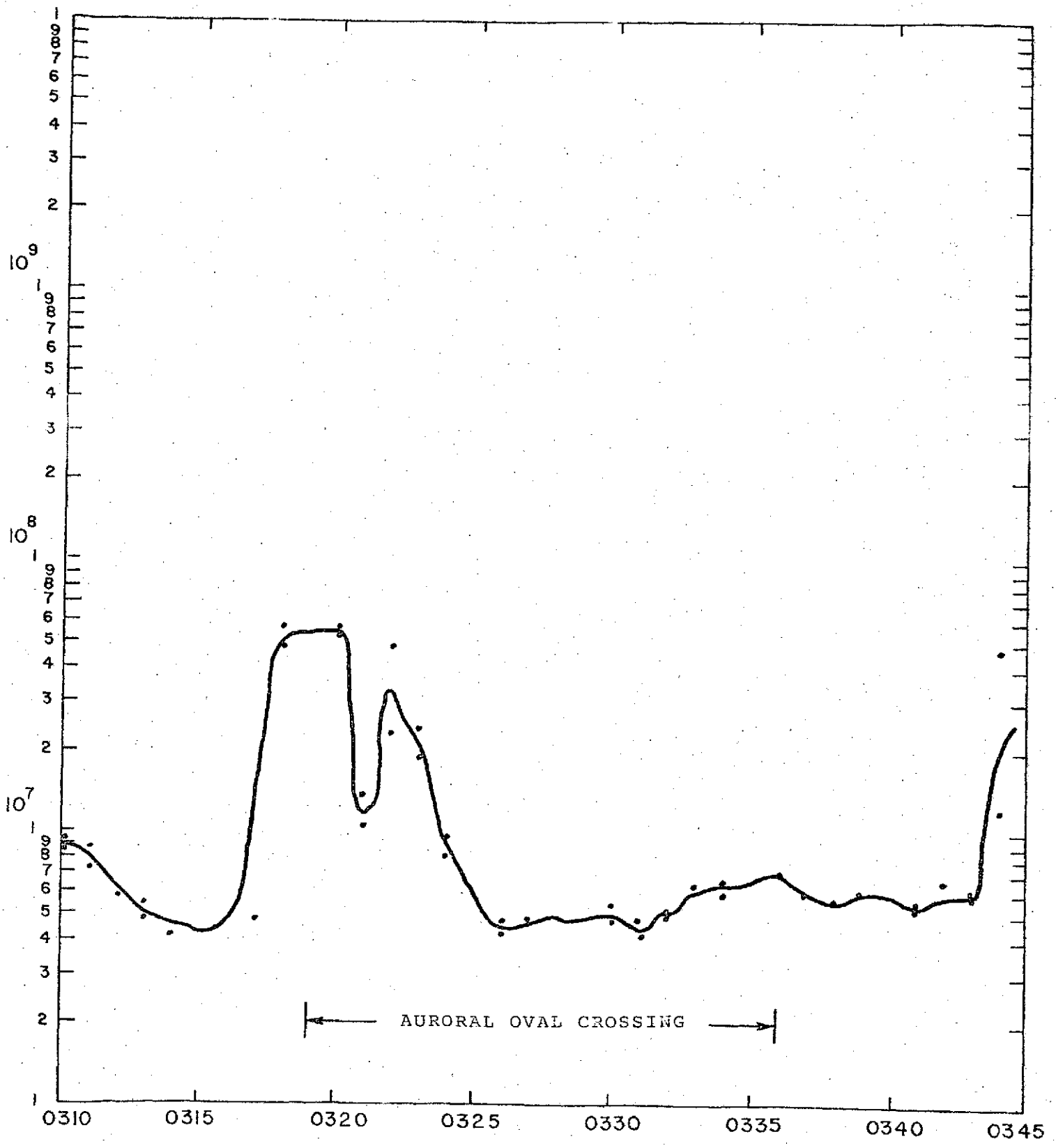


Figure 3-18. RAE I Noise Temperature at 2.2 MHz on Lower Vee Antenna - 0310 to 0345 UT - 3 November 1969

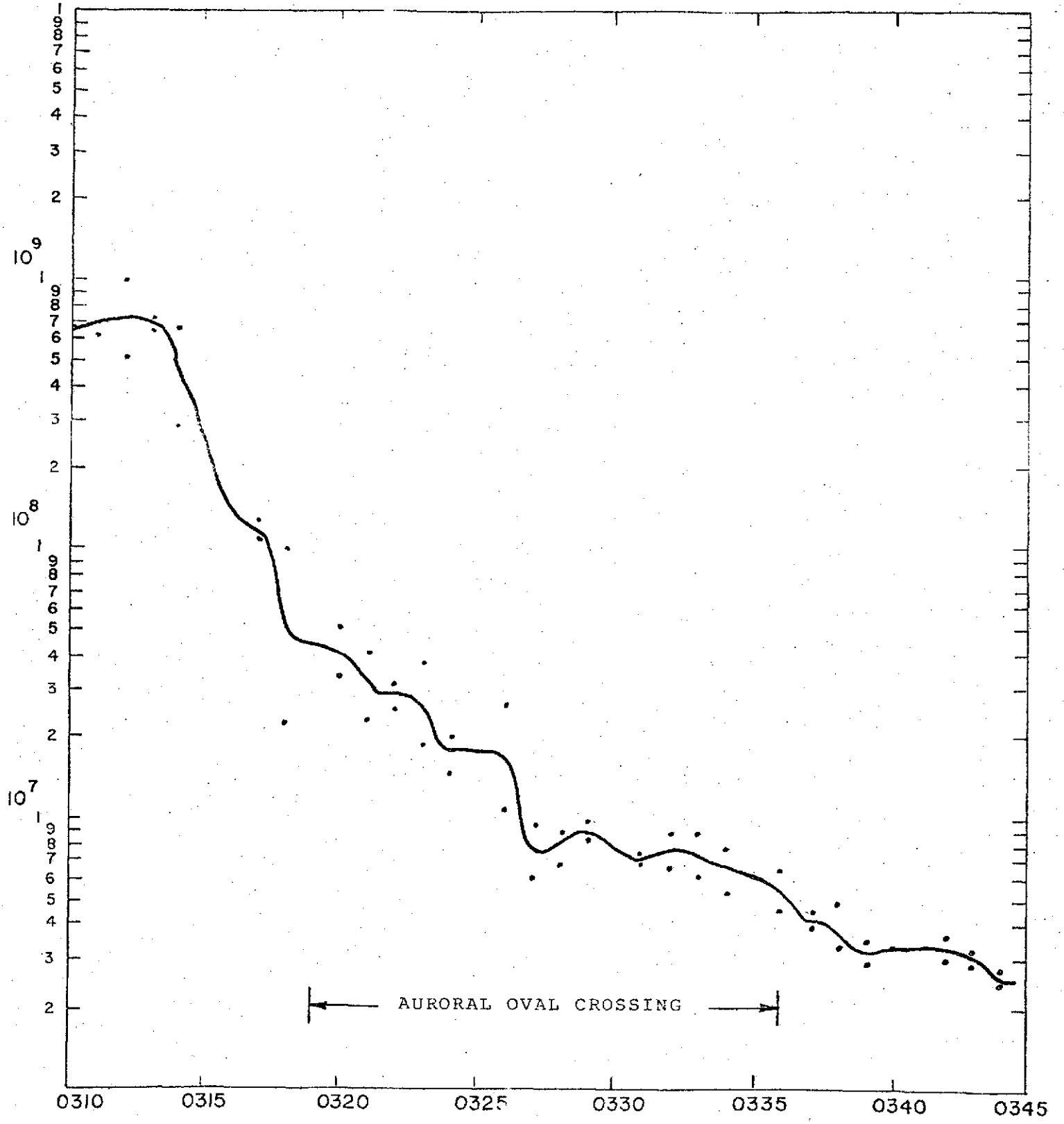


Figure 3-19. RAE I Noise Temperature at 3.9 MHz on Upper Vee Antenna - 0310 to 0345 UT - 3 November 1969

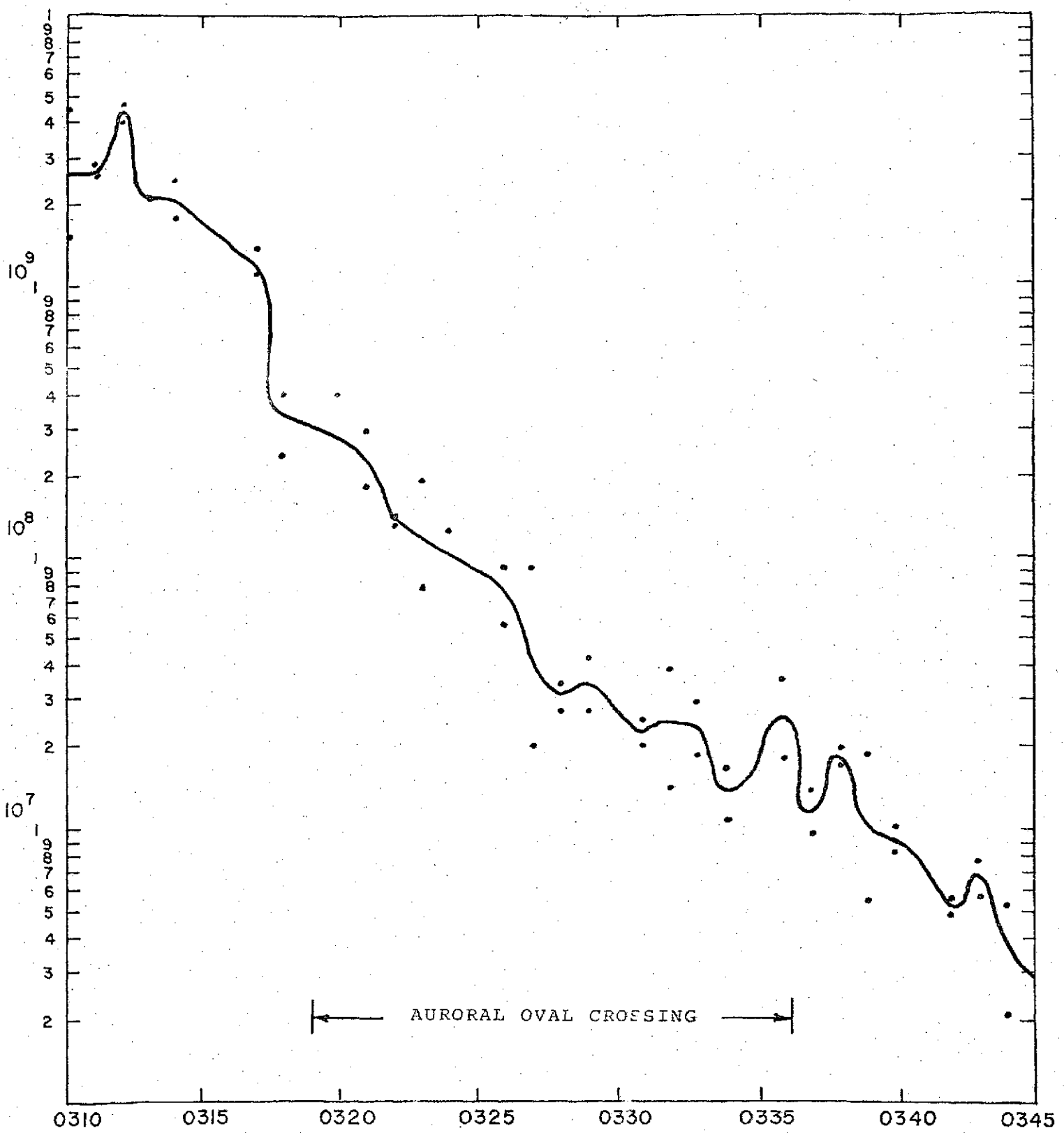


Figure 3-20. RAE I Noise Temperature at 3.9 MHz on Lower Vee Antenna - 0310 to 0345 UT - 3 November 1969

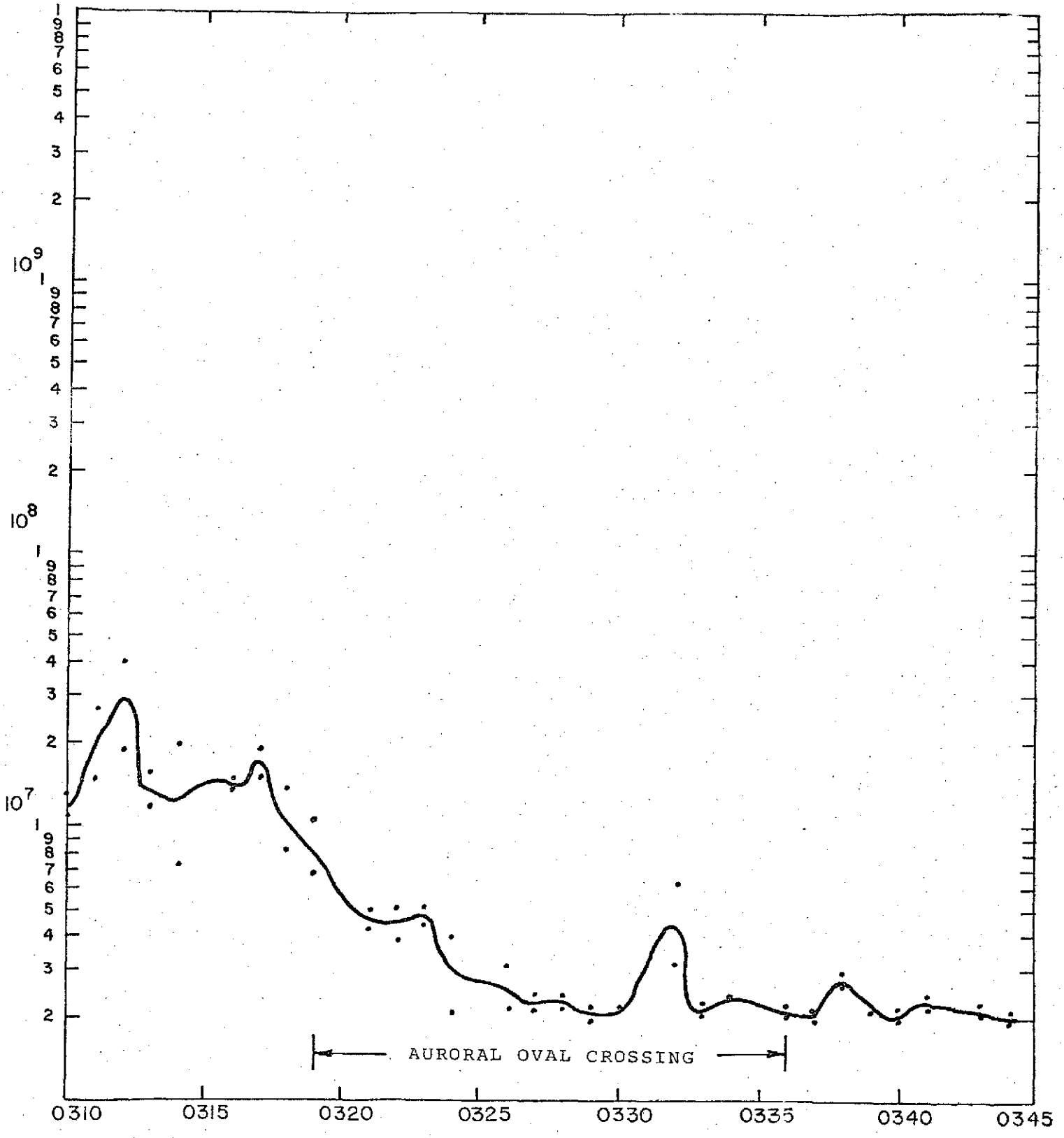


Figure 3-21. RAE I Noise Temperature at 4.7 MHz in Upper Vee Antenna - 0310 to 0345 UT - 3 November 1969

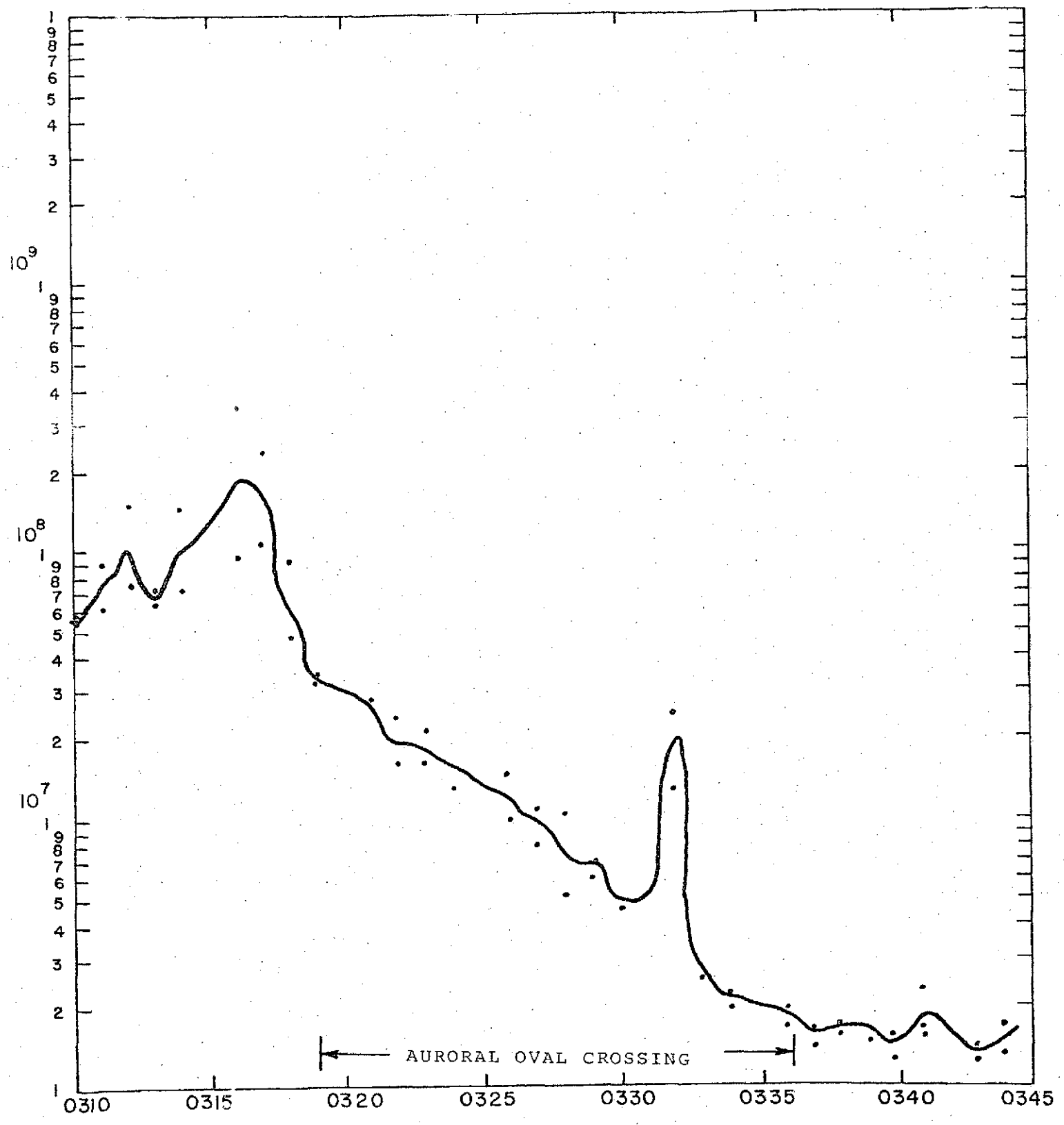


Figure 3-22. RAE I Noise Temperature at 4.7 MHz on Lower Vee Antenna - 0310 to 0345 UT - 3 November 1969

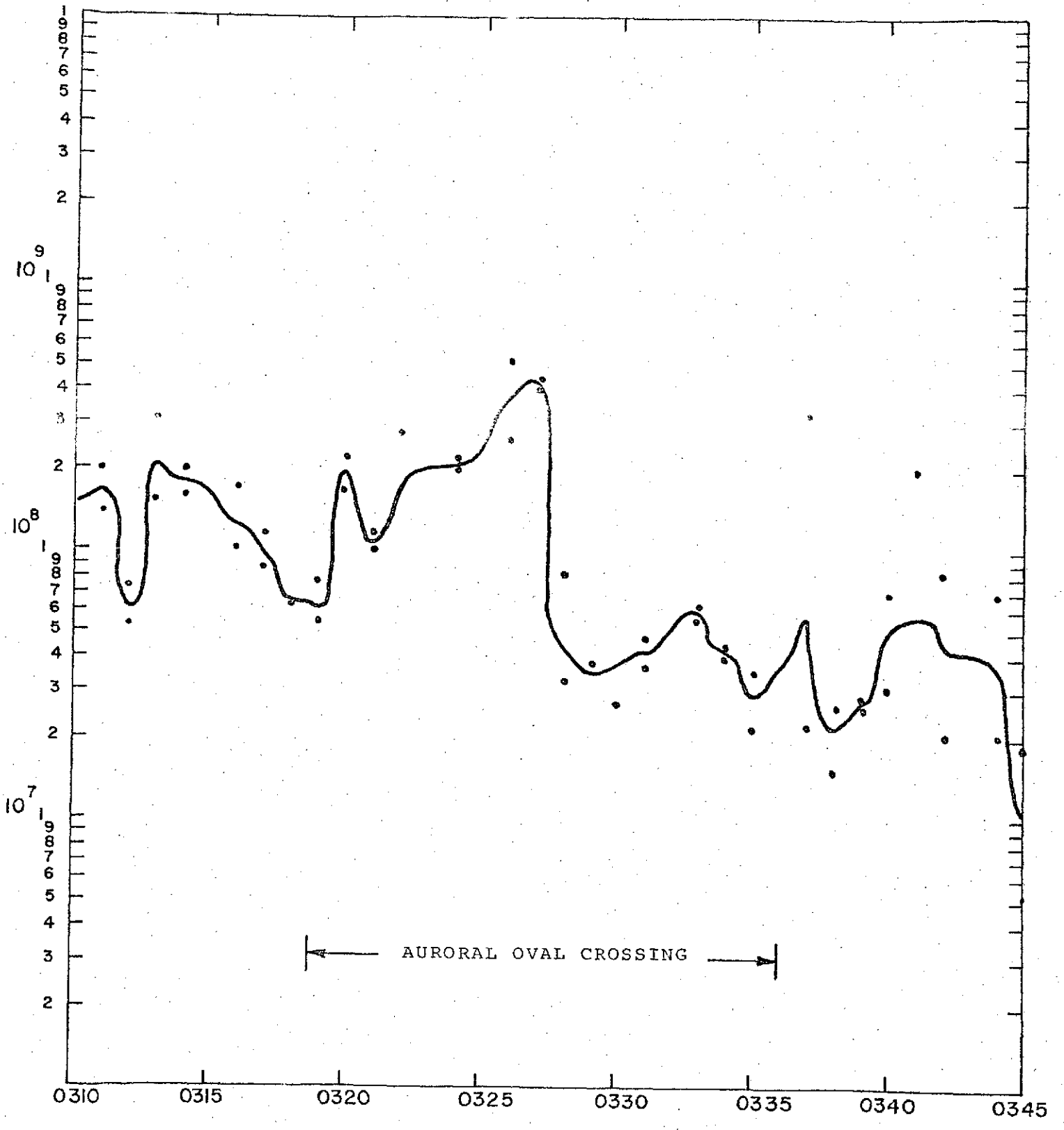


Figure 3-23. RAE I Noise Temperature at 6.5 MHz on Upper Vee Antenna - 0310 to 0345 UT - 3 November 1969

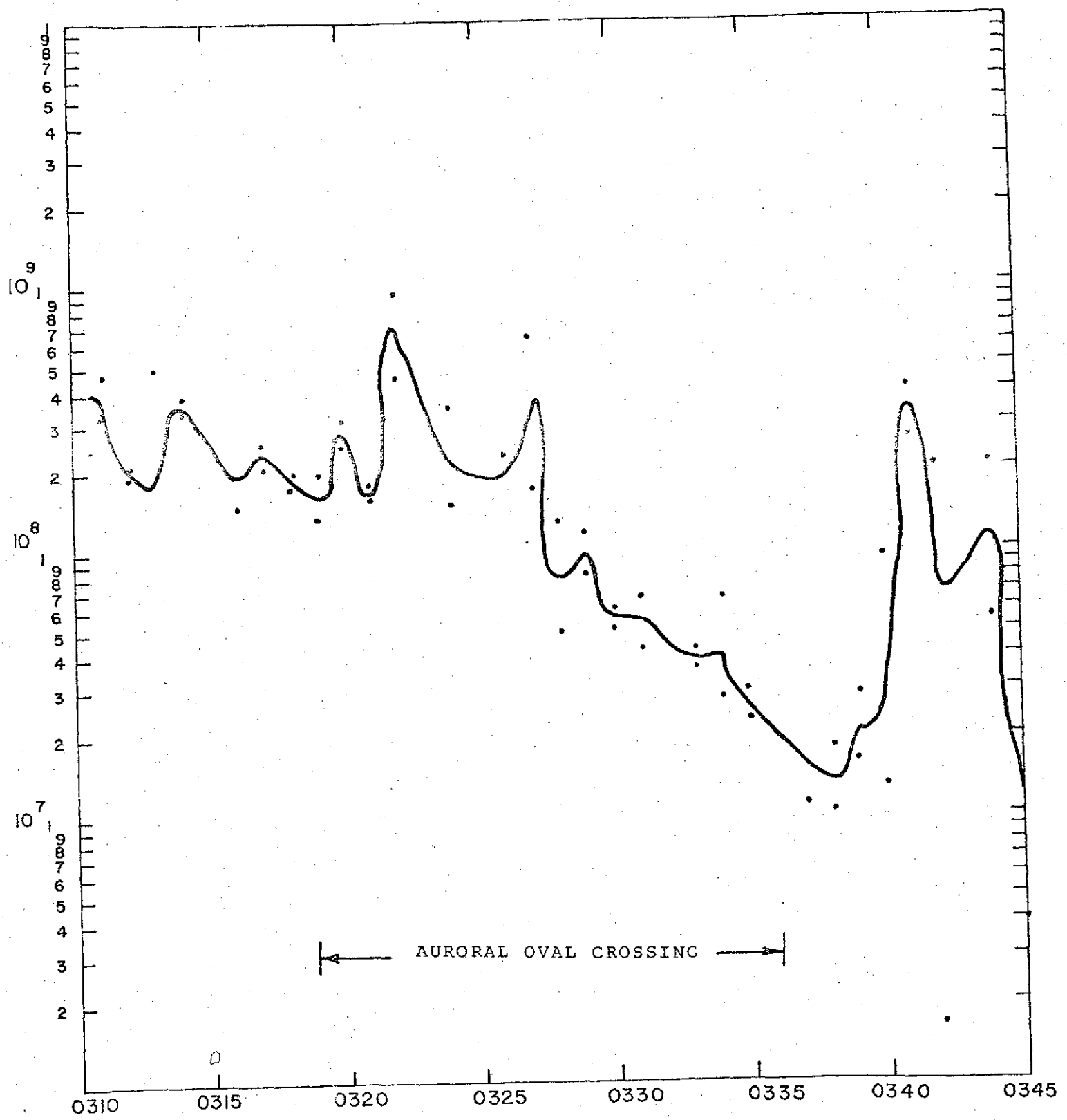


Figure 3-24. RAE I Noise Temperature at 6.5 MHz on Lower Vee Antenna - 0310 to 0345 UT - 3 November 1969

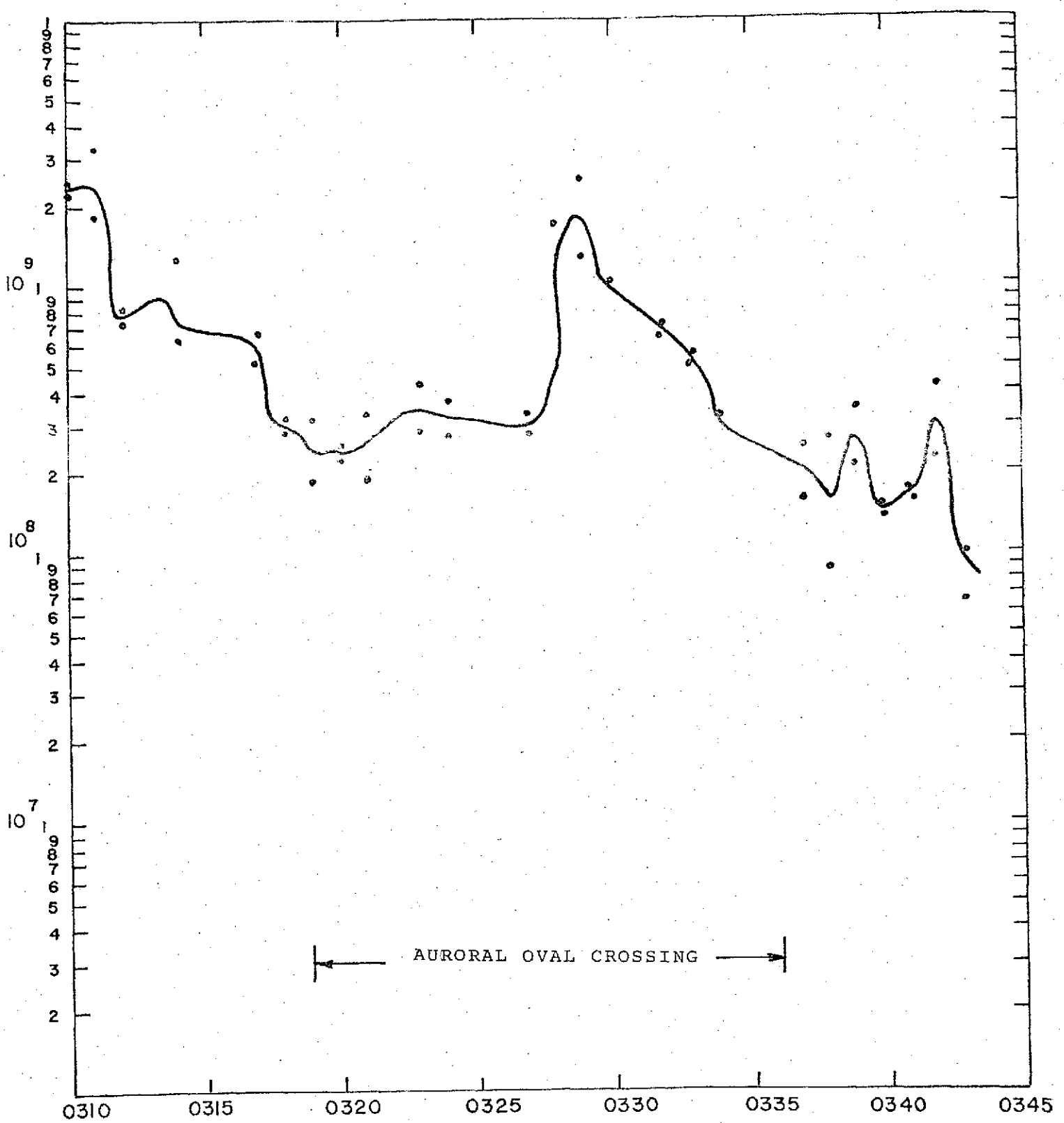


Figure 3-25. RAE I Noise Temperature at 9.18 MHz on Upper Vee Antenna - 0310 to 0345 UT - 3 November 1969

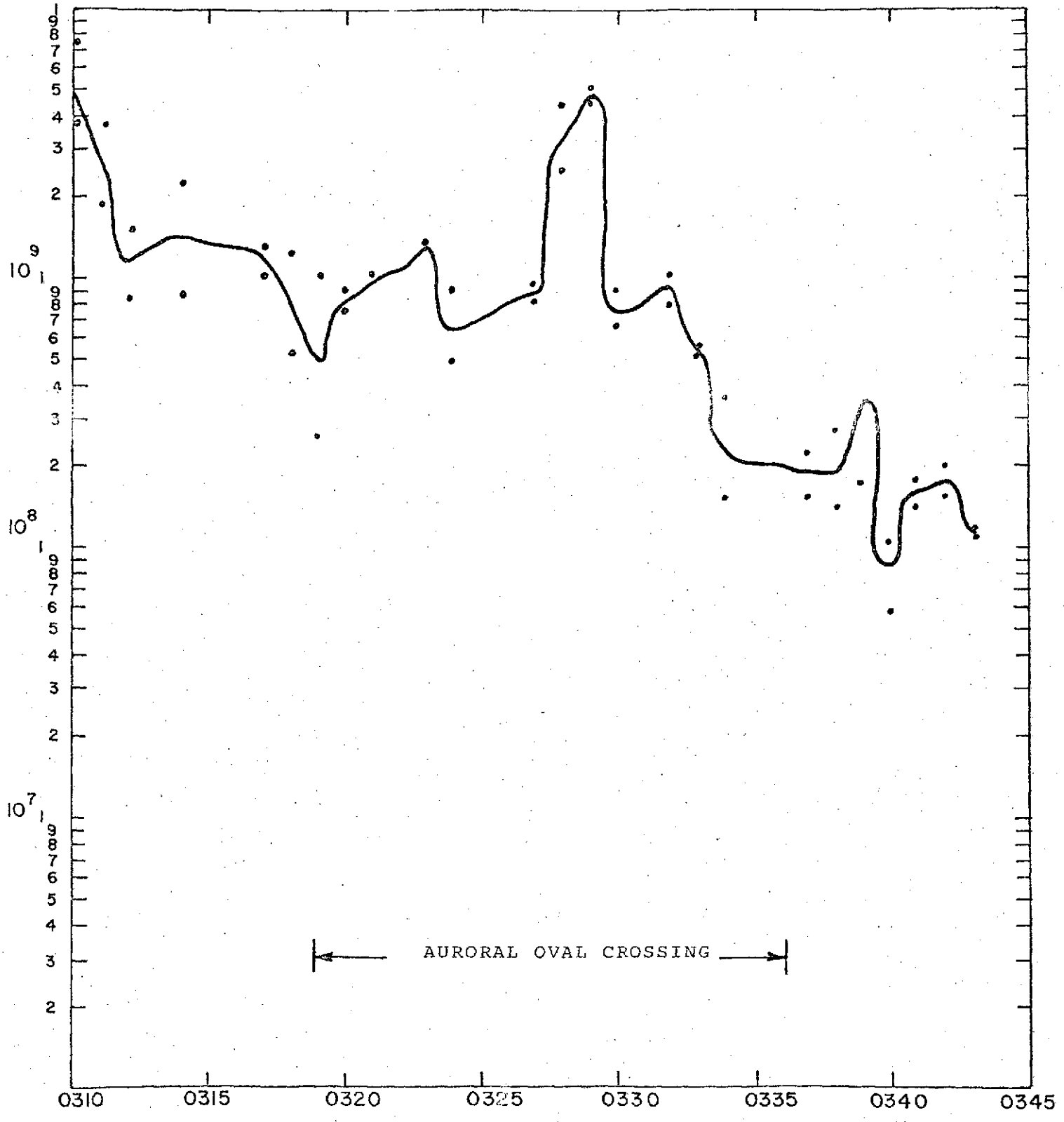


Figure 3-26. RAE I Noise Temperature at 9.18 MHz on Lower Vee Antenna - 0310 to 0345 UT - 3 November 1969

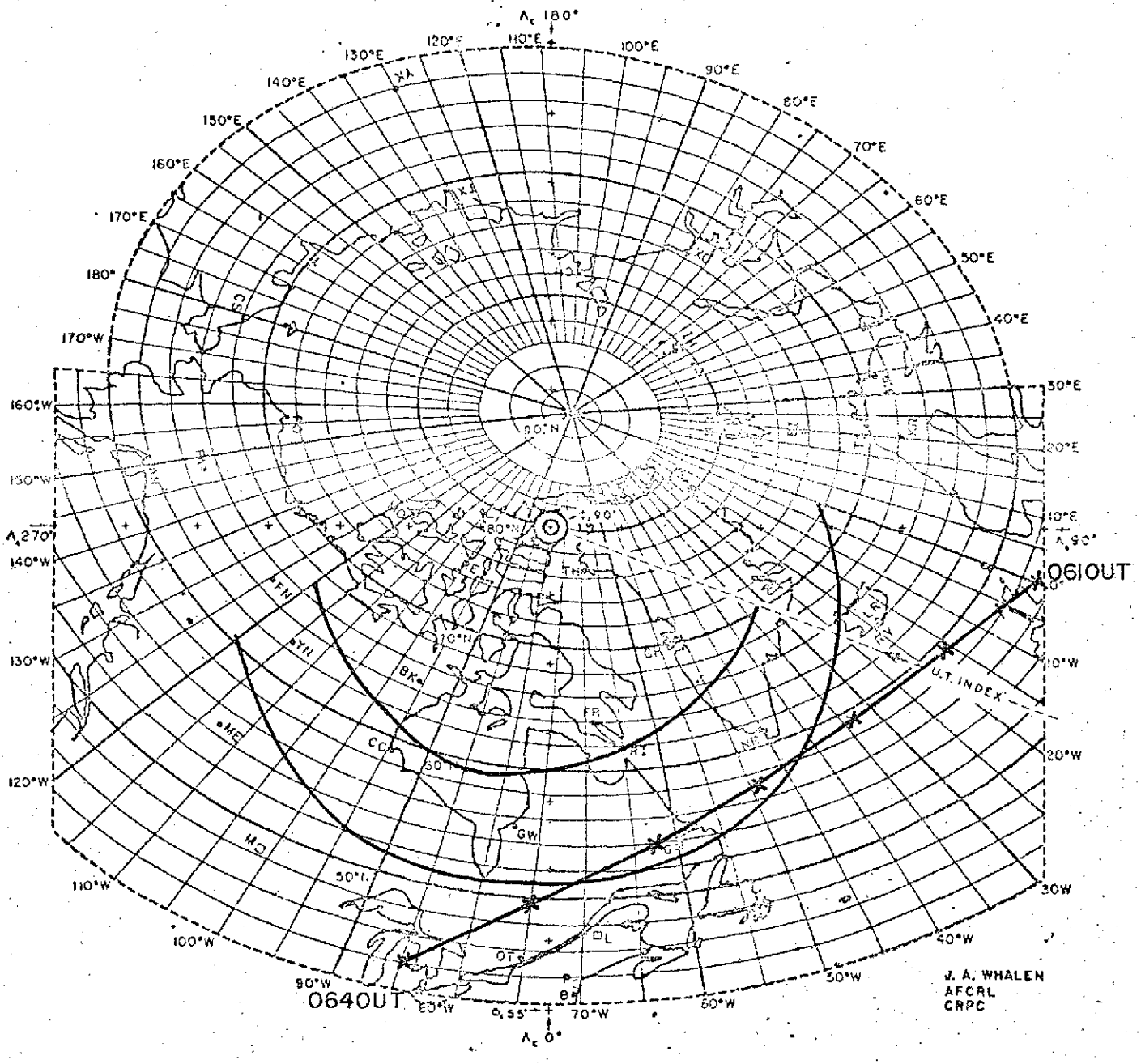


Figure 3-27. Location of Auroral Oval and RAE I Position for 4 May 1969 (0610-0640 UT)

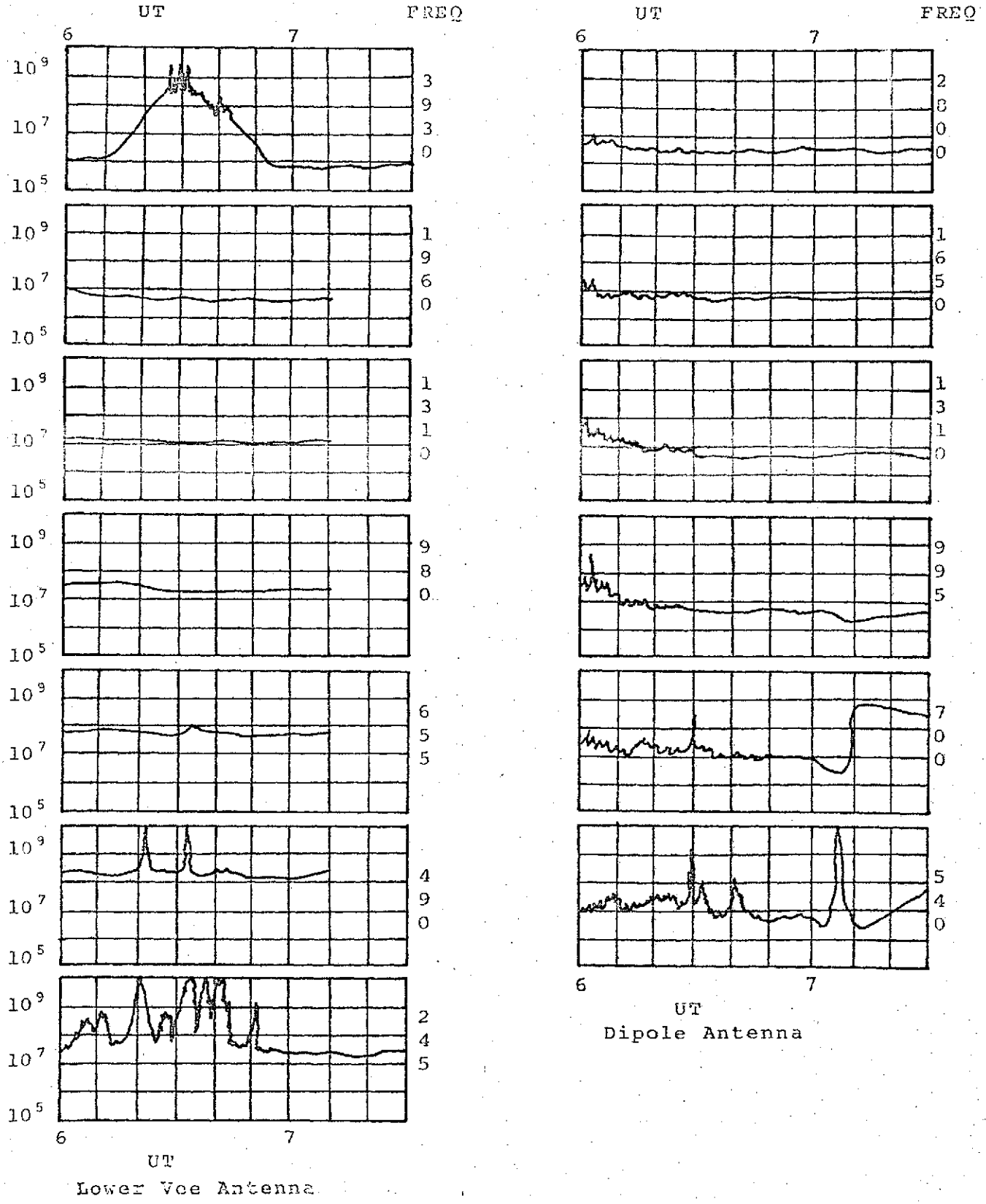


Figure 3-28. RAE Burst Receiver Data for 4 May 1969 (0610 - 0640 UT)

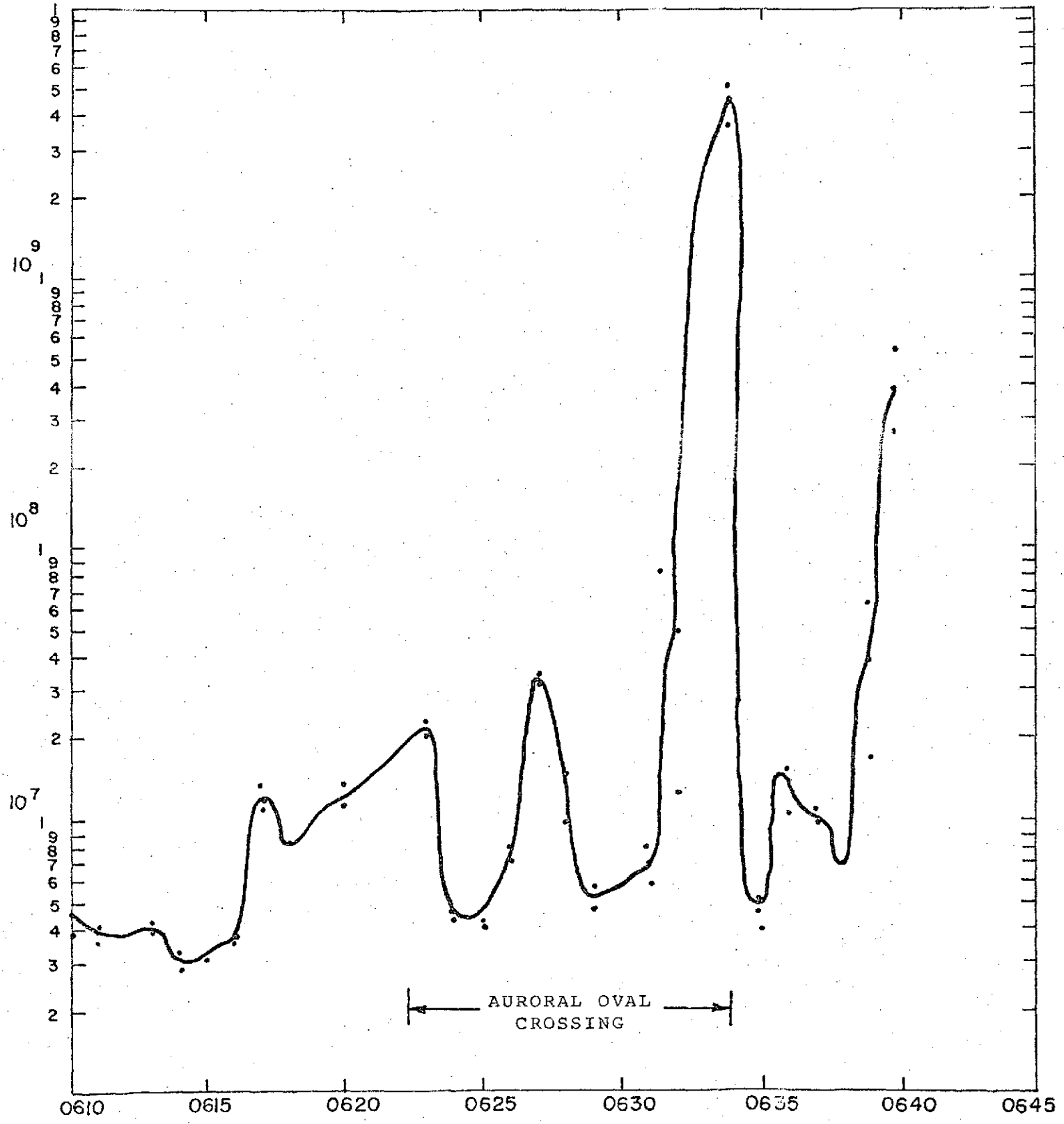


Figure 3-29. RAE I Noise Temperature at 450 kHz on Upper Vee Antenna - 0610 to 0640 UT - 4 May 1969

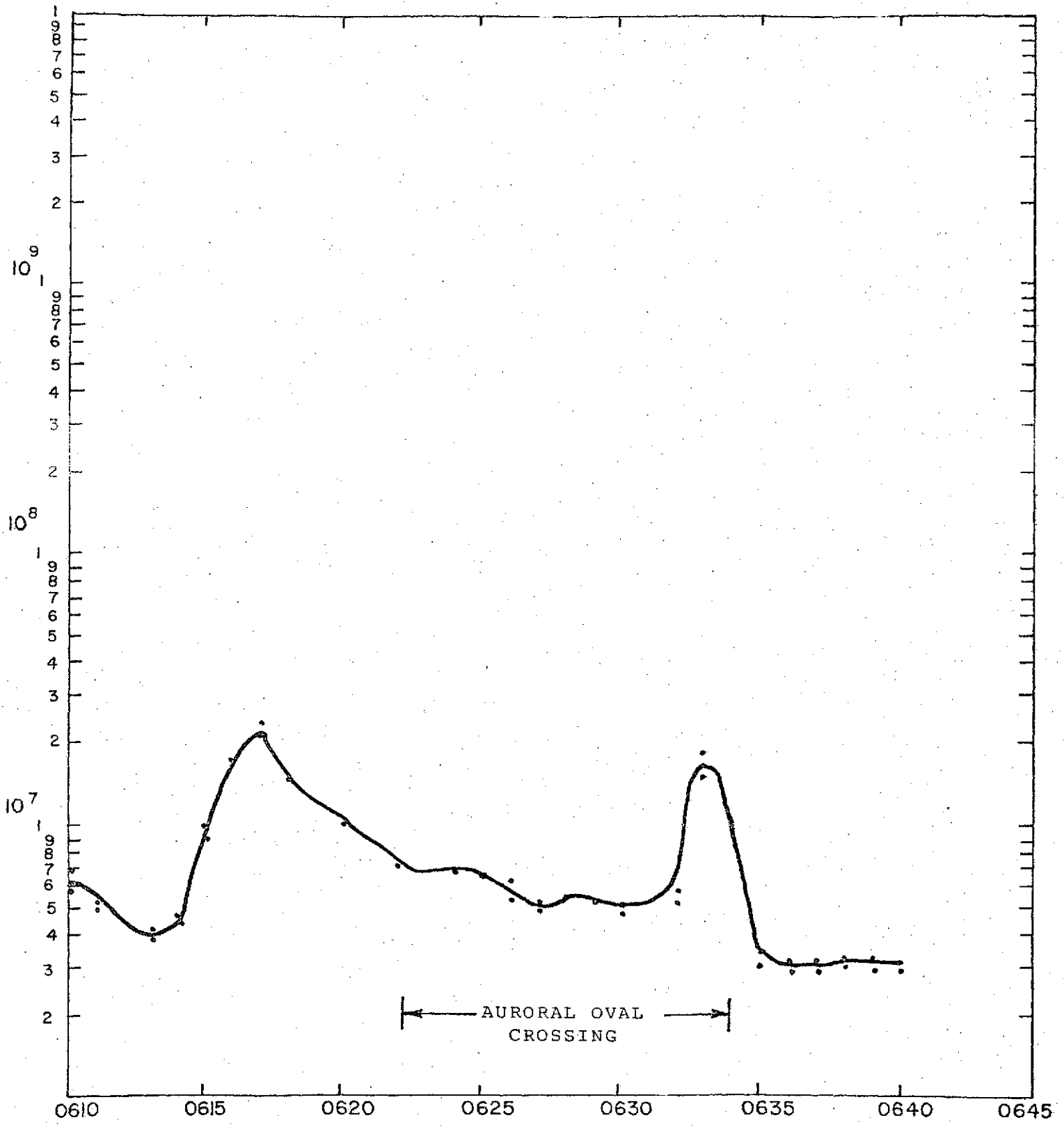


Figure 3-30. RAE I Noise Temperature at 700 kHz on Upper Vee Antenna - 0610 to 0640 UT - 4 May 1969

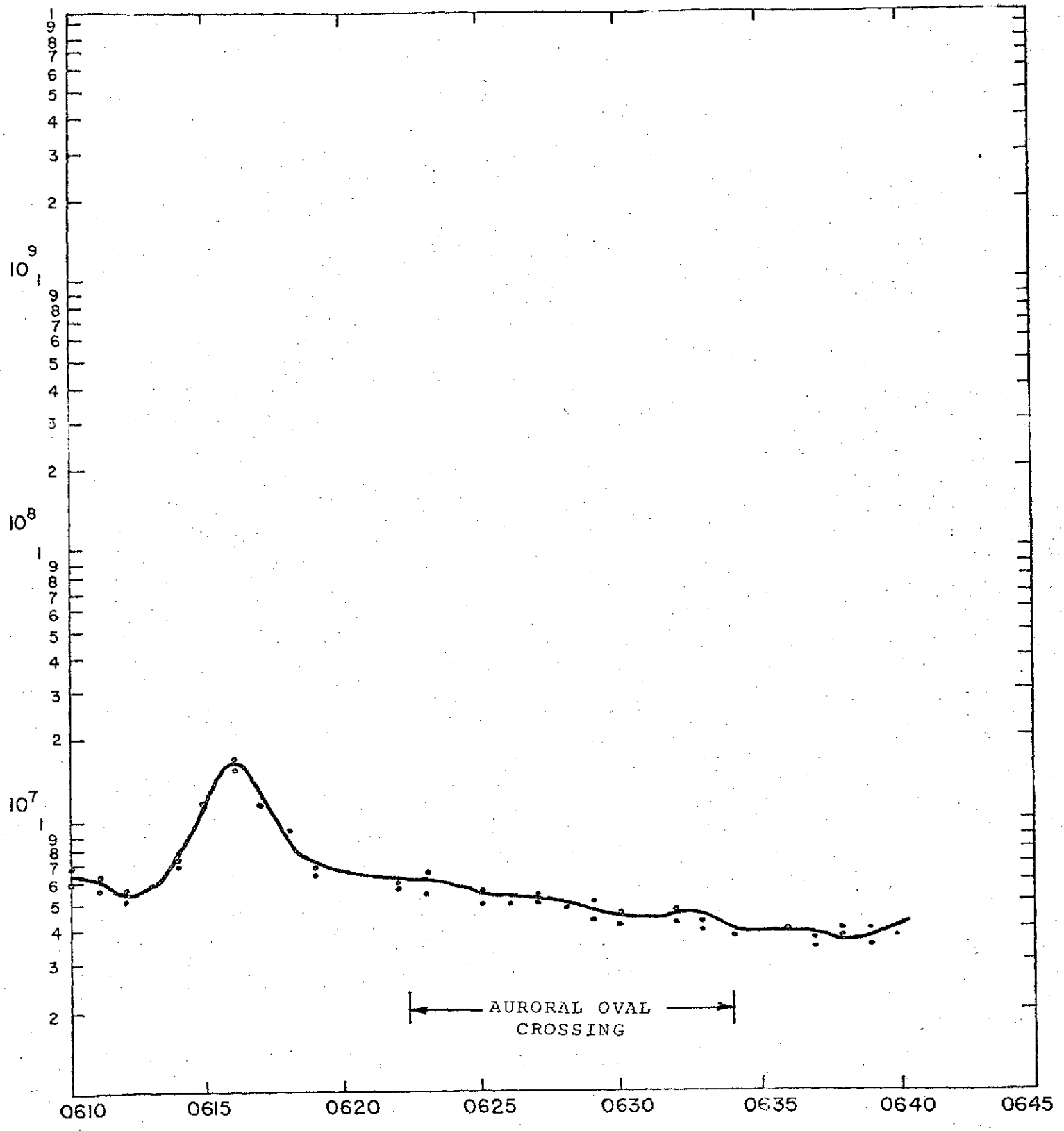


Figure 3-31. RAE-I Noise Temperature at 900 kHz on Upper Vee Antenna - 0610 to 0640 UT - 4 May 1969

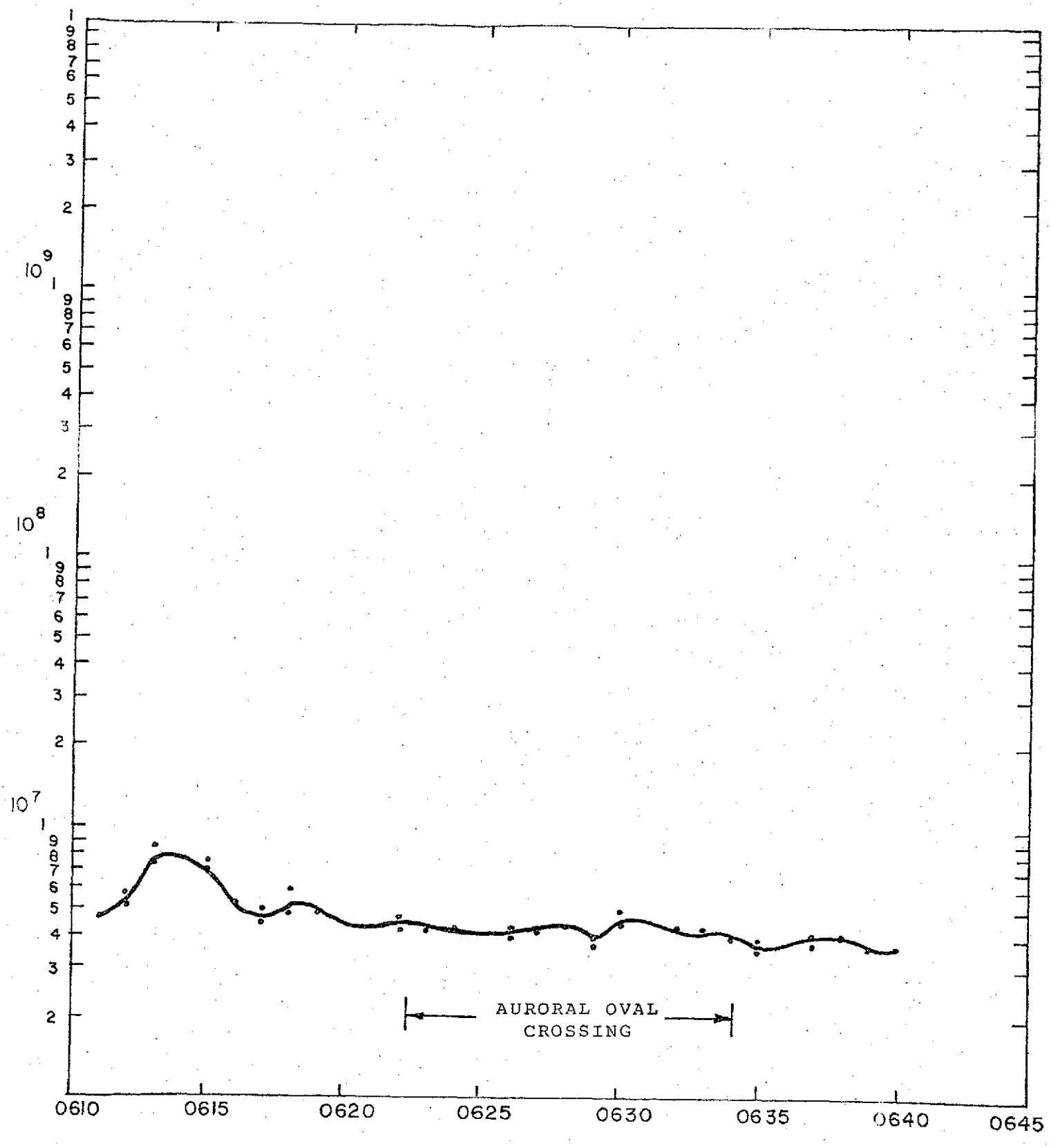


Figure 3-32. RAE I Noise Temperature at 1.31 MHz on Upper Vee Antenna - 0610 to 0640 UT - 4 May 1969

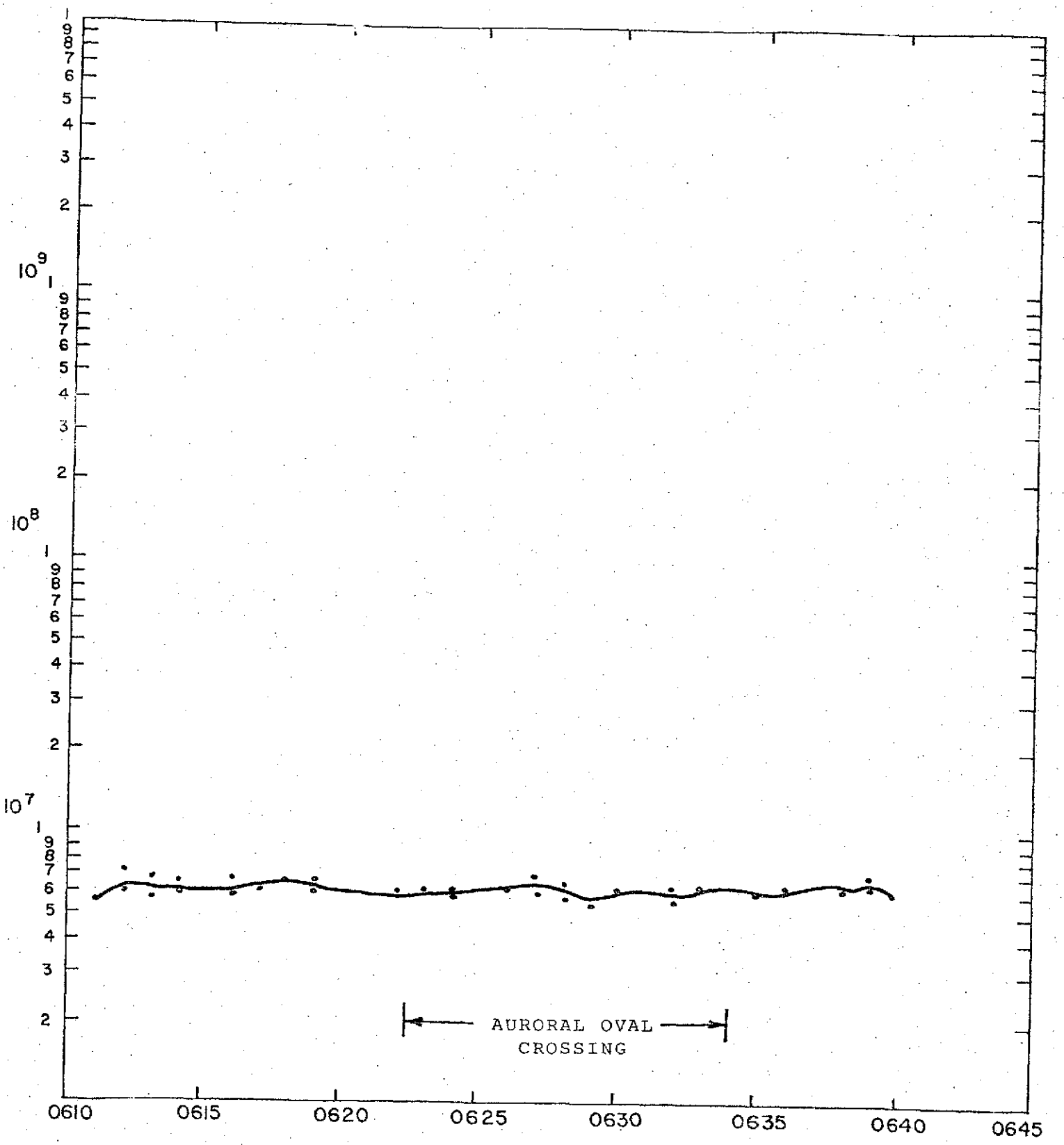


Figure 3-33. RAE I Noise Temperature at 2.2 MHz on Upper Vee Antenna - 0610 to 0640 UT - 4 May 1969

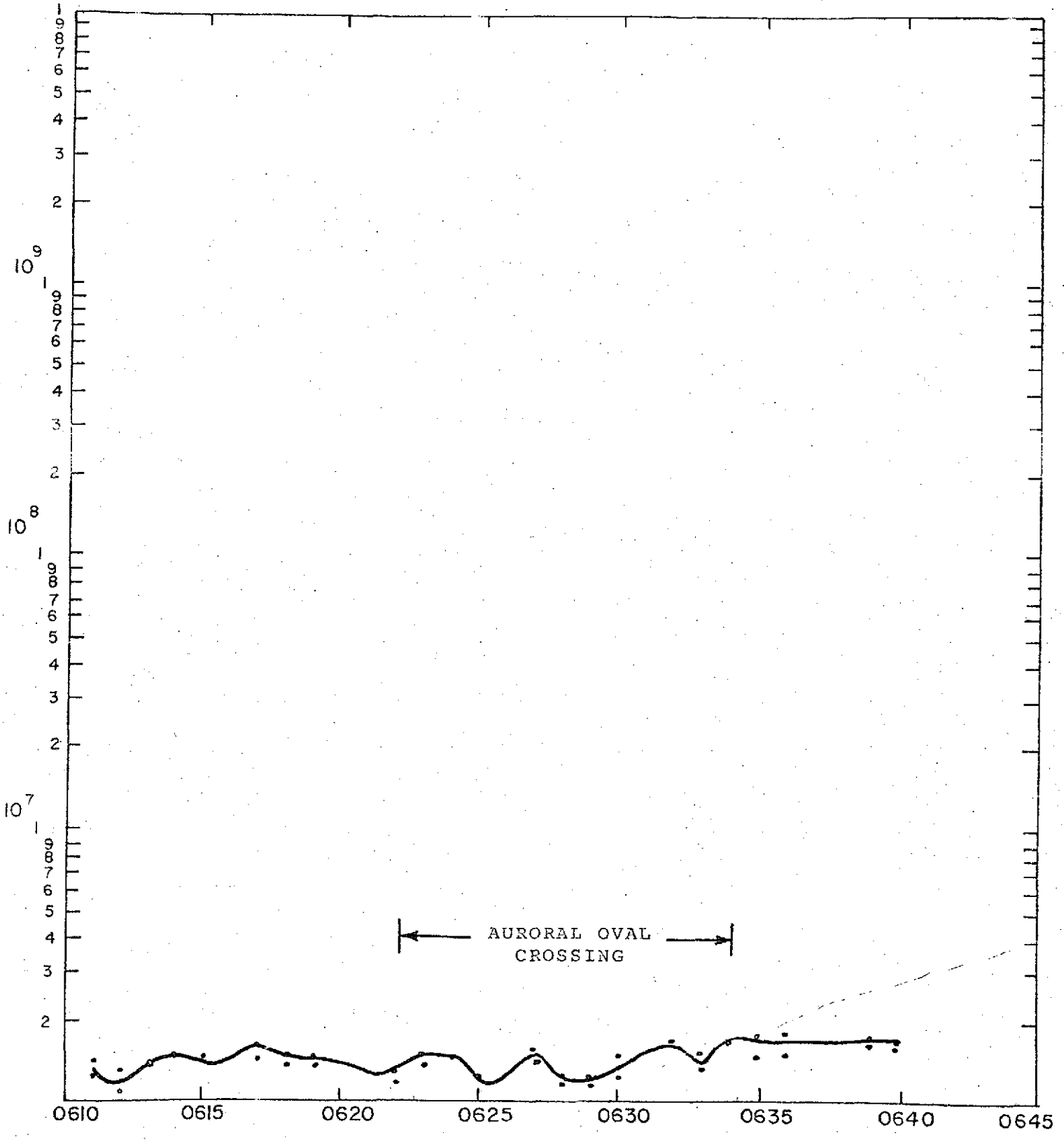


Figure 3-34. RAE I Noise Temperature at 3.93 MHz on Upper Vee Antenna - 0610 to 0640 UT - 4 May 1969

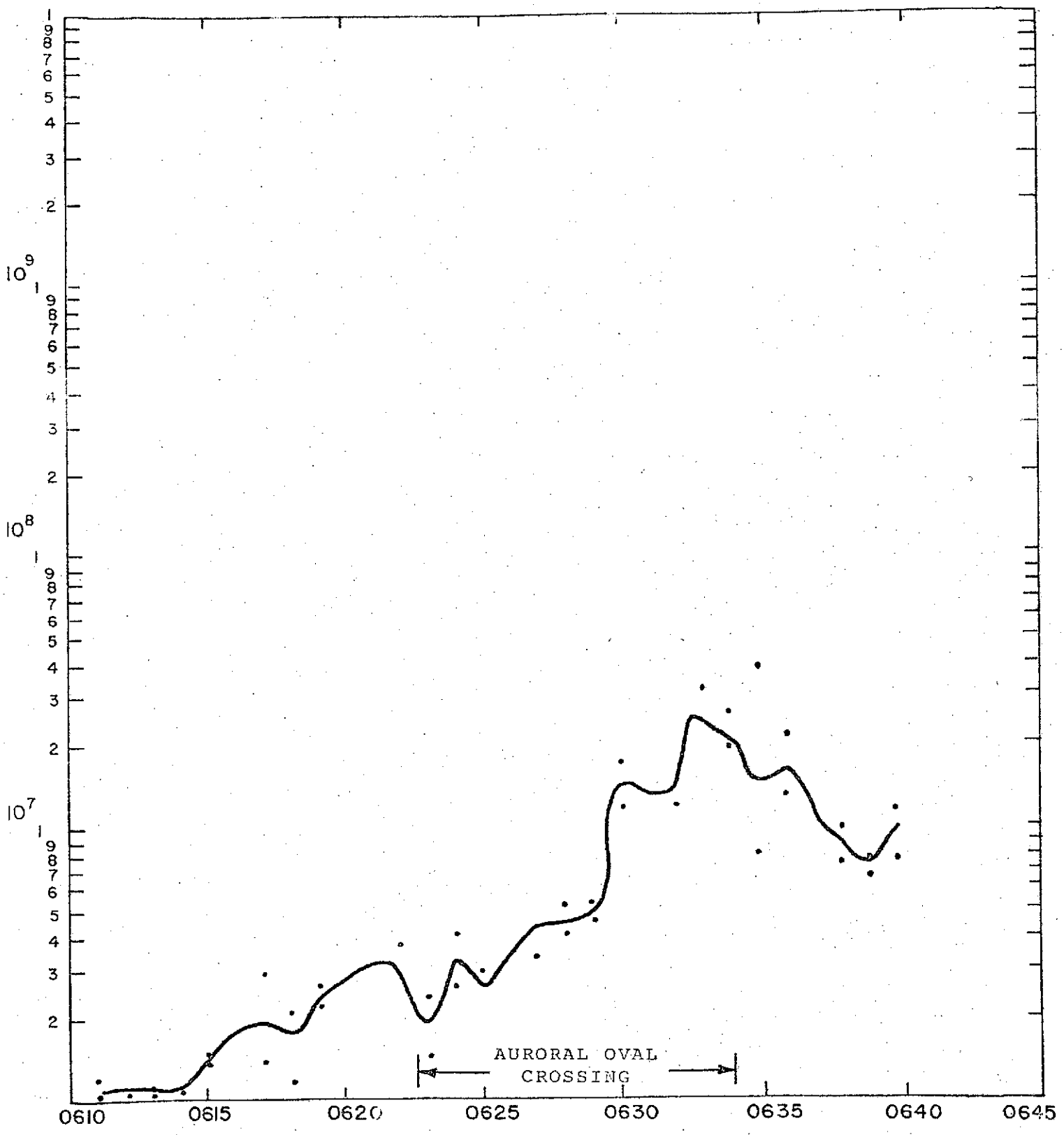


Figure 3-35. RAE I Noise Temperature at 3.93 MHz on Lower Vee Antenna -- 0610 to 0640 UT - 4 May 1969

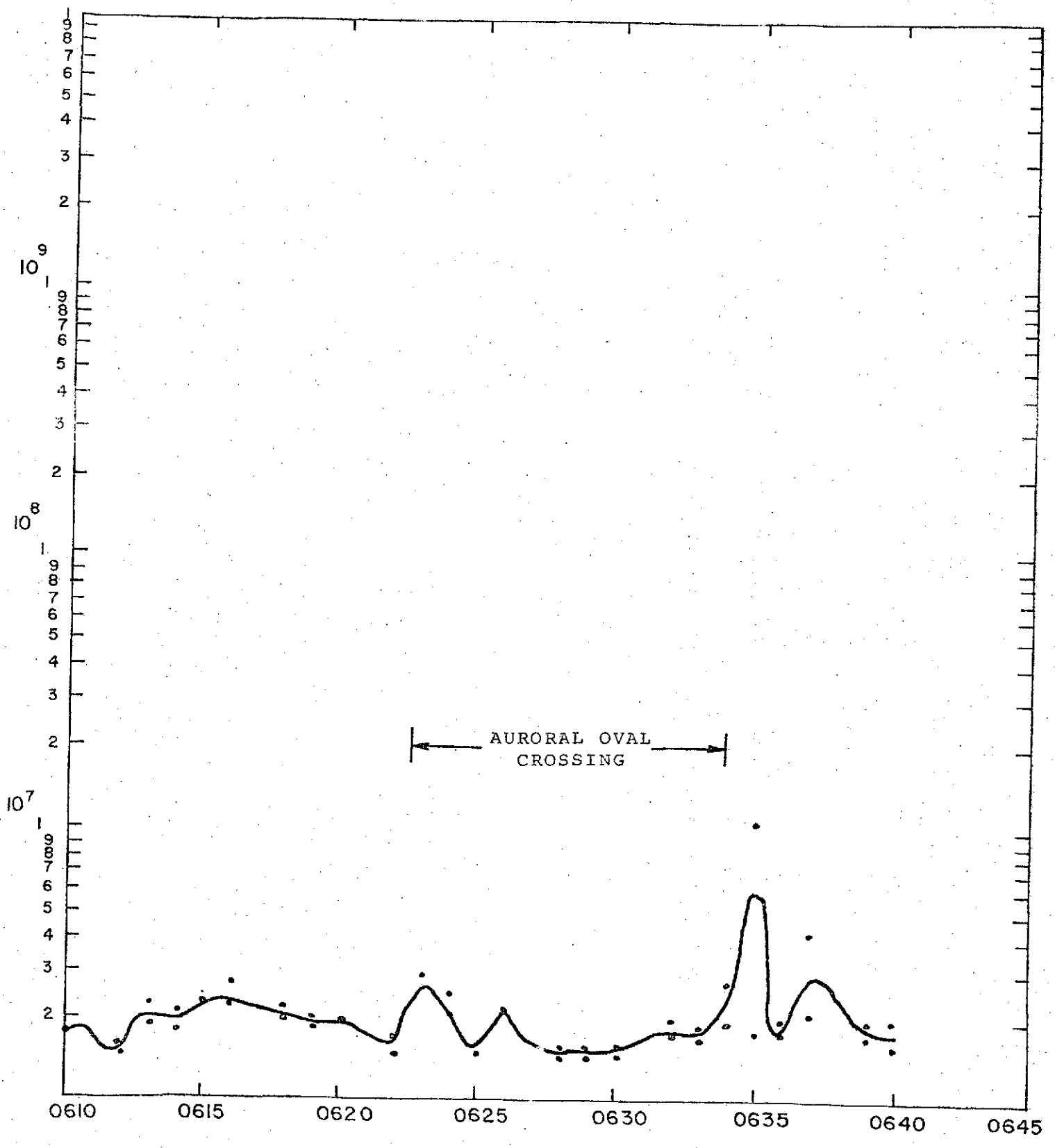


Figure 3-36. RAE I Noise Temperature at 4.7 MHz on Upper Vee Antenna - 0610 to 0640 UT - 4 May 1969

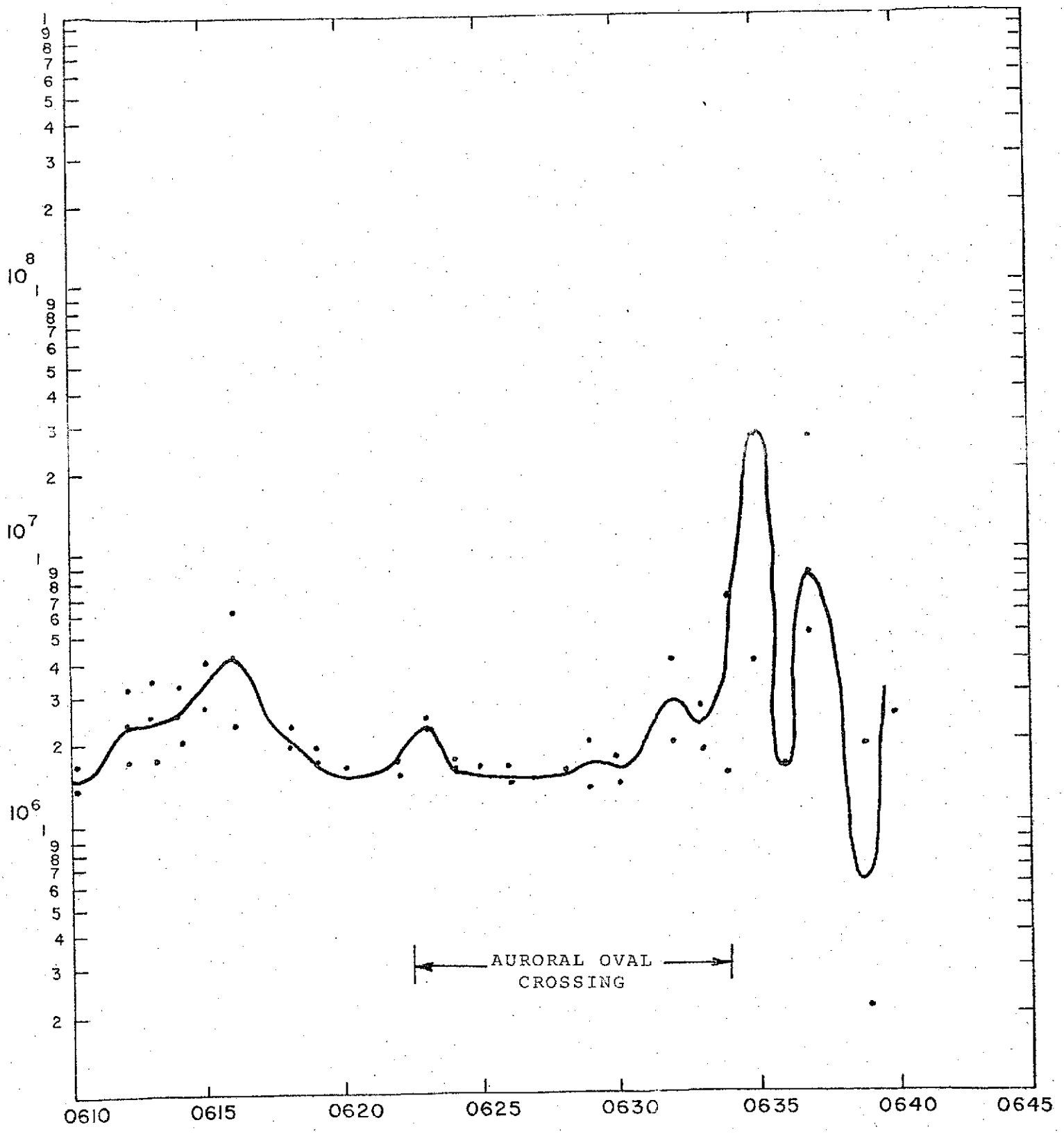


Figure 3-37. RAE I Noise Temperature at 4.7 on Lower Vee Antenna - 0610 to 0640 UT - 4 May 1969

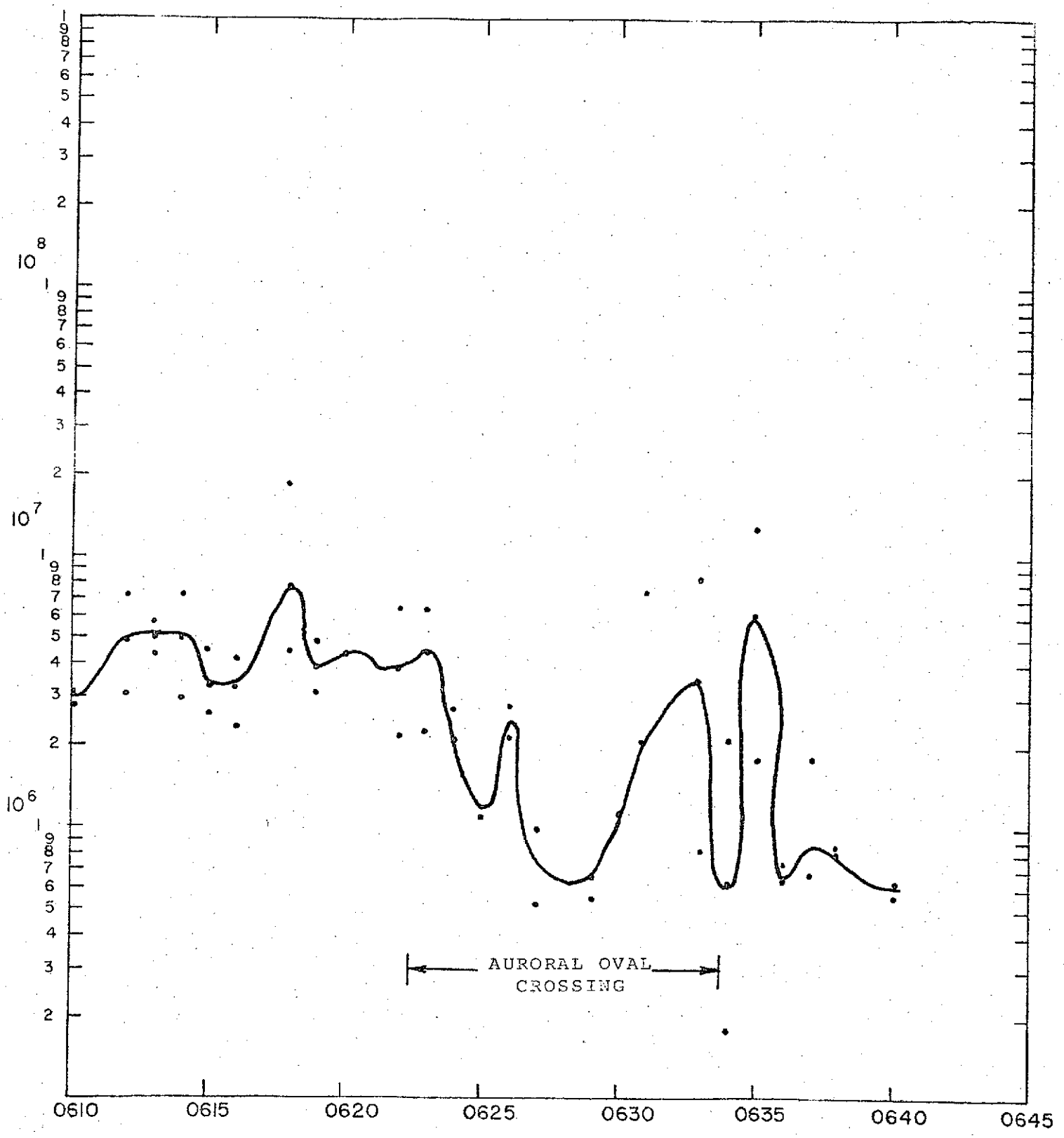


Figure 3-38. RAE I Noise Temperature at 6.55 MHz on Upper Vee Antenna - 0610 to 0640 UT - 4 May 1969

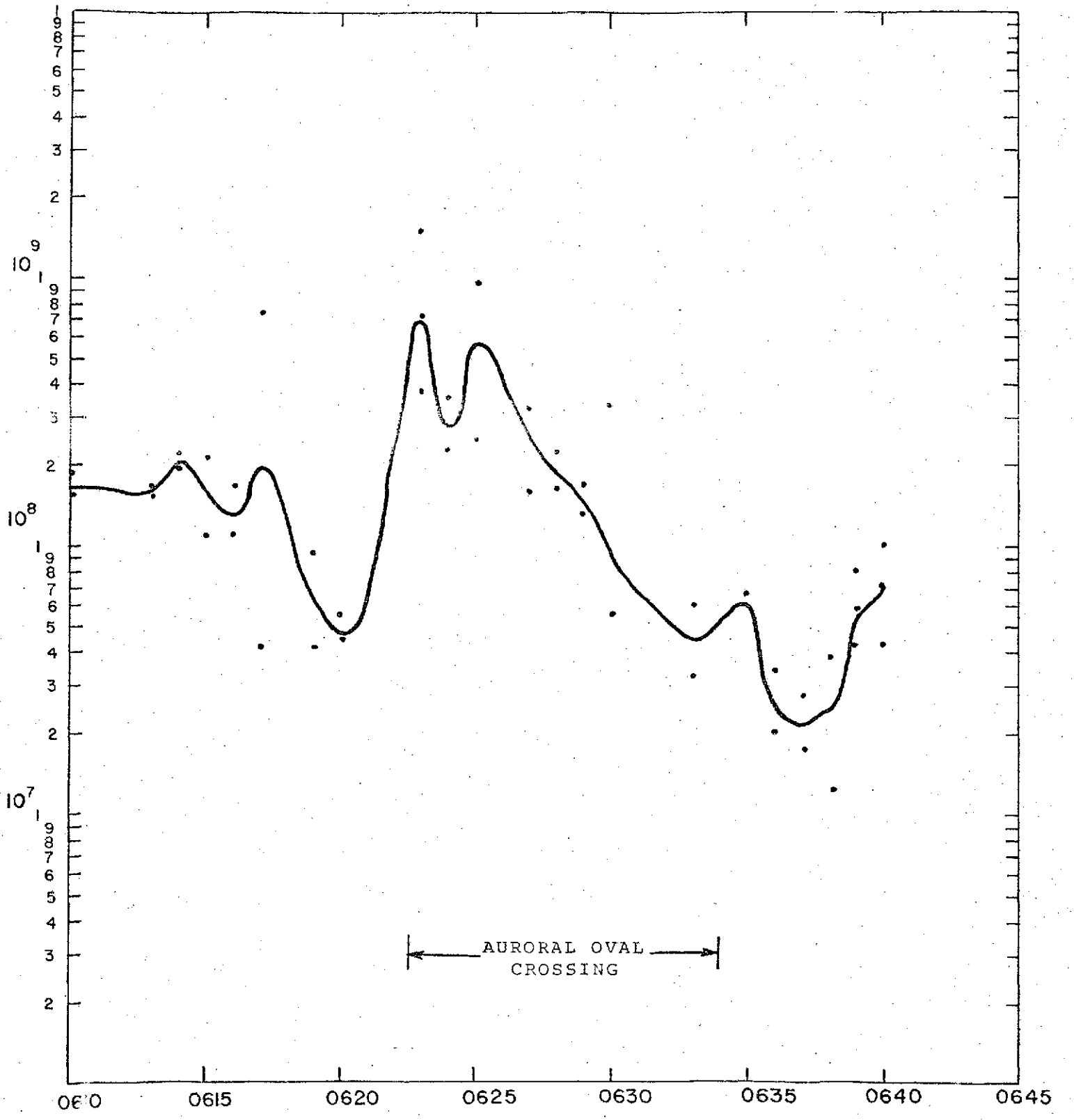


Figure 3-39. RAE I Noise Temperature at 9.18 MHz on Upper Vee Antenna - 0610 to 0640 UT - 4 May 1969

## 3.2.3 SUMMARY OF RESULTS

With regard to the analysis of high latitude phenomena, no clear picture has emerged. For certain, observations by the burst receiver show higher noise temperatures received by the satellite when it is over high latitudes. In general this appears to be the case for all times of day and for both hemispheres. Since the burst receiver monitors the temperature of the dipole antenna which has a large (donut shaped) beam width or viewing pattern, there is some difficulty in ascertaining the source of the increased noise level. Generally speaking, the observed noise level may increase on several or all of the frequencies from 540 kHz to 2.80 MHz as RAE 1 approaches the auroral region. Conversely when RAE 1 recedes from the auroral region the noise levels decrease to their low latitude level. This behavior or pattern is observed for various different levels of magnetic activity without any obvious correlation to the degree of magnetic activity. In some cases there is no clear change in received noise intensity as the satellite crosses over the auroral oval; however, in other instances there is a definite increase in observed noise temperature as the satellite crosses the auroral oval. Since the same pattern is generally observed, i.e. high noise levels over the high latitude regions and low noise levels over the low and equatorial latitudes, one could rule out galactic radiation as the source of this noise. This would follow from the argument that the galactic component should remain relatively constant and certainly not be distributed according to any geographic coordinates.

Furthermore, when considering the R-V receiver measurements with the upper and lower Vee antennas, the noise intensity is almost always greater on the lower Vee. This observation when taken in conjunction with the observation that the

noise intensity at the high frequencies drops off sooner than it does at lower frequencies leads to the conclusion that the radiation emanates from a region below the satellite, but above the peak of the $F_2$-layer. Two further arguments that RAE is not monitoring ground radiation are: 1) Radio noise measurements made at ground level indicate that radio noise levels decrease with increasing latitude and this is not observed by RAE; 2) Examination of RAE noise measurements during polar cap absorption and auroral absorption events (the times of which were supplied by R. Cormiero AFCRL) show no decrease in noise level, which would not be the case if one were observing ground radiation.

Most of the cases examined were for observations made mainly during the nighttime hours, since the high latitude geophysical processes of interest are primarily nighttime phenomena as discussed in Section 3.1. During this time the F-layer ionization decreases and so also does the lowest penetration frequency thus permitting ground radiation to reach the satellite. This effect would be further enhanced with the presence of the high latitude troughs. However, the measured increase in observed noise temperature most likely has its origin in the magnetosphere and represents emission from either precipitating charged particles or electrons trapped in the Earth's magnetic field for the reasons discussed above. Furthermore, daytime observations that were examined also reveal a similar pattern of increased noise level at high latitudes. Particle precipitation does take place on the day side of the Earth's magnetosphere, even though it is most intense in the pre-midnight sector. However, because of the very sporadic nature of the emissions it is not clear whether the noise intensities are strongest around midnight magnetic time, as one might expect if particle precipitation were the responsible generation mechanism.

## 3.3 RF Generation Mechanisms

### 3.3.1 SYNCHROTRON RADIATION FROM TRAPPED PARTICLES

Synchrontron radiation, or the radiation produced by trapped relativistic electrons spiraling down magnetic field lines, is important as a possible source of noise. This may include frequencies from VLF to HF. The objective of this section is to discuss, in brief outline, the synchrotron radiation mechanism as applied to a single trapped electron, to ensembles of trapped electrons, and to energetic electrons trapped in the outer Van Allen belt and precipitating particles near the auroral zone. The predictions of J.F. Vesecky are discussed (see Vesecky, 1969) regarding the possibility that a high latitude satellite may observe 5-20 MHz synchrotron radiation originating from magnetospheric regions above the auroral zones. Finally, the RAE event observed November 3, 1969 from 0310 to 0345 UT is discussed as an example of possible experimental verification of the prediction. The sources of information are extracted from articles in the open published literature and by data provided by RAE. In addition, the possible role of precipitating auroral electrons contributing to the RAE measurement is briefly discussed.

#### SINGLE TRAPPED ELECTRONS

In practice, the synchrotron radiation detected from any given region of the magnetosphere originates from an ensemble of particles (electrons being the most important) spiralling down the field lines. The particles will be distributed in

energy and also in the initial conditions that determine the pitch angle which is an important parameter governing the orbiting particles motion and spatial range. In any given magnetospheric region (the outer Van Allen belts for example) significant temporal variations in particle (electron) density are observed (Vesecky, 1969). The number of trapped particles may exhibit, for example, very large changes during times of magnetic storms (Williams and Palmer, 1965). The significance of the large temporal variation in particle density is that a large temporal variation in radiation may be expected as a consequence. It has been observed that disturbed conditions may increase the trapped particles in radiation belts and also the intensity of auroral particles precipitating at high latitudes.

The radiation from an ensemble of electrons depends, of course, on the characteristic radiation from a single particle, as determined basically by: the particle's energy (hence, its velocity), the pitch angle of the spiralling motion, the strength of the magnetic field B , the charge and mass of the particle and finally, the angle of the observer's position relative to the plane of the particle's motion.

The dynamics of a charged particle trapped by a magnetic field is analyzed in many texts. Of importance as regards radiation emission is the power intensity pattern produced by the orbiting charge for the cases of non-relativistic and relativistic electrons.

In the non-relativistic case, the pattern resembles that of a loop antenna as may be expected. The frequency of radiation is that of the orbiting electron, that is, its gyro frequency:

$$\omega_0 = \frac{eB}{m_0 \gamma} \qquad (3\text{-}1)$$

where: $\gamma = (1-\beta^2)^{-\frac{1}{2}}$

$$\beta = \frac{V}{C} \qquad (3\text{-}2)$$

The relativistic electrons, however, tend to throw their energy forward in a narrow beam. An estimate of the beam width is on the order of:

$$B.W. = \frac{m_0 c^2}{E_T} \qquad (3\text{-}3)$$

where $E_T$ is the total particle energy. In Figure 3-40 examples of patterns as a function of particle energy are shown, where $\theta$, and $\phi$ are the usual polar and azimuthal angles used to describe radiation patterns.

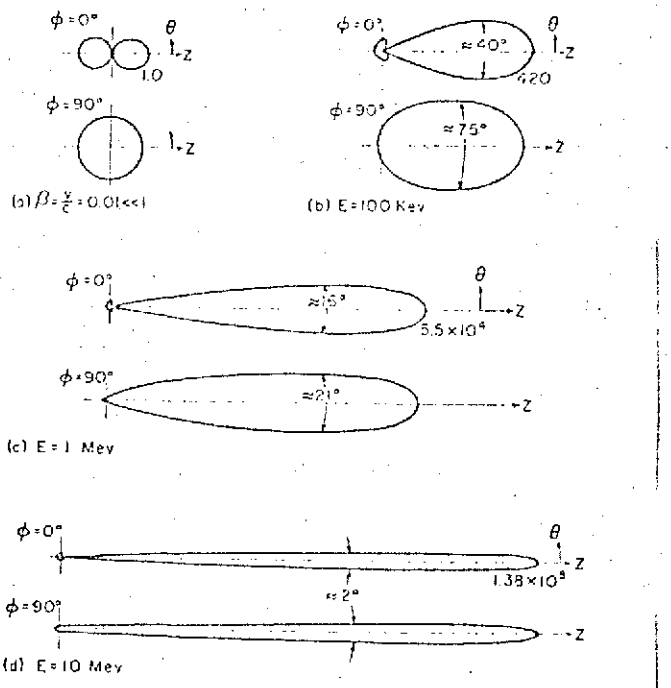


Figure 3-40. Examples of radiation patterns (total power).

The radiation in the non-relativistic case is often called cyclotron radiation. The relativistic electron's radiation is called synchrotron radiation. In the non-relativistic case, the radiation frequency is the orbiting gyro frequency. In the relativistic case, the observer views a pulse of radiation occurring at the particle's gyro frequency.

The Fourier analysis of this wave form then exhibits the harmonics (or line spectra) of the fundamental gyro frequency. The power spectrum for a relativistic trapped electron has been worked out by many investigators. A typical and much used example of the synchrotron power spectrum is given by Panofsky and Phillips as:

$$P_n(\Psi) = \frac{e^2 \omega_0 \beta^3 n^2}{8\pi^2 \varepsilon_0 R} \left[ J_n^1(n\beta \cos\Psi) + \frac{\tan^2\Psi}{B^2} J_n^2(n\beta \cos\Psi) \right] \quad (3\text{-}4)$$

where: $P_n(\Psi)$ is the power radiated per unit solid angle at the angle $\Psi$ for the nth harmonic.

$\omega_0$, $\gamma$, B are defined in equations (3-1) and (3-2)

$\psi$ = the angle out of particle's plane of motion to the observer.

R = radius of curvature which depends on particle energy E, pitch angle $\alpha$ and $B_o$ the magnetic field

B = magnetic flux density

n = number of harmonics

The harmonic frequencies are $n\omega_0$; n = 1, 2, etc.

An expression for the total power radiated by a trapped relativistic electron in the direction $\Psi$ out of the orbital plane is given by Peterson and Hower;

$$P(\Psi,f) = 3.4X10^{-45}\frac{Rf^2}{\beta^2}(1-\beta^2+\Psi^2)^2\left[K_{\frac{2}{3}}^2(\Psi) + \frac{\Psi^2}{1-\beta^2+\Psi^2}K_{\frac{1}{3}}^2(\Psi)\right] \quad (3-5)$$

where $\Psi = \frac{m}{3}(1-B^2+\Psi^2)^{3/2}$ (3-6)

A plot of the above expression for the in plane direction $\Psi=0$ at energies in the .128 MeV to 40 MeV is shown in the Figure 3-41 (Peterson and Hower, 1966).

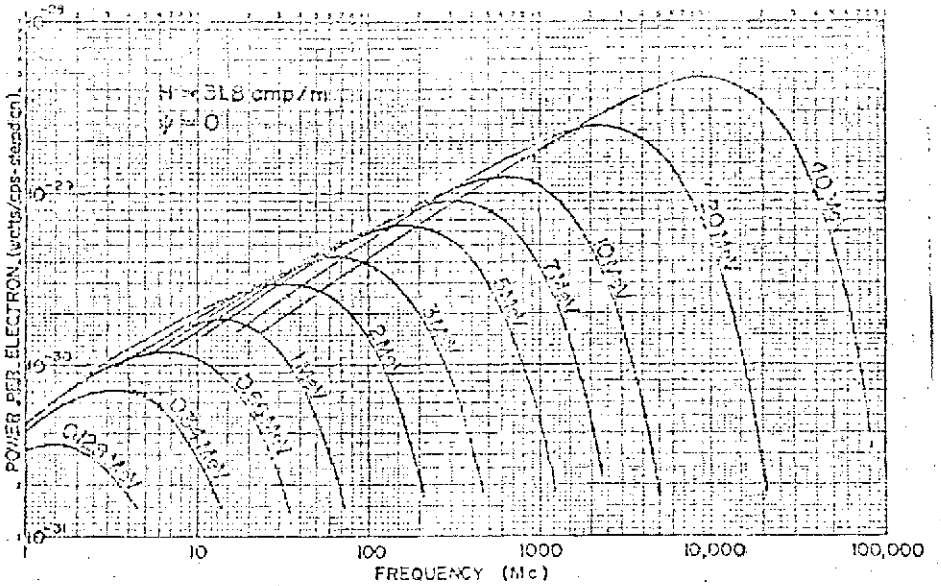


Figure 3-41. Spectra of single electrons (frequency).

The magnitude of the B field chosen to estimate the power per electron is 31.8 amp/m (typical of about 750 km over the auroral zone).

The curves can be easily adjusted to reflect the B field effect on radiation at any other part of the magnetosphere. If the new B is ¼ of 31.8 amp/m for example, then the curves must be shifted down so the peak is at ¼ the original peak, and shifted to the left, so the frequency at the peak is ¼ the original frequency. The Figure 3-42 (Peterson and Hower, 1966) gives an example of adjusting the power vs. f curve for a 10 MeV electron from B field 31.8 to 31.8/4.

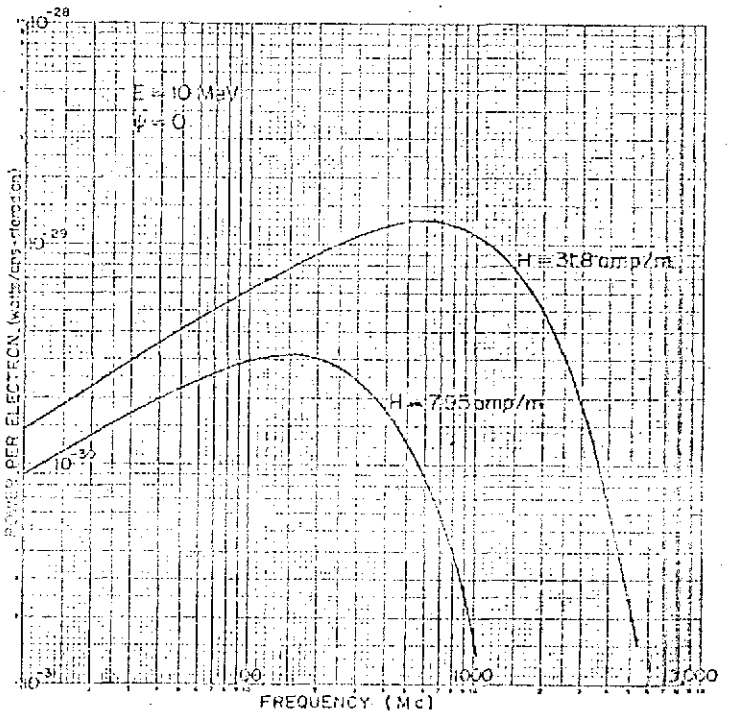


Figure 3-42, Effect of change in B on the spectrum of A 10 MeV electron.

It is readily noted from the plotted values of Figure 3-41 that, at any particular frequency, the more energetic electrons produce the most intense radiation. At the same time, at the lowest frequencies (1-10 MHz) the most energetic electrons (20-40 MeV) will produce less radiation than some of the lower energy particles. For any given frequency of radiation there is an optimum electron energy and the higher the emitted frequency, the higher the energy of the particle must be to produce significant radiation.

## ENSEMBLES OF ELECTRONS

To determine the radiation from an ensemble of electrons at a frequency f, it is required to have an estimate of the number density and energy of particles whose patterns will lie within a receiving antenna pattern. This is largely a geometrical problem. The estimate of power for a single electron pattern out-of-plane angle $\Psi$ will determine the extent of

the electron density region whose radiation will be received. If $P_r$ is the total received power of frequency f from a magnetospheric region of volume V, distance r from a receiver, then:

$$P_r = \iiint \frac{P(\Psi,f,E,B,\alpha)}{r^2} \rho(E,\alpha,r)\,dv\,dE\,d\alpha \text{ Watts/m}^2 \text{ cps} \qquad (3\text{-}7)$$

where: $P(\Psi,f,E,B,\alpha)$, is the total power of a single electron and $\rho$ is the number density of particles of energy E, etc. The above expression may also include a multiplicative attenuation term if the propagation medium is absorbing. The two possible mechanisms for absorption are: a medium of non-zero conductivity lying between receiving antenna and radiating region when collision frequency and charged particle density are high enough at the frequency considered; and the loss of radiated energy to increase the synchrotron "self-absorption" motion of electrons. For an auroral case similar to that of interest, the two have been shown to be insignificant(Vesecky, 1969). Obviously, the evaluation of equation (3-7) requires considerable knowledge of the radiating region. Conversely, a measurement of $P_r$ may allow an estimate of a property of the region such as the number density of particles.

To estimate the possibility of viewing synchrotron radiation from a region (e.g. outer Van Allen belt) along a ray path traversing the region, requires that the geometry and particle morphology be modelled sufficiently accurately based on measured data and suitable semi-empirical or theoretical models.

Once the morphology of a given region is determined, that is, the spatial, temporal and energy distribution of particles (electrons and protons) in a particular region of space so

that the $P(\Psi,f,E,B\alpha)$ and $\rho(E,\alpha,r)$ of equation (3-7) can be evaluated then the received power can be estimated. Equation (3-7) is then put into a more readily useful form which allows integration along a ray path from radiating region to receiver. These may be curved paths if the intervening medium varies systematically in refractive index. The intervening medium may also scatter or absorb energy. These effects must be accounted for if of significant magnitude.

Peterson and Hower (1966) have shown that it is convenient to express the received power in terms of the brightness b:

$$b = \frac{2kT}{\lambda^2} = \int P(\Psi,f,E,B,\alpha)\rho(E,\alpha,r)\,dr\,dE\,d\alpha \qquad (3\text{-}8)$$

and Vesecky has chosen to re-express equation (3-8) as follows (see Veseky, 1969):

$$b = \int_{s_0}^{\infty} J(f,s)\,ds \qquad (3\text{-}9)$$

where:

$$J(f,s) = \int_{0}^{\infty} P(f,E,s)N(E)\,dE \qquad (3\text{-}10)$$

$N(E)$ is the number density of particles having an energy lying within E and E+dE and s represents an arc length along the propagation path with the receiver at $s_0$.

Given the morphology of a particular radiating medium traversed by a ray path to a receiver, considerable simplifications can be introduced into the evaluation of b using equation(3-9), particularly for energetic particles $E \geq .5$ MeV.

Then it is convenient to take $\alpha = \frac{\pi}{2}$ and $\Psi=0$ as reasonable estimates.

## MORPHOLOGY OF PARTICLES AFFECTING RAE

The objective is to examine the possibility of synchrotron radiation contributing to or determining the noise received when RAE crosses the polar auroral regions. Since the position of RAE is known as it crosses the polar regions for any particular orbital pass (e.g. Figure 3-9), and also the antenna orientation and pattern for each frequency is known, it is possible to determine the possible directions where received noise must originate. The second directional bit of information is determined essentially by the direction of the magnetic field in regions where trapped or precipitating particles occur together with the expected distribution of pitch angles. These determine a range of planes which contain the direction of particle motion. For synchrotron radiation most radiation is confined to the planar direction. The amount of out-of-plane radiation (as determined by the angle $\Psi$) depends on the frequency. Finally, by matching up receiver antenna pattern direction and the directions of planes normal to field lines in regions of significant particle density and energy, the receiving rays can be estimated which provide maximum received radiation. The integration of equation (3-9) then allows determination of b.

Figure 3-43 shows examples (taken from Peterson and Hower) of the effect of frequency and electron energy on the single relativistic electron's beam width as measured approximately by the out-of-plane angle $\Psi$.

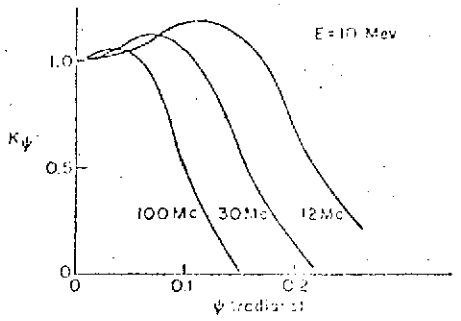


(a) Emission Pattern at Several Different Frequencies

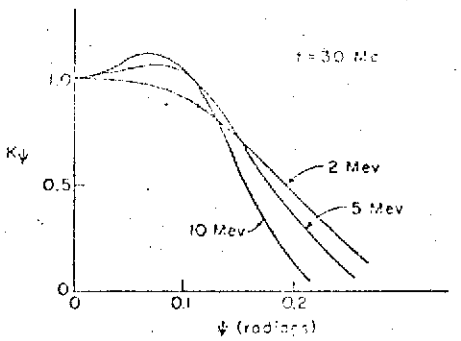


(b) Emission Pattern at Several Different Energies

Figure 3-43. Examples of emission patterns.

Some qualitative information regarding two regions that are candidate sources of synchrotron radiation in the .7 MHz-9.18 MHz range received by RAE in polar regions is presented in the following paragraphs.

## OUTER BELT AT HIGH LATITUDES

As noted by Hess (1968) measurements by satellites show that trapped fluxes normally stop fairly abruptly at some particular latitude and show a diurnal variation at high latitudes. Figure 3-44 depicts the latitudinal extent of stable trapped particles.

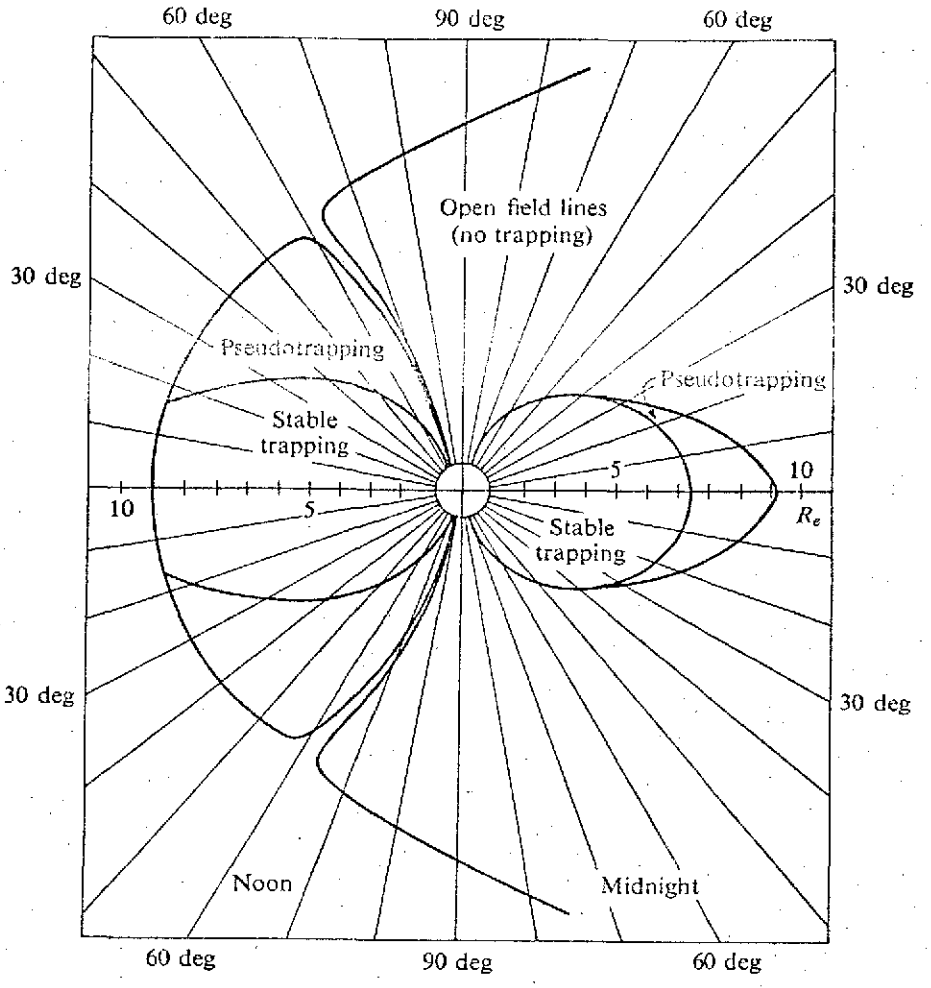


Figure 3-44. Calculated locations of the regions of quasitrapping (or pseudo trapping) in the magnetosphere. Particles mirroring inside those regions are unable to complete a 180-deg drift around the Earth. Those injected into the left side will be lost into the tail; those injected into the right portion will abandon the magnetosphere through the boundary on the day side [60].

Figure 3-45 indicates the limit of trapping (in the invariant coordinate system) with respect to a normalized flux J (see Hess, 1968):

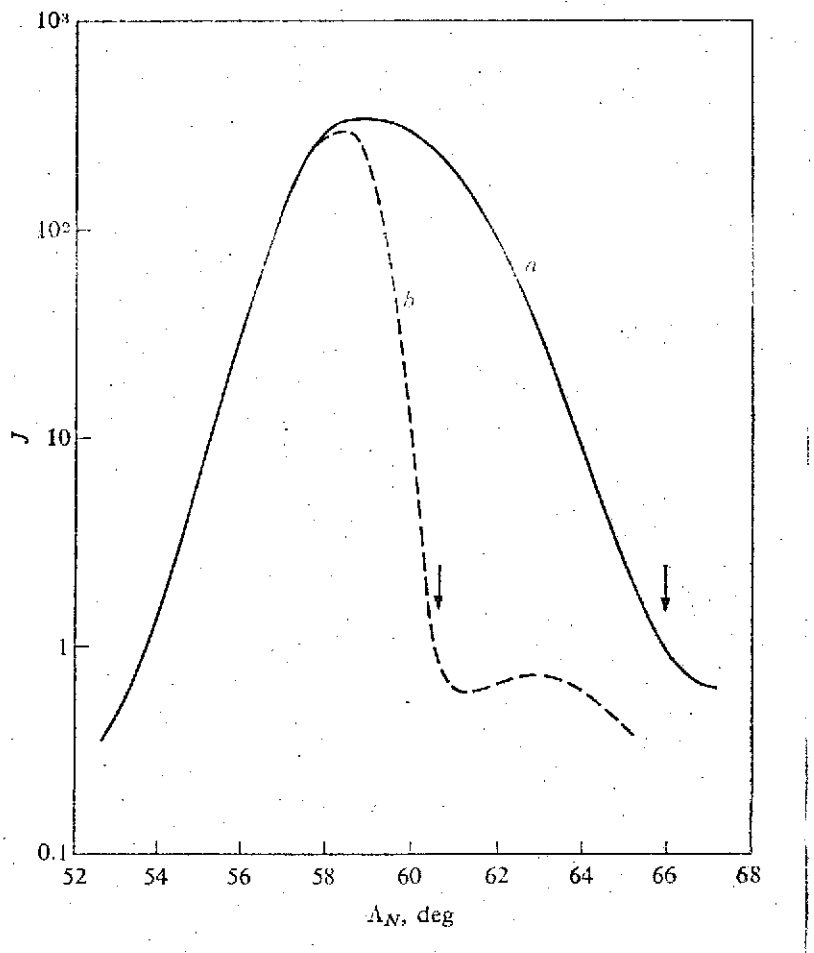


Figure 3-45. Behavior of the upper limit of trapping $\Lambda_N$ (shown by arrow) before the magnetic storm of April 1 to 2, 1964 (curve *a*) and during the main phase of this storm (curve *b*). The decrease in $\Lambda_N$ is consistent with the measured increase in tail field during this storm [53].

Typical energy spectra for protons and electrons in the outer belt are presented below (see Hess, 1968). A characteristic of proton flux is that it is quite stable in time, whereas electron fluxes are highly variable in time. For both particles, an exponential model of particle flux as a function of particle energy is widely used for curve fitting measured data.

Figure 3-46 gives the value of $E_o$ relating flux J and energy E by:

$$J = K \exp\left(-\frac{E}{E_o}\right) \qquad (3\text{-}11)$$

based on measured data for a range of pitch angles over L shell regions L=2 to L=7. Curves may be extrapolated to L=10.

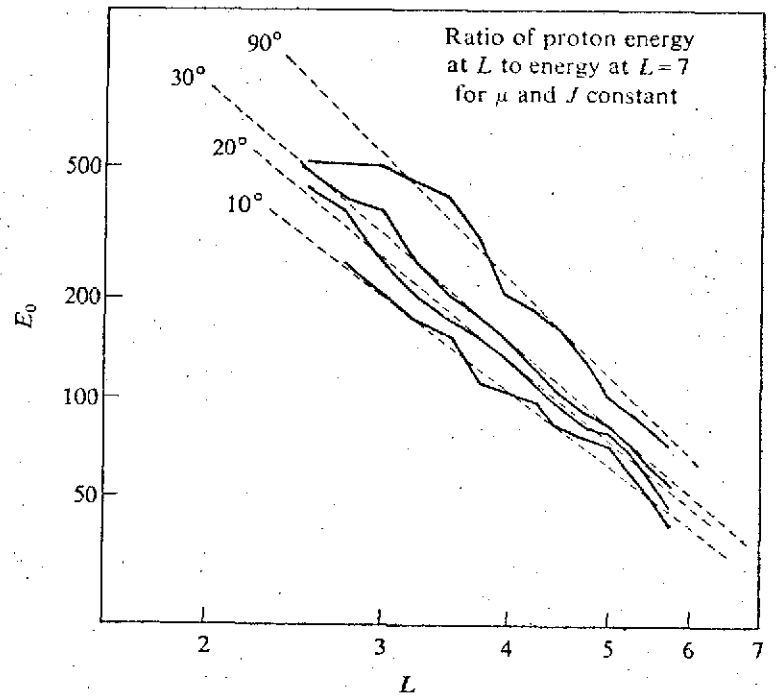


Figure 3-46. Comparison of measured e folding energies $E_o$ from data of Davis and Williamson [1] with calculated energy variation of protons during radial-drift conserving $\mu$ and $J$ for various initial pitch angles at $L = 7$ [6].

Similarly, Figure 3-47 and Figure 3-48 show typical flux of energy E electrons over L shells ranging from L=1.74 to L=8.20.

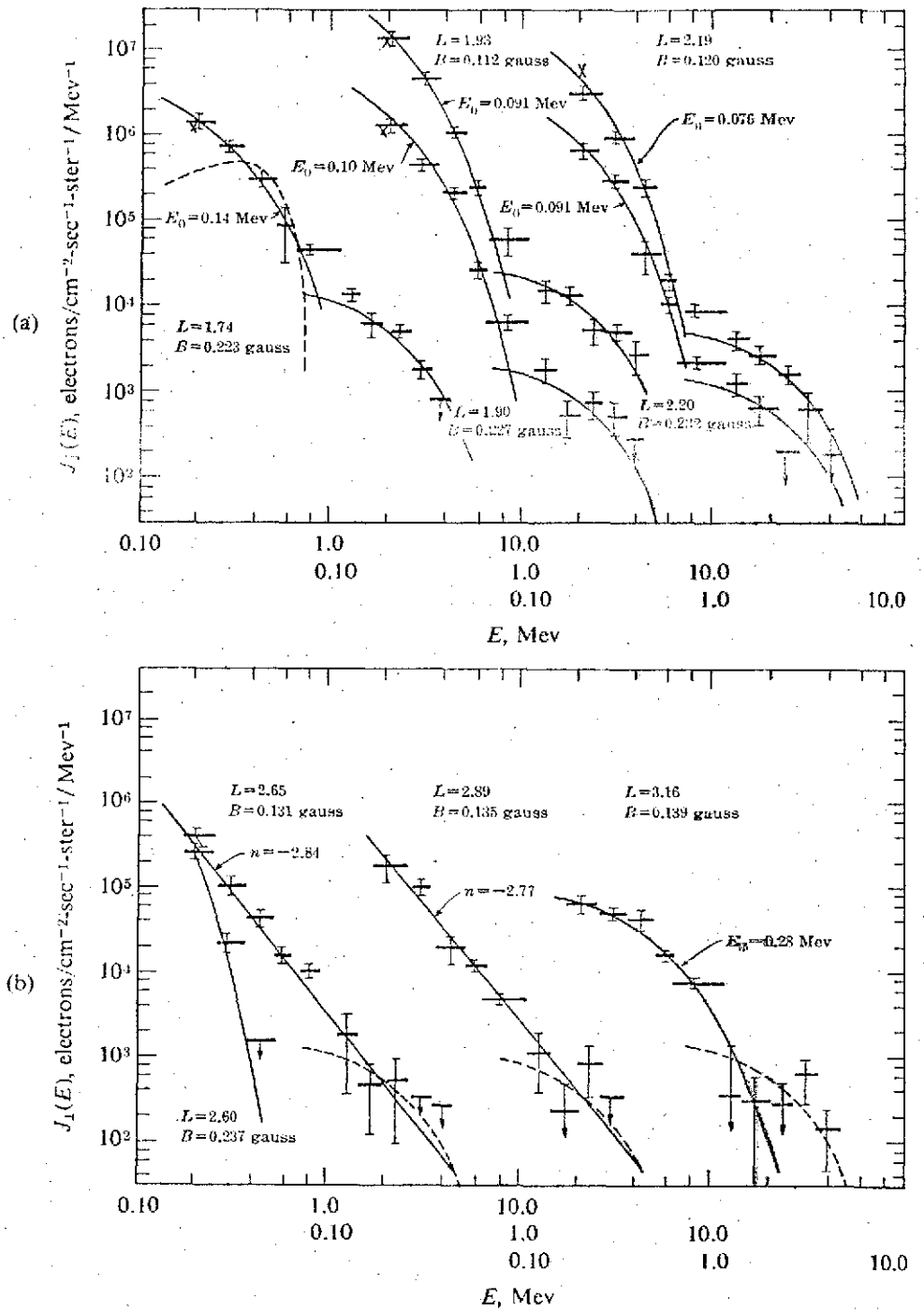


Figure 3-47. Typical differential electron-energy spectrum measured on Satellite 1964-45a on August 15, 1964. (a) $1.7 < L < 2.2$. Exponential distributions are fitted to the soft component, and an equilibrium fission-data spectrum is fitted to the hard component. The neutron $\beta$-decay spectrum is given as a dashed line with the data of $L = 1.74$. (b) For $2.4 < L < 3.2$. Power laws are fitted to two sets of data. The data at $L = 3.16$ are fit better by an exponential system. Fission $B$ spectram fitting the high-energy points are given as dashed lines.

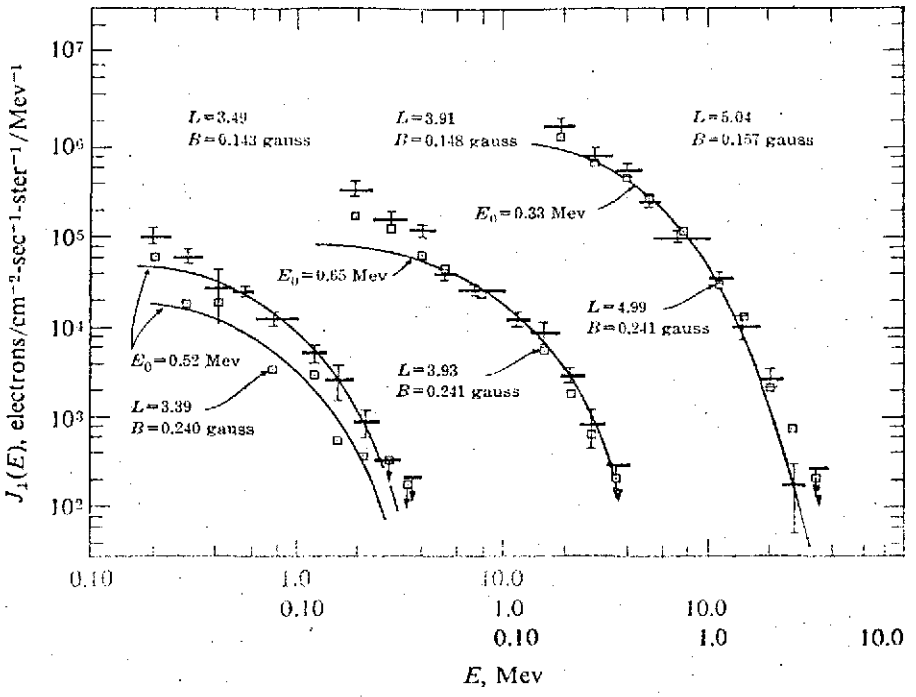


(c)

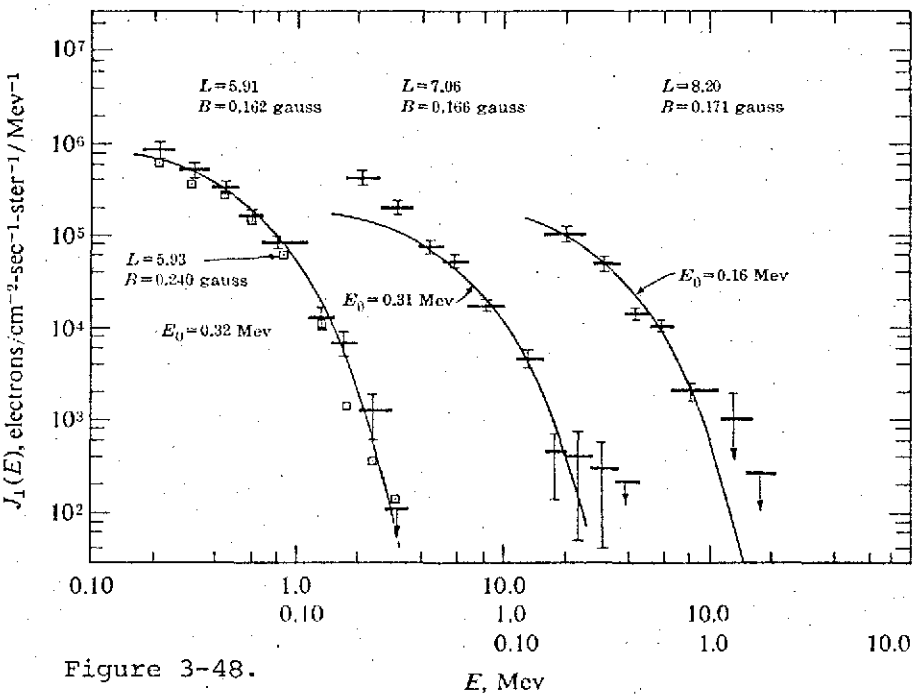


(d)

Figure 3-48.

Typical differential electron-energy spectrum measured on Satellite 1964-45a on August 15, 1974

(c) For $3.4 < L < 5.0$. Exponential spectra fit the data above 0.5 Mev. (d) For $5.9 < L < 8.2$. Exponential spectra fit the data given.

An exponential modeling of electron flux J by energy E is given by equation (3-11)

Diffusion of both protons and electrons is an important process partially determining spatial and temporal distribution of the particles (see Hess, 1968).

Figure 3-49 provides data and estimates of electron fluxes in the inner zone (see Hess, 1968).

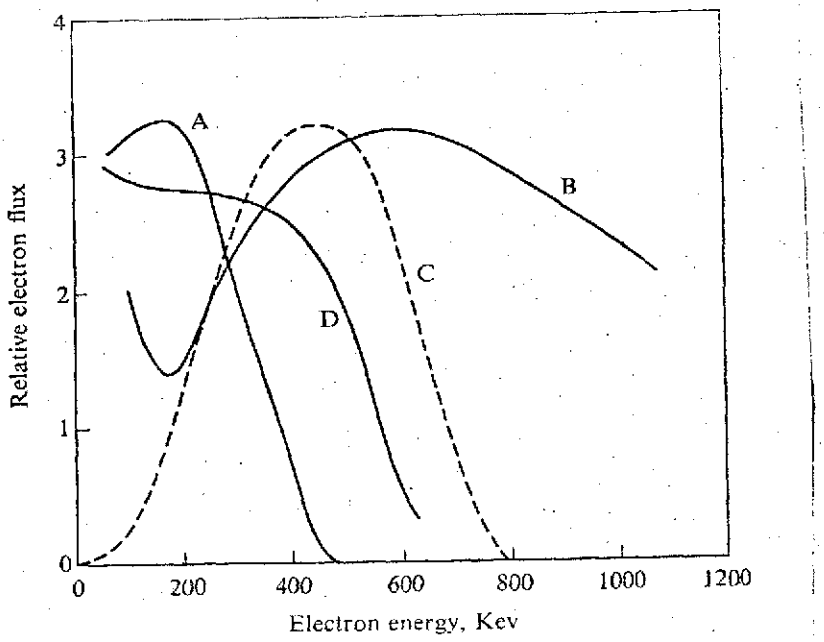


Figure 3-49, Various energy spectra of inner-zone electrons. A indicates the spectrum measured by Holly *et al.* [46], B the spectrum measured by Mann *et al.* [48], C the calculated electron spectrum [52], and D the spectrum measured by Imhof *et al.* [47].

The information in Figures 3-45 through 3-48 yield E, $\alpha$ and $\rho$ which, together with frequency versus energy estimates of Figure 3-42, allow estimates of brightness b according to equation (3-8) when the spatial morphology of B and fluxes are more precisely given.

## AURORAL PRECIPITATING PARTICLES

It is assumed that the region of precipitating particles lies within the pseudotrapping region shown in Figure 3-44. It is apparently accepted that most of the particle energy brought into auroral zones is of energies E < 30 keV, with the possibility of significant numbers of higher energy also present. The data of many experiments of energy flux measurement is summarized in Figure 3-50 (see Hess, 1968) for electrons. The spectra of protons is probably roughly similar.

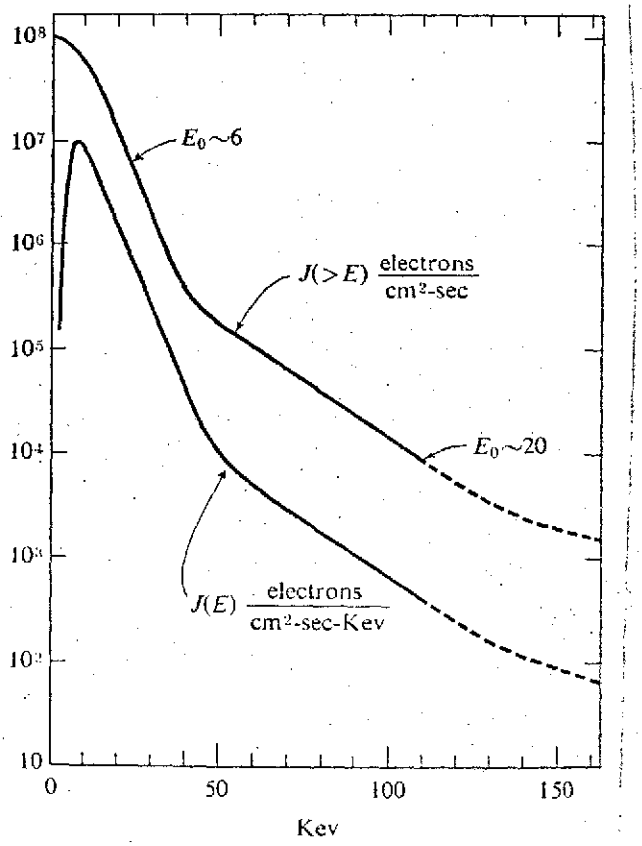


Figure 3-50. Typical electron-energy spectra of precipitating auroral electrons based on various experimental data. Both a differential and energy spectra are shown. The high-energy region shown as a dotted line is not yet well known.

Figure 3-51 (see Hess, 1968) in effect provides evidence that the origin of precipitating auroral electrons is not primarily from the region of stably trapped electrons and protons. The rationale is that usually the fluxes of precipitating and stably trapped particles increase at the same time, hence, the stably trapped particles are not the immediate and significant source of precipitating particles.

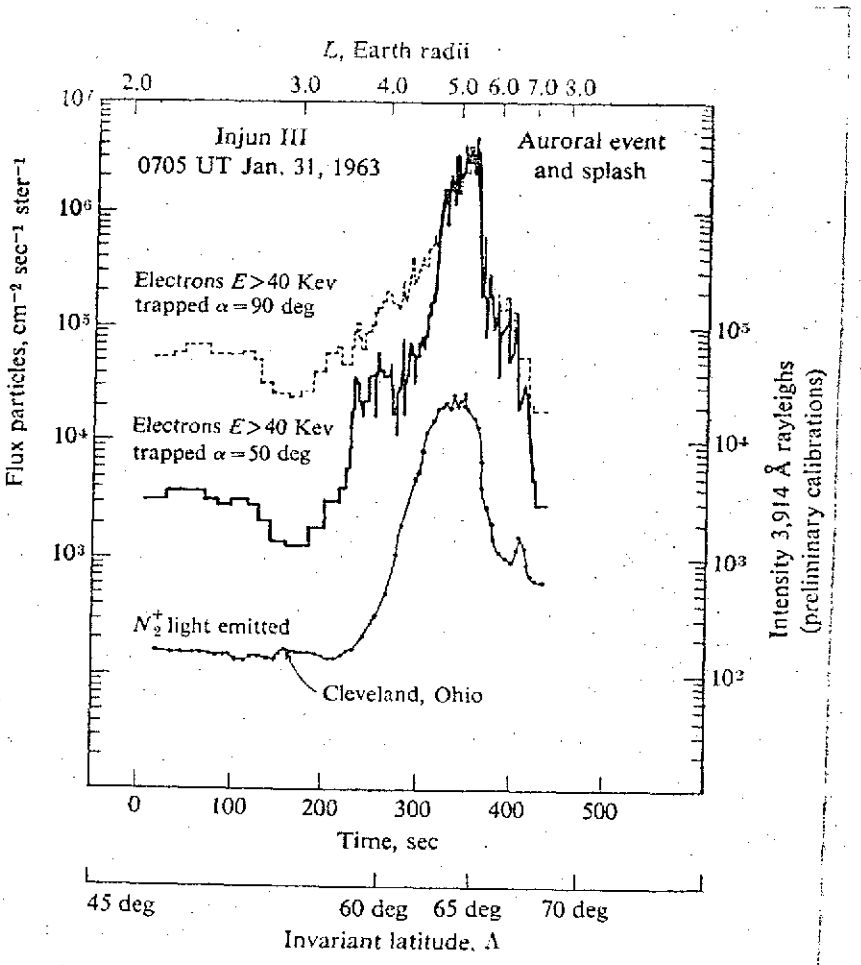


Figure 3-51 Measurements of trapped and precipitated particles and 3914 Å auroral emission from a pass of the Injun III satellite showing the simultaneous increases of trapped and precipitating particle fluxes [14].

The direction of synchrotron radiation originating from precipitating auroral particles will be in a plane approximately normal to the magnetic field lines originating in a region about the auroral oval and projected upward in altitude.

## VESECKY'S PREDICTION OF HIGH ALTITUDE RECEPTION OF 5-20 MHz

Vesecky undertook calculation of synchrotron radiation brightness b according to equations 3-7 , 3-8 , and 3-9 and a model of outer belt radiation fluxes of relatively high energy by Vette. The latter is a codification based on numerous satellite measurements (see Vesecky, 1969). Figure 3-52 shows a plan view of an (optimum) region of synchrotron radiation at an altitude of 4,000 km. Since the most intense radiation from this region lies in a plane normal to the earth's magnetic field lines, it may be detected by satellites at higher altitudes. Vesecky's analysis shows that frequencies in the range 5-20 MHz should be energetic enough during some disturbed events to be detectable above cosmic noise. These frequencies are in the range observed to be most energetic from the outer belt.

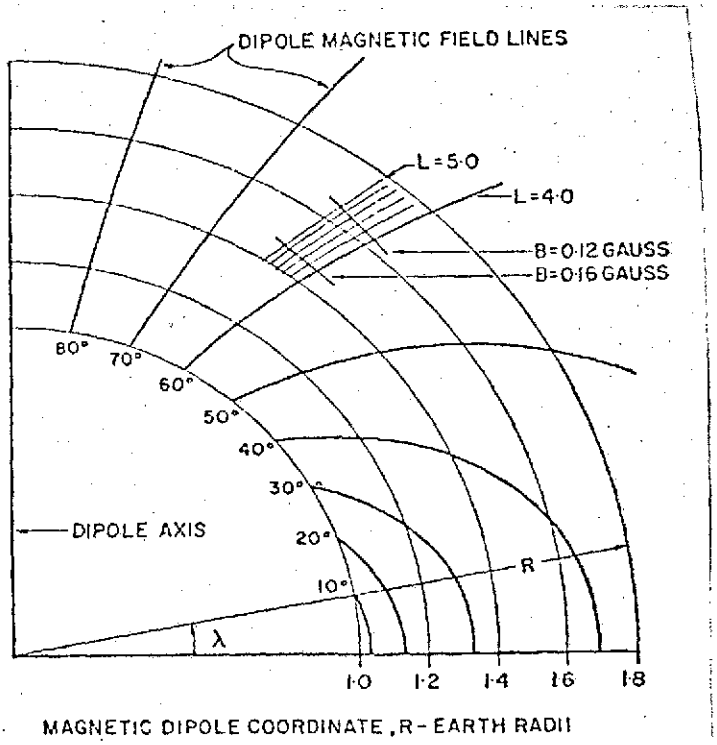


Figure 3-52. A VIEW TAKEN PERPENDICULAR TO THE DIPOLE AXIS OF A DIPOLE MODEL FOR THE GEOMAGNETIC FIELD SHOWING THE $(R, \lambda)$ COORDINATES OF THE DOMINANT EMITTING REGION. Ray paths being considered will pass through the emitting region toward the observer while perpendicular to the plane of the figure.

Figure 3-53 shows levels of cosmic noise brightness and examples of possible synchrotron noise during disturbed events.

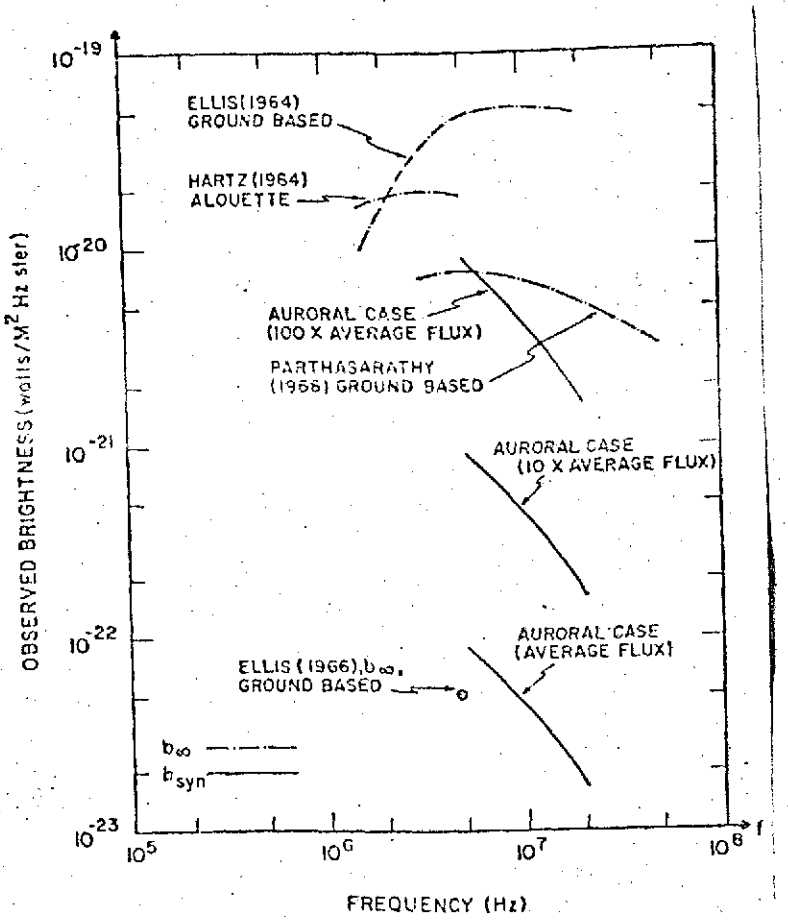


Figure 3-53 COMPARISON OF SYNCHROTRON EMISSION FROM ABOVE THE AURORAL REGIONS ($b_{syn}$) WITH SEVERAL ESTIMATES OF THE COSMIC NOISE BACKGROUND ($b_\infty$).

Figure 3-54 depicts the results of brightness calculations originating from the region shown in Figure 3-52 for the frequencies 5-20 MHz. For details of these calculations see Vesecky, 1969.

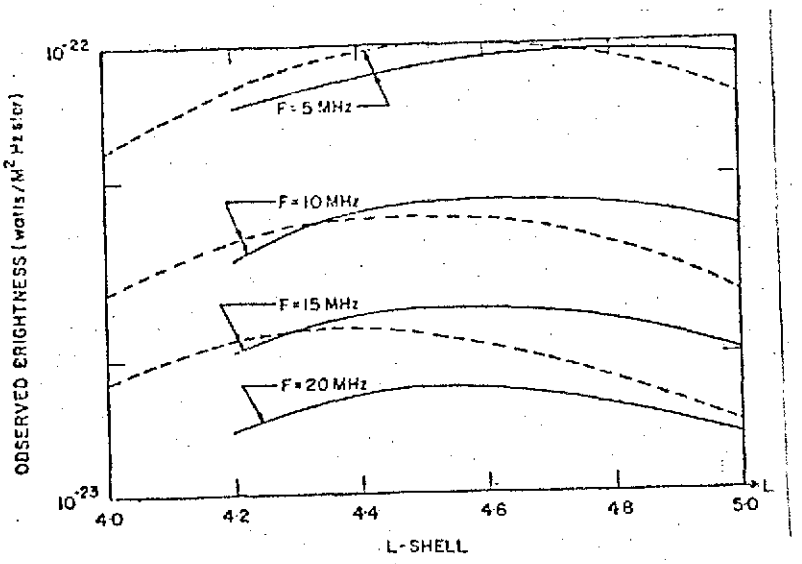


Figure 3-54. Distribution of observed brightness with the region in $(B, L)$ space from which the dominant contribution comes at frequencies in the 5–20 MHz range; the solid line implies $B \approx 0{\cdot}16$ G and the dashed line $B \approx 0{\cdot}12$ G.

Finally, it is noted that most of the auroral region orbital passes during PCA events presented in this report do support the predictions of Vesecky for the higher end of the frequency range. Note that the RAE orbit at 6,000 km, which is above the 4,000 km emitting region shown in Figure 3-52, , and conditions are approximately those postulated by Vesecky for detection of 5-20 MHz. Examination of data indicates enhanced radiation arrives through the lower Vee antenna side lobes or from below.

Remaining for speculation is the detection of frequencies well below the 5 MHz lower level predicted using Vette's outer belt model. It is noted however, that the spectrum of precipitating particle energy is in the lower energy ranges. Thus, even though individual electrons at the lower energies provide little power (see Figure 3-41) the pattern becomes more omnidirectional which fact increases the region and number of particles whose radiation can contribute. Figure 3-41 also indicates that higher energies up to about 1 MeV contribute to the radiated frequencies below 1 MHz, but the contributing regions will be more restricted because of narrow radiation pattern.

## CONSIDERATIONS CONCERNING SYNCHROTRON RADIATION IN RAE DATA

Analysis of RAE data from PCA events indicate generally that radiation is received on antenna side lobes or from below the satellite. The estimated background shows the upper Vee to be most energetic which fits the view that cosmic radiation is most efficiently received from the top Vee. Figure 3-55 shows a plot of upper and lower Vee background and noise enhancement as the auroral region is approached. This is the event of November 3, 1969 during which the subsatellite track entered the oval boundaries. Very similar looking data occur for passes where the oval is not intersected or even passed very closely. This is still consistent with the picture of synchrotron radiation generated by precipitating and trapped particles.

It is noted that the RAE data may provide experimental information on both large scale and small scale irregularities. The scattering from small scale irregularities would provide diffraction patterns that can be relatively narrow or broad as the spatial separation is many wavelengths or few. The two measurements at each frequency (separated by four seconds) in effect samples the diffraction fine structure.

The RAE data shows a variety of four second interval energy separations. These can be viewed as the effect of the satellite passing through the small scale diffraction fringes. It is possible that a suitable analysis of this data can provide estimates of the statistics of small scale irregularities.

The fine structure is superimposed on large variations of energy which may be viewed as the effect of the satellite swinging into the highly directional synchrotron radiation propagating through a predominately forward scattering medium which implies large scale scattering irregularities.

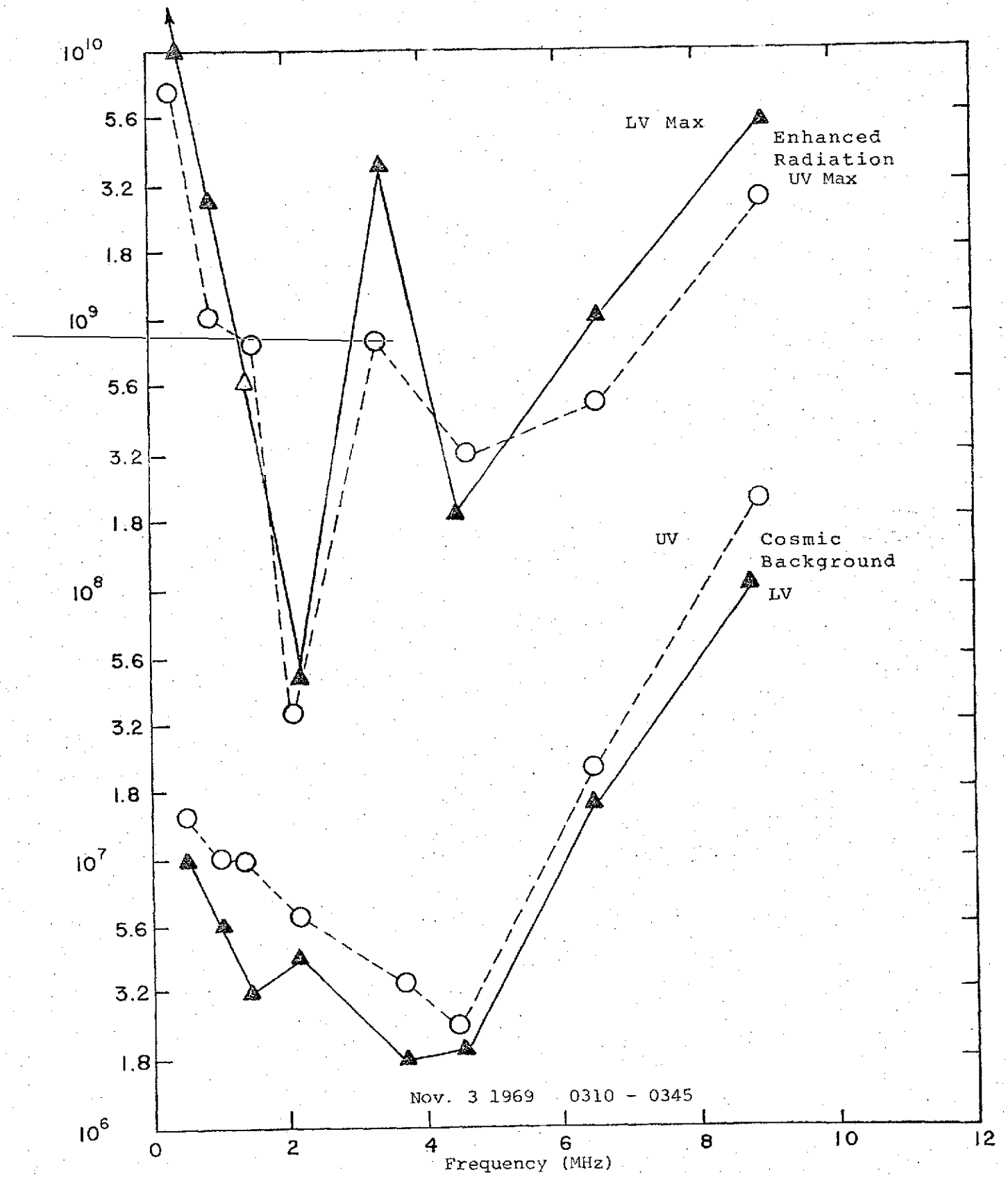


FIGURE 3-55. NOISE ENHANCEMENTS FOR UPPER AND LOWER VEE FOR 3 NOVEMBER 1969.

The rather broad range of frequencies generated and detected by synchrotron radiation provides a ready made frequency source over about a decade of frequencies.

## 3.4 Other Geophysical and Man Made Phenomena

### 3.4.1 South Atlantic Geomagnetic Anomaly

Since it is expected that RF emissions from precipitating particles in the auroral regions will increase RAE noise temperatures, it is reasonable to expect that particle precipitation in other regions of the world will have the same effect. Magnetospherically trapped energetic electrons drift eastward, and as those on low L shells (L~3) approach the South Atlantic magnetic anomaly from the west, they precipitate into the upper atmosphere because their mirror altitudes are lowered by the reduced magnetic field strength in the anomaly (C. Pike, et al., 1968). We judged it possible that these energetic electrons will generate RF noise emissions as they enter the upper atmosphere and enhance the noise power measured by RAE in its passage over the region.

We have investigated some ten RAE orbits just south east of Recife, Brazil over the region of the anomaly and compared these passes with corresponding orbits at the same latitudes both east and west of the magnetic anomaly to determine the relative importance of electron precipitation from low L shells and possible noise enhancement from RF emissions. The orbits chosen were taken from Spring, Summer and Fall months of 1969 at 6.55 and 9.18 MHz. After careful examination of the data, no definite indications of either enhanced or depressed noise levels were found. Paths west of the anomaly over the South American continent show somewhat higher noise but this is easily attributable to the increase in thunderstorm activity over the continent. For control passes east of the anomaly over the South Atlantic, there are no substantial differences in received noise power as compared to RAE orbits over the South Atlantic anomaly. On the basis of this analysis one would

be forced to conclude that there appears to be neither measurable enhancement or depression of the noise power over the region of the geomagnetic anomaly. However, recalling the discussion of the RAE noise contours in Section 2.2, five seasonal contours give clear indications of enhanced average noise power over the anomaly on both 6.55 and 9.18 MHz respectively. The remaining nine contours show little or no enhancement over the region. We have not been able to formulate a convincing explanation of this behavior. The structural manifestations are very clear, but on the basis of the depth and scope of the analysis performed, we are unable to explain the apparently conflicting results. To resolve these difficulties a more extensive analysis of the RAE data supplemented by a more detailed examination of the process occurring in the neighborhood of the anomaly, i.e., emission processes, F-layer enhancements, enhanced D-region absorption processes, is required.

### 3.4.2 RF EMISSION DURING ARTIFICIAL AURORA PRODUCTION

In January 1969 a rocket-borne electron accelerator was launched from Wallops Island for the purpose of creating detectable artificial auroras (W. Hess, et al., 1971, T. Davis, et al., 1971). As pointed out in Section 3.3, precipitating particles may produce RF emissions over a broad spectrum depending on the particle energies and a number of other complex factors. The precipitating particles result from the natural interplay of the solar plasma and Earth's magnetic field, or they may be artificially introduced in a manner similar to the rocket-borne particle generator, or by nuclear detonation.

Generally, one can expect that HF emissions may be produced by accelerating electrons with energies within the range of those generated during the Wallops Island rocket launch, i.e. 1 to 10 keV. Consequently, we were presented with an opportunity to examine RAE data during the January 1969 experiment, to determine whether there were any perturbations in the data attributable to enhanced HF emission generated by the artifically injected electrons.

Detection of the potentially enhanced level of RF emission required a detailed examination of the RAE data, the state of the local ionosphere, magnetic and solar activity information, and prevailing meteorological conditions. The meteorological conditions are of particular importance since the rocket was launched shortly after the passage of a cold front and the atmospheric noise, consisting primarily of sferics associated with the front, may have been quite severe. It was our judgement that the results of this study would give a further indication of the ability to differentiate between the many noise generation mechanisms generally operative near Earth's surface.

As has been the case in the past while investigating thunderstorm activity, our attempt to observe HF emissions of artificial aurora has been completely thwarted since RAE orbits did not traverse the appropriate geographic locale at those observational times judged critical to the investigation. Since electrons can remain trapped by the magnetic field for some time before their energy is dissipated, additional periods following the time of rocket launch were investigated. These investigations have failed to reveal any significant perturbations attributable to

radiation from trapped, artifically injected electrons. Consequently, due to the unfavorable relation between RAE's orbital position and the time of electron injection, it is our judgement that it is not possible to arrive at any firm conclusion regarding enhancements of noise power due to synchrotron radiation from the injected electrons.

# 4.0 CONCLUSIONS

Results of the continuing investigation of RAE I observations of worldwide terrestrial radio noise and geophysically significant regions of the Earth have proved to be very fruitful when viewed in toto. The fourteen seasonal noise contours based on RAE observations of HF noise indicate that while there is general agreement with the CCIR predictions regarding the gross characteristics of terrestrial HF noise, there are many significant differences. The RAE and CCIR contours begin to diverge at the higher latitudes, over the Northern Chinese and Russian mainlands, and frequently over ocean regions, particularly over the North Central Pacific. Large noise levels at the higher latitudes are attributed to RF emission processes in the magnetosphere. Differences over China and Russia are partially attributable to high power transmitters on the mainland in addition to the lack of empirical data over this region as evidenced by CCIR. The lack of ground-based measurements over ocean regions leads one to believe that the CCIR predictions are suspect over the oceans. On the other hand, the RAE contours are exclusively the result of measured data. Overall, the RAE contours are a valuable contribution to our knowledge of the noise environment.

Regarding the analysis of high latitude phenomena no clear picture has emerged. In almost all cases, noise temperatures are greater at high latitudes than mid-latitudes for all times of day in both hemispheres. The fact that the noise temperature is nearly always greater on the lower Vee coupled with the fact that the noise temperature at

higher frequencies drops off sooner than at lower frequencies leads one to conclude that the radiation emanates from a region below the satellite but above the peak of the $F_2$-layer. This conclusion is in agreement with the predictions of Vesecky (1969).

A further observation is that noise levels do not decrease appreciably during polar cap absorption and auroral absorption events. This behavior is not what would be expected if the radiation emanated from the ground. This observation tends to reinforce the conclusion that at high latitudes magnetospheric RF emissions enhance noise levels as indicated above.

With regard to known geophysical effects, such as the PCA and midlatitude trough, the RAE data do not reveal their existence clearly as do ground-based riometers and satellite-borne ion traps. There does not appear to be a benefit in the RAE data worth the detailed statistical analysis that would be required to reveal the presence of the PCA or trough.

There does appear to be a large amount of data available on the noise generated by precipitating particles in near space. There is a great deal of variability and structure in this data when viewed as a function of time, location or frequency. The meanings and inferences of these RAE data to the kinds of particles existing in space, their source and the mechanism of entry into the Earth's magnetic field have yet to be appreciated.

RAE measurements of noise levels over the South Atlantic geomagnetic anomaly have resulted in a number of apparently conflicting observations. On the one hand, pronounced high noise levels are observed on five seasonal contours for Spring, Summer and Fall for the 0-8 and 16-24 local time blocks on both 6.55 and 9.18 MHz. On the other hand, the remaining 9 seasonal contours display nothing unusual over this region. Further, the individual RAE orbits over the anomaly when compared to control orbits both east and west of the anomaly show very little differences. On the basis of the analysis performed to date, there are no satisfactory conclusions to be presented. A deeper understanding of phenomena observed over the South Atlantic geomagnetic anomaly requires more extensive analysis and additional independent measurements over the region.

The artifical aurora experiment of January 1969 was not amenable to analysis since RAE did not traverse the appropriate geographic region at those observational times judged critical to the investigation. There was no indication of enhanced noise due to radiation from trapped artifically injected electrons at times sometime after the launch. Our judgement is that it was not possible to arrive at any firm conclusion regarding enhancements of noise power due to synchrotron radiation from the inserted electrons.

# REFERENCES


Bailey, D. K., 1964,"Polar-Cap Absorption," Planet, Space Sci., 1964, Vol. 12.

Bowman, G. G., 1969, "Ionization Troughs Below the F2-layer Maximum," Planet, Space Sci., Vol. 17.

Carpenter, D. L., 1963, "Whistler Evidence of a 'Knee' in the Magnetospheric Ionization Density Profile," J. Geophys. Res. Vol. 68, No. 6.

Cormier, R., 1974, Private Communication

Chernosky, E. J., 1974, Private Communication

Davis, T.N., T. J. Hallinan, G. D. Mead, J. M. Mead, M. C. Trichel, W. N. Hess, 1971, JGR, Vol 76, No. 25.

Dessler, A. J., Effect of Magnetic Anomaly on Particle Radiation Trapped in Geomagnetic Field, J. Geophys. Res. Vol. 64, No. 7, 1959.

Herman, J. R., 1972, "High Latitude Spread-F and Ionospheric Troughs," Proc. OHD Tech. Review Meeting of 3-4 May 1972, Vol 2, Pg. 149.

Herman, J. R. , J. A. Caruso and R. G. Stone, 1973, "Radio Astronomy Explorer (RAE) I Observations of Terrestrial Radio Noise," Planet, Space. Sci., Vol 21, No. 3.

Hess, W. N., 1968, "The Radiation Belt and Magnetosphere," Blaisdell.

Jelly, D. H., and L. E. Petrie, 1969, "The High Latitude Ionosphere," Proc. IEEE, Vol. 57, Pg. 1005.

Muldrew, D. G., 1965, "F-Layer Ionization Troughs Deduced From Alouette Data," J. Geophys. Res., Vol. 70.

Novaco, James. C., 1973, "Galactic Background Maps at 3.93 and 6.55 MHz, Goddard Space Flight Center, Report No. X-693-73-182.

Panofsky, and Phillips, 1956, "Classical Electricity and Magnetism," Addison and Wesley.

Peterson, A. M. and G. F. Hower, 1966, "Theoretical Model of Synochrotron Radiation and Comparison with Observations of Radiation Trapped in the Earth's Magnetic Field," (Ed. B. M. McCormack).

Pike, C. P., J. R. Herman and G. J. Gassmann, "Conjugate F-Region Enhancement Related to the South Atlantic Magnetic Anomaly," Radio Sci., Vol. 13, No. 7, 1968.

Reid, G. C., 1963, "A Study of the Enhanced Ionization Produced by Solar Protons During a Polar Cap Absorption Event," J. Geophys. Res., Vol. 66, No. 12.

Sharp, G. W., 1966, "Midlatitude Trough in the Night Ionosphere," J. Geophys. Res., Vol. 71, No. 5.

Vesecky, J. F., 1969, "Radio Frequency Synchrotron Radiation from Trapped Electrons Above the Auroral Zones," Planet. Space Sci., Vol. 17, pp. 389 to 402.

Weber, R. R., J. K. Alexander, R. G. Stone, 1971, Radio Science, 6, 1085.

Williams, D. J. and W. F. Palmer, 1965, "Distortion in the Radiation Cavity as Measured by an 1100 km Polar Orbiting Satellite," J. Geophys. Res. 70.

Whalen, J. A., 1970, "Auroral Oval Plotter and Nomograph For Determining Corrected Geomagnetic Local Time, Latitude and Longitude for High Latitudes in the Northern Hemisphere," AFCRL-70-0422.